Stabilization, Extension and Unification of the Lattice Boltzmann Method Using Information Theory

by

Tyler Wilson

A thesis submitted in conformity with the requirements
for the degree of Doctor of Philosophy
Graduate Department of Mathematics
University of Toronto

Abstract

Stabilization, Extension and Unification of the Lattice Boltzmann Method Using Information Theory

Tyler Wilson
Doctor of Philosophy
Graduate Department of Mathematics
University of Toronto
2016

A novel Lattice Boltzmann method is derived using the Principle of Minimum Discrimination Information (MinxEnt) via the minimization of Kullback-Leibler Divergence (KLD). Approximations of this method yields the single relaxation time (SRT-LBM), two relaxation time (TRT-LBM), multiple relaxation time (MRT-LBM) Lattice Boltzmann Methods as well as Entropic Lattice Boltzmann Method (ELBM) and Ehrenfest Step LBM (EF-LBM). Specifically it is shown that these methods can be understood as approximations of a method for constrained KLD minimization. By carrying out the actual single step Newton-Raphson minimization (MinxEnt-LBM) a more accurate and stable Lattice Boltzmann Method can be implemented. To demonstrate this, 2D Poiseulle flow, 1D shock tube and lid-driven cavity flow simulations are carried out and compared to SRT-LBM, TRT-LBM MRT-LBM and EF-LBM.

To my Mom and Dad.
You did this. I just put my name on it.

Acknowledgements

Firstly, I would like to express my sincere gratitude to my advisors Prof. Mary Pugh and Prof. Francis Dawson for the continuous support of my work and most of all for their seemingly endless patience. Their guidance helped me in all the time of research and writing of this thesis. I could not have imagined having better advisors and mentors for my Ph.D study. I, and my family, cannot thank you both enough.

I would like to thank the third member of my thesis committee: Prof. Almut Burchard, for her insightful comments and encouragement, particularly when things looked most bleak. In addition, I would like to thank Prof. Clinton Groth and Prof. Robert McCann. Both have been extremely generous with their time, not only in agreeing to serve on my defense committee, but for all the helpful conversations along the wandering path of this work. To Prof. Adrian Nachman, thank you for agreeing to serve on my defense committee. In a real and practical sense, this wouldn't be possible without your kind help.

Throughout the many twists and turns of my research I reached out to a number of experts in the field including Prof. Li-Shi Luo, Prof. Michael Sukop and Prof. Tony Ladd. A heartfelt thanks to each of you for taking the time out of your busy lives to offer honest, interesting and thoughtful feedback to an unknown student from thousands of kilometers away.

As any student can attest, a single word of this thesis could not have been written if not for the financial support of many people along the way. Chief among them I would like to thank Angella Hughes and the Board of Directors of Xogen Technologies for the considerable investment in my work and my future. Not only from the financial side of things but also for providing me a long list of professional and personal growth experiences that have already proven to be invaluable. Also, thank you to the University of Toronto for allowing me the opportunity to assist and teach a number of classes throughout the years. Teaching has truly been one of the most rewarding experiences of my young career and something that will certainly be part of my future. Finally, this work was also generously supported by the Natural Sciences and Engineering Research Council of Canada and MITACS. Therefore, thank you to the people at NSERC, MITACS and also to the taxpayers of Canada, most of whom have not been given the opportunities I have and yet selflessly contributed to this work.

Thank you to all of my friends, colleagues, students and teammates who provided so many interesting and enjoyable times during my stay at the University of Toronto. You served as just enough to distraction to keep me sane, but not quite enough to prevent this work from being completed.

Last and certainly not least, thank you to my family. To my beautiful (and inhumanly patient) wife I couldn't have accomplished any of this without your unwavering support. Along the way you fostered this work, but also set the highest standard for my ongoing effort to be a better citizen of society. Your energy, kindness and compassion are truly endless. Lastly, thank you to my daughter whose hugs and laughter makes all of this, and everything else, worth it.

Contents

List of Tables

List of Figures

Chapter 1

Introduction

The Lattice Boltzmann Method (LBM) is a mesoscale discrete velocity model that has become an increasingly popular method (see Figure 1.1) for simulating fluid flows, particularly in complex geometries like porous flow (see [1] for a recent review). It employs a carefully coordinated discretization of physical space, velocity space and time, to track the evolution of a vector valued mass expectation distribution, $\mathbf{f}$ (whose vector components are called "populations.") This evolution is carried out in a cycle of "streaming" and "collision" steps (see §2.1). Historically, the LBM evolved [2, 3, 4, 5, 6, 7, 8] from the Lattice Gas Automata, or LGA (for an excellent treatment of the LGA see [9, 10]). The LBM was created to address undesirable features of the LGA such as statistical noise. Thus, the original interpretation of the LBM was that it was a generalization of the LGA.

The second interpretation of the LBM is that the LBM is a special finite difference form of the continuous Boltzmann Equation [11, 12, 13, 14]. The finite difference view of the LBM allowed researchers to explore various aspects of the LBM by performing the discretization using various quadratures and lattices.

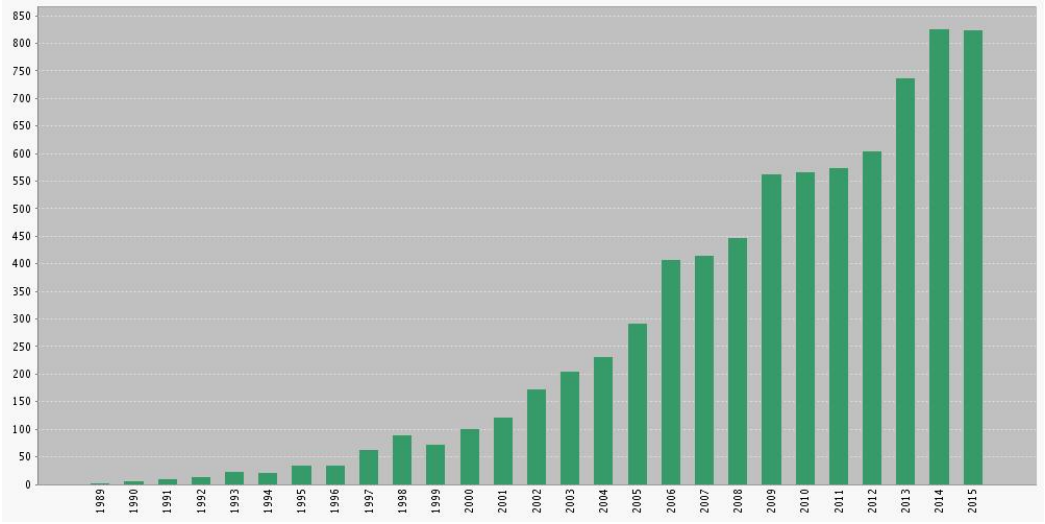

Figure 1.1: Number of publications containing "Lattice Boltzmann" keyword in Web of Science from 1989 until the end of 2015

Despite this progress it became clear that the LBM can suffer from numerical instabilities. According to Sterling and Chen,

> it is well known among LB researchers that instability problems arise frequently. When the LB method is viewed as a finite-difference method for solving the continuum discrete-

> velocity Boltzmann equations, it becomes clear that numerical accuracy and stability issues should be addressed.[15]

Increasing the stability of the LBM became the focus of significant effort. One cause of instability is that even if the mass expectation populations start positively valued they can become negative during the course of a typical simulation. As a result, one of the natural places to start to improve stability was to ensure that all mass expectation populations remained non-negative [16]. Although this helped, it did not ensure stability [17].

Much of the work done to address the stability issues of the LBM over the last twenty plus years has been to attempt to endow the Lattice Boltzmann Method with some of the features of LGA. This is because, despite the flaws of the LGA, it had some built-in advantages. Quoting Boghosian and co-workers,

> One often overlooked advantage of lattice-gas models is their unconditional stability. By insisting that lattice-gas collisions obey a detailed-balance condition, we are ensured of the validity of Boltzmann's H theorem, the fluctuation-dissipation theorem, Onsager reciprocity, and a host of other critically important properties with macroscopic consequences. [18]

Indeed, a growing number of researchers felt that the lack of unconditional stability (particularly with thermal Lattice Boltzmann Methods) was due to the lack of a so-called "H-Theorem" for the LBM.

The classical H-Theorem of Boltzmann in 1872 was a key development in statistical mechanics. A translation of his original paper is given in [19]. For a gas of spherical particles undergoing elastic collisions Boltzmann was able to show that given a *continuous* mass expectation distribution, $f(\mathbf{x}, \mathbf{v}, t)$, one could define an H-function,

$$H[f] = \iint f(\mathbf{x}, \mathbf{v}, t) \ln f(\mathbf{x}, \mathbf{v}, t)\, d\mathbf{v} d\mathbf{x}, \tag{1.1}$$

which was monotonically non-increasing in time. The thermodynamic entropy is related to this function by,

$$S_{\text{thermo}} = -k_B H,$$

where k_B is the Boltzmann constant. Using variational methods one can easily verify that the Maxwell-Boltzmann distribution,

$$f^{\text{MB}}(\mathbf{x}, \mathbf{v}, t) = \frac{\rho}{(2\pi RT)^{D/2}} e^{-\frac{|\mathbf{v}-\mathbf{u}|^2}{2RT}} \tag{1.2}$$

is the unique minimizer of (1.1) under the physical constraints,

$$\rho(\mathbf{x}, t) = \int_{\mathbb{R}^D} f(\mathbf{x}, \mathbf{v}, t)\, d\mathbf{v} \tag{1.3}$$

$$\rho(\mathbf{x}, t)\, \mathbf{u}(\mathbf{x}, t) = \int_{\mathbb{R}^D} \mathbf{v}\, f(\mathbf{x}, \mathbf{v}, t)\, d\mathbf{v} \tag{1.4}$$

$$R\frac{D}{2}\, \rho(\mathbf{x}, t)\, RT(\mathbf{x}, t) = \frac{1}{2} \int_{\mathbb{R}^D} |\mathbf{v} - \mathbf{u}(\mathbf{x}, t)|^2\, f(\mathbf{x}, \mathbf{v}, t)\, d\mathbf{v} \tag{1.5}$$

where D is the physical dimension, R is the specific gas constant, $\rho(\mathbf{x}, t)$ is the density at $\mathbf{x} \in \mathbb{R}^D$ and time $t \in \mathbb{R}$, $\mathbf{u}(\mathbf{x}, t)$ is the macroscopic velocity and $T(\mathbf{x}, t)$ is the temperature. This has the

interpretation that without additional forces or interactions, the velocity distribution of a gas of elastically colliding particles will evolve into the Maxwell-Boltzmann distribution over time. The Maxwell-Boltzmann distribution serves as both a stationary state as well as an attractor for the system.

The Lattice Boltzmann method alternates between "streaming" steps and "collision" steps. In the collision step, the collision instantaneously replaces the pre-collision mass expectation distribution $\mathbf{f}^{\text{pre}}(\mathbf{x}, t)$ with a post-collision distribution $\mathbf{f}^{\text{post}}(\mathbf{x}, t)$. The streaming step then "streams" the post-collision populations to neighbouring nodes, producing pre-collision expectation distributions at time $t + \Delta t$.

The original Single Relaxation Time Lattice Boltzmann Method (SRT-LBM, also called LBGK LBM) collision step,

$$\mathbf{f}^{\text{post}}(\mathbf{x}_j, t_n) = \mathbf{f}^{\text{pre}}(\mathbf{x}_j, t_n) + \frac{1}{\tau}\left(\mathbf{f}^{\text{eq}}(\mathbf{x}_j, t_n) - \mathbf{f}^{\text{pre}}(\mathbf{x}_j, t_n)\right), \tag{1.6}$$

has a stationary state (called the equilibrium distribution, $\mathbf{f}^{\text{eq}}$) that does not serve as an attractor. In fact, one can easily convince oneself that starting with a seemingly harmless initial state, repeated application of (1.6) will lead to unbounded growth of $\mathbf{f}$, particularly if some components of $\mathbf{f}^{\text{pre}}$ are very different from the corresponding components of $\mathbf{f}^{\text{eq}}$. This suggested to some authors that the LBM should be equipped with an H-Theorem. According to Chen et al,

> We point out that the fundamental origin of the instability in [thermal Lattice Boltzmann models] can be attributed to the violation of a global H-theorem. On the contrary, [isothermal Lattice Boltzmann models] systems do not suffer from such a problem. [20]

This was expanded upon by Succi,

> The violation of the global H-Theorem manifests itself whenever the temperature field acquires a spatial dependence. On the other hand, though the transition probabilities are not unity, they become constants in the isothermal LB models, which explains why the above problem disappears for isothermal LB models. This essential difference between thermal and isothermal lattice models lies at the heart of the significantly better stability of the latter. [21]

Even though athermal (without a well defined physical temperature) and isothemral (having a well defined, uniform, constant temperature) Lattice Boltzmann Methods seemed to be more stable than their thermal counterparts, a number of researchers still noted instabilities in isothermal simulations and attributed them to lack of an H-Theorem[22, 18, 23, 24]. Attempts to equip the LBM with an H-Theorem, or incorporate some notion of entropy, have spanned the last 15 years and are generally referred to as "entropic methods".

To equip the LBM with an H-Theorem one must provide an functional (hereafter called an "entropy") that is monotonically decreasing in time. In addition, the corresponding equilibrium and collision step must accurately reproduce the desired physics of the system.

The first attempts to equip the LBM with an H-Theorem were to retain the SRT-LBM collision step (1.6) and instead of using the original and most popular polynomial equilibrium [8], (2.16), one chooses an equilibrium distribution that minimizes a chosen entropy functional, subject to constraints that ensure proper dynamics [25, 26, 27]. Karlin et al [28] proposed that any such entropy should be convex and when the corresponding equilibrium is used in the SRT-LBM collision, (1.6) one must recover the Navier-Stokes equations up to second order in the macroscopic velocity, $\mathbf{u}$.

Entropy functions that satisfy these requirements are called "perfect entropy functions." Though Karlin et al. were able to find such a perfect entropy function for 2 cases (a 1 dimensional, 3 velocity

lattice, and a 2 dimensional 9 velocity lattice), finding an entropy function for a given lattice is non-trivial in general and in some situations may be impossible. Also, Wagner [29] showed that one cannot find a perfect entropy function for Lattice Boltzmann implementations that use an equilibrium that is a polynomial in $\mathbf{u}$.

Requiring that the equilibrium be a polynomial was sufficient (but not necessary) to ensure that model would be Galilean invariant, which was one of the requirements for LBMs with H-Theorems set by Succi et al. in [21]. (However, non-polynomial equilibrium Galilean invariant models were suggested by Boghosian and coworkers [23, 30]). The other two requirements outlined in [21] were that the equilibrium should be realizable (bounded between 0 and 1) and also solvable (expressible as an explicit function of the local macroscopic properties).

All of the above requirements put tremendous restrictions on finding a suitable equilibrium while keeping the SRT-LBM collision step. An alternative path to equipping the LBM with an H-Theorem would be to find a novel collision step that is not the SRT collision (1.6) . The most popular of these alternative collision steps is the Entropic Lattice Boltzmann Method (ELBM) and was first described by Karlin et al. in 1999 [28]. This method constructs a collision step based on knowledge of the entropy function only. Though the collision step may include an equilibrium distribution, in general the ELBM circumvents the need for finding an equilibrium distribution with specific attributes. Early work with the ELBM [22, 31] used the perfect entropy functions developed in [28] but eventually a more popular entropy function based on Boltzmann's original H-function (1.1) was suggested [32],

$$S[\mathbf{f}] = \sum_i \mathbf{f}_i \ln \frac{\mathbf{f}_i}{W_i}, \tag{1.7}$$

where $\mathbf{f}_i$ is the ith component of $\mathbf{f}$ and the W_i are weights that depend on the choice of lattice (for example, see §2.1.6). An explicit corresponding equilibrium for this entropy function that conserves mass and momentum can in fact be found [32] (see (5.2)). Since then many tests of the ELBM collision step have used this function in some manner (for an example [33, 34, 35], and others). An excellent review of the early work on equipping the LBM with an H-Theorem can be found in [21] and [36].

In addition to attempts to equip the LBM with an H-Theorem, other entropic methods have been explored such as non-equilibrium entropy limiters [37], and Ehrenfests' coarse-graining [38, 39, 40]. The assumption that the LBM should (or even *could* incorporate entropic principles was not universally accepted. A wide range of other attempts have been made to improve the stability of the LBM. Chief among them is the Multiple Relaxation Time Lattice Boltzmann Method (MRT-LBM) [41, 42, 43, 44, 45, 46, 47, 48]. There is a bit of a split in the LBM community, between the advocates of entropic methods, and advocates of MRT-LBM.

In fact, critics of entropic methods claim that there are many issues with entropic methods. One major issue is that they can be comparatively computationally expensive. Some authors claim that the benefits of entropic methods may be overstated [49, 39, 50, 51], impossible to implement in certain conditions [52], and impractical [53].

Despite the popularity of entropic methods and MRT-LBM methods, a host of other techniques claim to increase stability as well. These include changing the boundary conditions [54, 55],"link-based" two-relaxation time-methods [56, 57, 58], least squares finite element LBM [59], regularized LBM [60], additional velocities [61], "Onsager-like" relation collision step [62], double MRT-LBM (for thermal flows) [63]. However, we will limit our focus on entropic methods and relaxation-time

methods.

We share the view that a notion of entropy plays an important role in the stability of the LBM and that entropy violations are a cause of numerical instabilities. In addition we claim that stability improvements from MRT-LBM methods and other entropic methods are manifestations of the same underlying principle, and that these approaches are not mutually exclusive and can, in fact, be unified.

The LBM has been largely used for fluid flow applications (though some non-fluid applications do exist, for example [64]) and for near-equilibrium flows in particular. Indeed, the relationship between the relaxation times used in implementations of the LBM and simulated fluid properties is typically derived by applying a Chapman-Enskog analysis and assuming near-equilibrium, low Mach number and a small Knudsen number. Only after the result of the Chapman-Enskog analysis is compared to the pre-determined governing equations: the Navier-Stokes equations (see for example,[12]) is one able to specify values for some relaxation times. This leads one to wonder if the LBM could be used in a wider range of non-fluid and/or far from equilibrium applications without an a priori knowledge of the governing macroscopic equations.

In this thesis we describe a novel, third interpretation of the LBM. This new interpretation is based on the Principle of Minimum Discrimination Information (or Minimum Cross Entropy) MinxEnt. We will show that MinxEnt is in fact a stronger condition than the H-Theorem for lattice simulations and, as such, simulations satisfying MinxEnt will necessarily satisfy an H-Theorem and in turn help stabilize the Lattice Boltzmann Method based on it. We will call this LBM based on MinxEnt, "MinxEnt-LBM" (see Figure 1.2).

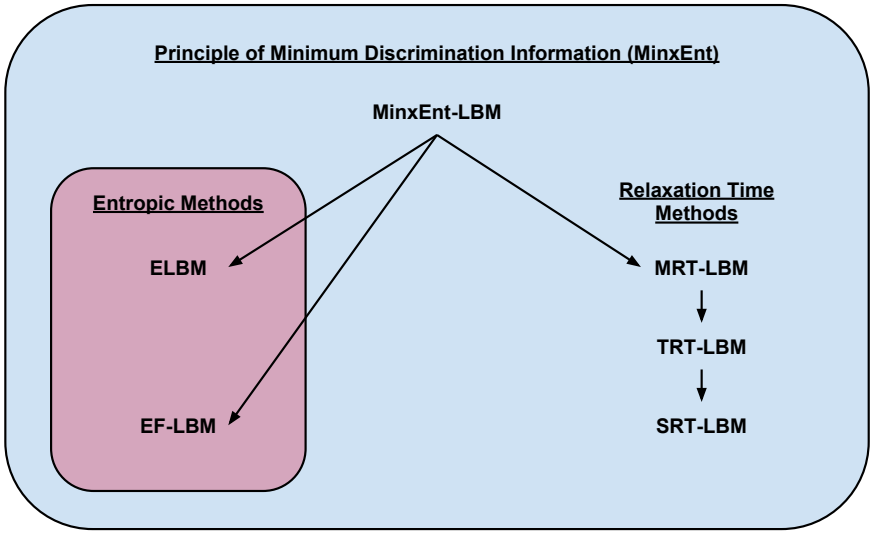

Figure 1.2: The relationship of other LBMs to MinxEnt-LBM. Methods at the tips of arrows can be shown to be special case of the method at tail

Further, we will show that MRT-LBM, entropic LBM (ELBM) and Ehrenfest Step LBM (EF-LBM) [39, 40, 65] are all different, simplified approximations of the MinxEnt-LBM scheme. We

compare the MinxEnt-LBM scheme to these other LBM schemes for benchmark problems: 1-D shock tube and 2D lid-driven cavity flow.

Finally, in constructing the MinxEnt-LBM framework we will see how it naturally suggests avenues to allow the method to be extended beyond fluid flow applications and to systems in which the governing macroscopic equations are not known ahead of time.

This thesis is organized in the following way: the LBM, and some of its current variations are described in Section 2. Section 3 outlines the foundation of our method, MinxEnt. Section 4 outlines the MinxEnt-LBM framework and includes the unification of other LBMs as different approximations of MinxEnt-LBM. Section 5 gives some numerical results and Section 6 offers final thoughts and future work.

Chapter 2

Lattice Boltzmann Methods

In kinetic theory [66], the evolution of macroscopic properties often involves understanding the behaviour of a mass expectation density, f, (hereafter called a "distribution"),

$$f = f(\mathbf{x}, \mathbf{v}, t).$$

For example in a fluid simulation, knowledge of the mass expectation distribution allows one to calculate macroscopic properties of the fluid such as density, momentum and temperature,

$$\rho(\mathbf{x}, t) = \int_{\mathbb{R}^D} f(\mathbf{x}, \mathbf{v}, t)\, d\mathbf{v} \tag{2.1}$$

$$\rho(\mathbf{x}, t)\, \mathbf{u}(\mathbf{x}, t) = \int_{\mathbb{R}^D} \mathbf{v}\, f(\mathbf{x}, \mathbf{v}, t)\, d\mathbf{v} \tag{2.2}$$

$$R\frac{D}{2}\, \rho(\mathbf{x}, t)\, RT(\mathbf{x}, t) = \frac{1}{2} \int_{\mathbb{R}^D} |\mathbf{v} - \mathbf{u}(\mathbf{x}, t)|^2\, f(\mathbf{x}, \mathbf{v}, t)\, d\mathbf{v} \tag{2.3}$$

The usual kinetic theory approach to calculating the evolution of f is based on solving the Boltzmann Equation (BE) [66]:

$$\frac{\partial f}{\partial t} + \mathbf{v} \cdot \nabla_{\mathbf{x}} f + \frac{\mathbf{F}}{m} \cdot \nabla_{\mathbf{v}} f = C[f] \tag{2.4}$$

where $\mathbf{F}$ is the external force and $C[f]$ is the change in f due to collisions (typically called the "collision term"). In practice using computers to approximate solutions of the BE is very challenging because of the collision term.

Understanding f is also the fundamental objective of the Lattice Boltzmann Method (LBM). In fact it has been shown that a specific discretization of the BE, under various approximations for of the collision term leads to versions of the LBM [11, 12, 13, 67, 14].

In this section we will describe the Lattice Boltzmann Method, as well as outline some of the variants that can be found in the literature. For a more detailed explanation of the connection between f and macroscopic properties of a system, see Appendix A.

2.1 LBM Simulation Procedure

Consider a finite time step, δ_t. Given a distribution f at time t we approximate f at time $t + \delta_t$ with a two-step process; a "collision step" followed by a local "streaming step."

In the instantaneous collision step, a *local* operator (denoted Δ) takes $f^{\text{pre}} = f$ at time t and maps it to f^{post} at time t:

$$\text{Collision Step:} \qquad f^{\text{post}}(\mathbf{x}, \mathbf{v}, t) = \Delta[f^{\text{pre}}(\mathbf{x}, \mathbf{v}, t)],$$

In this context, "local" means local in $\mathbf{x}$: the post-collision distribution at position $\mathbf{x}$ is determined by the pre-collision distribution at position $\mathbf{x}$ only — the pre-collision distributions at points other than $\mathbf{x}$ have no effect. This is one of the powerful features of LBM; it is very suitable for parallel computation.

Given the post-collision distributions, $\mathbf{f}^{\text{post}}$, at time t at all locations $\mathbf{x}$, constructs pre-collision distributions at time $t + \delta_t$ by "sending components" of the f^{post} to neighbouring locations in the natural manner determined by their velocities

$$\text{Streaming Step:} \qquad f^{\text{pre}}(\mathbf{x} + \mathbf{v}\,\delta t, \mathbf{v}, t + \delta_t) = f^{\text{post}}(\mathbf{x}, \mathbf{v}, t),$$

The streaming step moves the values of the distribution *unchanged* from position to position according to their velocities. This is usually known as "free streaming" or "free transport." The fact that distributions do not evolve by free transport is addressed by the collision step.

A defining feature of the LBM is the discretization of space into a lattice, Λ, with a commensurate discretization of the velocities. Let $\mathbf{x}, \mathbf{v} \in \mathbb{R}^{\mathbf{D}}$ be a position and a velocity respectively. If the system occupies a region of physical space, $\Omega \subset \mathbb{R}^D$ then $\mathbf{x} \in \Omega$. The velocity, $\mathbf{v}$, is unconstrained: $\mathbf{v} \in \mathbb{R}^D$. The LBM tracks the evolution of a discrete, vector-valued distribution, $\mathbf{f}(\mathbf{x}, t)$, which is defined at only a regular, uniform, discrete set of positions and velocities. That is,

$$\mathbf{x} = \mathbf{x}_j, \in \Omega \cap \Lambda$$

where Λ is a lattice in $\mathbb{R}^D$ and

$$\mathbf{v} = \mathbf{v}_i \in \{\mathbf{v}_1, \mathbf{v}_2, \ldots, \mathbf{v}_b\}$$

where $\{\mathbf{v}_1, \mathbf{v}_2, \ldots, \mathbf{v}_b\}$ is the set of allowed velocities. Given a time-step δt, the velocities must satisfy $\mathbf{x}_j + \mathbf{v}_i\,\delta t \in \Lambda$ for all $i \in \{1, \ldots, b\}$ and all $\mathbf{x}_j \in \Omega \cap \Lambda$ in order for the velocity discretization to be compatible with Λ at δt. The vector-valued distribution, $\mathbf{f}(\mathbf{x}_j, t)$ is related to the continuous distribution by components:

$$\mathbf{f}_i(\mathbf{x}_j, t) \approx f(\mathbf{x}_j, \mathbf{v}_i, t)$$

A typical LBM simulation would proceed as follows, making note that the order of streaming and collision step does not matter in practice:

1. Discretize space, velocity, and time: Above, $\mathbf{x} \in \Omega \subset \mathbb{R}^D$, $\mathbf{v} \in \mathbb{R}^D$, $t \in \mathbb{R}$, and the mass expectation distribution, f, takes on values in $\mathbb{R}$. As discussed in detail in §2.1.6, a finite set of velocities $\mathbf{v}_i, i \in \{1, \ldots, b\}$ is chosen; see Figure 2.3 for an example of a lattice in $\mathbb{R}^2$ and set of nine velocities. A fixed time step, δt, is also chosen with time discretized accordingly: $t_n = n\,\delta t$ with $n \in \mathbb{N}$. A compatible lattice Λ is constructed and then intersected with Ω; this results in a discrete set of points $\mathbf{x}_j \in \Lambda \cap \Omega$. The distance between nearest neighbour nodes is uniform and denoted δ_x. How this discretiztion is done is an open topic in LBM research. Because of the discretization of velocity, the distribution $f(\mathbf{x}_j, \cdot, t_n) : \mathbb{R}^D \to \mathbb{R}$ is approximated with a vector $\mathbf{f}(\mathbf{x}_j, t_n) \in \mathbb{R}^b$.

2. Initialize distributions: At $t = 0$, at each node $\mathbf{x}_j$, all b components of the (now discrete) distribution $\mathbf{f}^{\text{pre}}(\mathbf{x}_j, 0)$ are assigned, in such a way that the macroscopic initial conditions,

such as density, mean velocity, etc, at $\mathbf{x}_j$ are satisfied.

3. Compute macroscopic quantities: Using $\mathbf{f}^{\text{pre}}(\mathbf{x}_j, t_n)$, macroscopic quantities such as density and mean velocity, are then calculated using discretized versions of (2.1) - (2.3) at each node $\mathbf{x}_j$ (see §2.1.6).

4. Compute local equilibrium: Using the macroscopic quantities, calculate a local "equilibrium distribution" $\mathbf{f}^{\text{eq}}(\mathbf{x}_j, t_n)$ at each node $\mathbf{x}_j$; see §2.1.1 and §2.1.6.

5. Collision Step: The pre-collision and equilibrium distributions are used to define the post-collision distribution at time t_n:

$$\mathbf{f}^{\text{post}}(\mathbf{x}_j, t_n) = \Delta[\mathbf{f}^{\text{pre}}(\mathbf{x}_j, t_n), \mathbf{f}^{\text{eq}}(\mathbf{x}_j, t_n)]$$

for all $\mathbf{x}_j \in \Lambda \cap \Omega$. See §2.1.2 to §2.1.5 for a discussion of some standard choices for the collision operator Δ.

6. Streaming step: At every node $\mathbf{x}_j \in \Lambda \cap \Omega$, each component of the distribution at time t_n is streamed according to

$$\mathbf{f}_i^{\text{pre}}(\mathbf{x}_j + \mathbf{v}_i\, \delta t, t_{n+1}) = \mathbf{f}_i^{\text{post}}(\mathbf{x}_j, t_n) \qquad \forall i \in \{1, \ldots, b\} \tag{2.5}$$

to create the pre-collision distribution $\mathbf{f}^{\text{pre}}$ at time t_{n+1}. Implicit in (2.5) is that $\mathbf{x}_j + \mathbf{v}_i\, \delta t = \mathbf{x}_{j'}$ for some j'; this requires that the lattice Λ and the velocity discretization are compatible (see §2.1.6).

7. Iterate: Having determined $\mathbf{f}^{\text{post}}(\mathbf{x}_j, t_{n+1})$ at all nodes, repeat steps 3-6 to determine $\mathbf{f}^{\text{pre}}(\mathbf{x}_j, t_{n+2})$ and so on.

A schematic workflow of the LBM is shown in Figure 2.1

Boundary conditions are imposed as needed either during the collision step, or the streaming step; see §2.1.7.

2.1.1 Equilibrium Distributions

Here we give two popular choices for the equilibrium distribution.

Maxwell-Boltzmann Based Equilibrium

For systems involving classical fluid particles, the most widely used equilibrium distribution [8] is based on the continuous Maxwell-Boltzmann Distribution:

$$f^{\text{eq}}(\mathbf{x}, \mathbf{v}, t) = \frac{\rho}{(2\pi RT)^{D/2}} e^{-\frac{|\mathbf{v}-\mathbf{u}|^2}{2RT}}. \tag{2.6}$$

It should also be noted that for other types of fluids (quantum fluids for example) the Maxwell-Boltzmann Distribution may not be the appropriate equilibrium for that system.

Entropy Based Equilibrium

As discussed in the introduction, one path to equipping an LBM with an H-Theorem is to choose an equilibrium that maximizes an entropy function subject to constraints. In an isothermal simulation

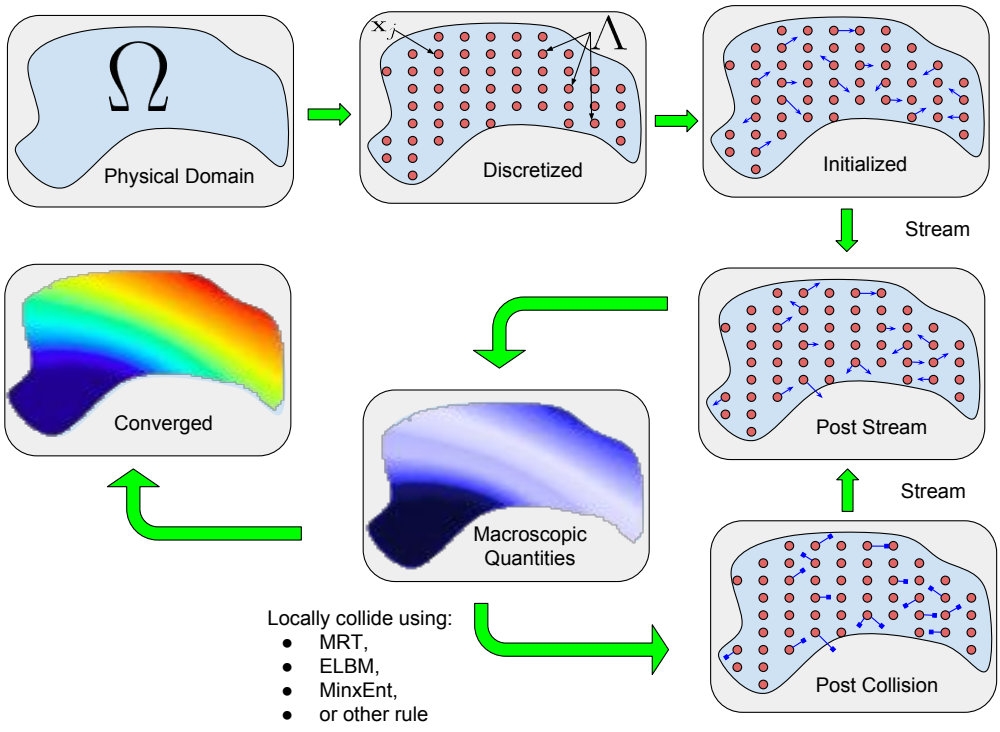

Figure 2.1: Schematic workflow of the LBM method beginning in the top left with the physical domain and proceeding to discretization, initialization, streaming and collision steps

these constraints are conservation of mass and momentum,

$$\rho(\mathbf{x},t) = \int_{\mathbb{R}^D} f(\mathbf{x},\mathbf{v},t)\, d\mathbf{v}$$
$$\rho(\mathbf{x},t)\,\mathbf{u}(\mathbf{x},t) = \int_{\mathbb{R}^D} \mathbf{v}\, f(\mathbf{x},\mathbf{v},t)\, d\mathbf{v}$$

The resulting equilibrium distribution which maximizes the entropy subject to hydrodynamic constraints will be discussed in §5.1.1.

2.1.2 Collision Step: Single Relaxation Time (SRT-LBM)

The collision step accounts for changes to the components of the distribution arising from collision between fluid particles.

The first, most popular and simplest collision step is based the linearization of the kinetic collision term [3, 4] and further approximating by assuming a single relaxation time τ [5]:

$$\Delta[\mathbf{f}^{\text{pre}}(\mathbf{x}_j,t_n),\mathbf{f}^{\text{eq}}(\mathbf{x}_j,t_n)] = \mathbf{f}^{\text{pre}}(\mathbf{x}_j,t_n) + \frac{1}{\tau}\left(\mathbf{f}^{\text{eq}}(\mathbf{x}_j,t_n) - \mathbf{f}^{\text{pre}}(\mathbf{x}_j,t_n)\right). \tag{2.7}$$

$\mathbf{f}^{\text{eq}}(\mathbf{x}_j,t_n)$ is an equilibrium distribution (see §2.1.1) and τ is some predetermined relaxation time that is related to the fluid viscosity; this relationship is lattice dependent and is discussed for a specific lattice in §5.1.2 . This single relaxation time approach was made more popular in [8] and assumed the name Lattice BGK (LBGK) owing to its similarity to the Bhatnagar-Gross-Krook kinetic equation [68]. For this reason it is common in the literature to refer to LBMs using the single

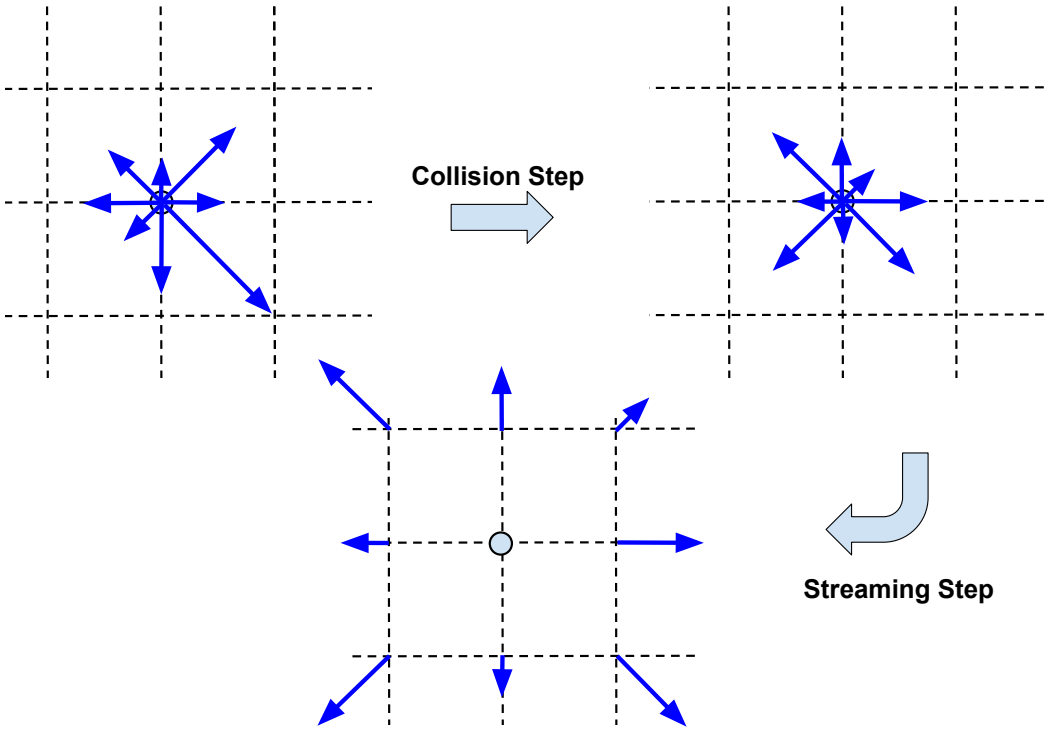

Figure 2.2: Top left: pre-collision distribution $\mathbf{f}^{\text{pre}}(\mathbf{x}_j, t_n)$. Top right figure: the resulting $\mathbf{f}^{\text{post}}(\mathbf{x}_j, t_n)$ after the collision step Bottom figure: the streamed components of the top right figure distribution $\mathbf{f}^{\text{pre}}(\mathbf{x}_j + \mathbf{v}_i\delta_t, t_{n+1})$.

relaxation time collision step as "LBGK."

2.1.3 Collision Step: Multiple Relaxation Time (MRT-LBM)

Historically, two major problems researchers encountered when implementing the SRT-LBM were that

1. one couldn't specify the Prandtl number for a simulation
2. numerical instabilities

The Prandtl number is the ratio of a fluid's kinematic viscosity and its thermal diffusivity; fluids can have the same kinematic viscosity but have different Prandtl numbers. Owing to its single adjustable parameter (τ), SRT-LBM fixes both the kinematic viscosity and the Prandtl number. In an attempt to rectify this issue and the stability problems, researchers returned to the more general linearized collision term of [3, 4] which allowed for multiple relaxation times during the collision step [41, 42, 43, 44, 45, 46, 47, 48]. This is accomplished via the collision operator:

$$\Delta[\mathbf{f}^{\text{pre}}(\mathbf{x}_j, t_n), \mathbf{f}^{\text{eq}}(\mathbf{x}_j, t_n)] = \mathbf{f}^{\text{pre}}(\mathbf{x}_j, t_n) + \mathbf{T}^{-1}\mathbf{B}\mathbf{T}\left(\mathbf{f}^{\text{eq}}(\mathbf{x}_j, t_n) - \mathbf{f}^{\text{pre}}(\mathbf{x}_j, t_n)\right) \tag{2.8}$$

where $\mathbf{B}$ is a diagonal matrix of relaxation times and $\mathbf{T}$ is an invertible matrix taking the vector $\mathbf{f}$ into "moment space." Note that the SRT-LBM collision step (2.7) can be recovered from the MRT-LBM collision by assuming $\mathbf{B} = \frac{1}{\tau}\mathbf{I}$. The class of "Two Relaxation Time" (TRT-LBM) collision

steps was suggested by Ginzburg et al. [69]. In the TRT-LBM, the entries of $\mathbf{B}$ can take only one of two values.

2.1.4 Collision Step: Entropic Lattice Boltzmann Method (ELBM)

Given a convex entropy function, $S(\mathbf{f})$, (sometimes written as H in the literature) and "bare collision," $\mathbf{\Delta}$ (which may, or may not involve an equilibrium distribution) the ELBM collision step is designed to lower the value of S and is carried out in two steps:

1. Calculate α where α satisfies:
$$S\left(\mathbf{f}^{\text{pre}}\right) = S\left(\mathbf{f}^{\text{pre}} + \alpha\mathbf{\Delta}\right)$$

2. Compute the collision
$$\mathbf{f}^{\text{post}}(\mathbf{x}_j, t_n) = \mathbf{f}^{\text{pre}}(\mathbf{x}_j, t_n) + \beta\alpha\mathbf{\Delta}(\mathbf{x}_j, t_n)$$

where $0 < \beta < 1$ is a number related to the kinematic viscosity of the fluid. Constructing the collision step in this way ensures that the entropy of the post-collision distribution is less than the pre-collision distribution. Note that the value of α must be calculated (if possible) at every $\mathbf{x}_j$ and every t_n; this slows down the procedure.

2.1.5 Collision Step: SRT-LBM with Ehrenfest Steps (EF-LBM)

Another attempt to stabilize the LBM using entropic ideas is based on Ehrenfest coarse graining [70]. The EF-LBM collision equips the LBM with an entropy limiter which monitors the simulation for spatial points at which some type of local entropic criteria is violated [39]. This approach has been shown to be successful in reducing instabilities in 1-D shock tube simulations [39, 40, 49, 50, 37, 51] and 2D lid driven cavity flow [51].

Similar to the ELBM, EF-LBM wants the value of a given an entropy function, $S(\mathbf{f})$, to decrease during the collision step. However, rather than insist S always decreases EF-LBM instead monitors the local nonequilibrium entropy, ΔS, defined as,

$$\Delta S(\mathbf{f}^{\text{pre}}) \equiv S(\mathbf{f}^{\text{eq}}) - S(\mathbf{f}^{\text{pre}}). \tag{2.9}$$

ΔS serves as an indicator of locations that the collision step may increase S. If ΔS is below some threshold, a regular SRT-LBM (2.7) collision step is taken. Otherwise, if the threshold is exceeded, the collision step is altered at the offending location. For example the collision step in the popular version of EF-LBM is,

$$\Delta[\mathbf{f}^{\text{pre}}(\mathbf{x}_j, t_n), \mathbf{f}^{\text{eq}}(\mathbf{x}_j, t_n)] = \begin{cases} \mathbf{f}^{\text{pre}}(\mathbf{x}_j, t_n) + \frac{1}{\tau}\left(\mathbf{f}^{\text{eq}}(\mathbf{x}_j, t_n) - \mathbf{f}^{\text{pre}}(\mathbf{x}_j, t_n)\right) & \text{if } \Delta S\left(\mathbf{f}^{\text{pre}}\right) < \text{tolerance} \\ \mathbf{f}^{\text{pre}}(\mathbf{x}_j, t_n) + \frac{1}{2\tau}\left(\mathbf{f}^{\text{eq}}(\mathbf{x}_j, t_n) - \mathbf{f}^{\text{pre}}(\mathbf{x}_j, t_n)\right) & \text{otherwise.} \end{cases} \tag{2.10}$$

We can see from (2.10) that if ΔS is above tolerance, the approach of EF-LBM is to reduce the change in $\mathbf{f}$ that occurs during collision step, effectively making the collision step more "gentle." It is also interesting to note that if $\tau \approx \frac{1}{2}$, the effect of using (2.10) is to set $\mathbf{f}^{\text{post}}$ to approximately the equilibrium. This is important because it is well known that numerical instabilities in SRT-LBM grow as τ nears $\frac{1}{2}$.

2.1.6 Discretization: D2Q9 Scheme Example

How the lattice Λ and the set of admissible velocities are chosen crucially impacts the accuracy of the LBM. Typically the scheme is chosen for the accurate calculation of the hydrodynamic moments of the flow, at least for the case of the Maxwell-Boltzmann based equilibrium distribution (2.6). Consider the expected value of ϕ for some function $\phi(\mathbf{v})$:

$$\int_{\mathbb{R}^D} f^{\text{eq}}(\mathbf{x},\mathbf{v},t)\,\phi(\mathbf{v})\,d\mathbf{v} = \frac{\rho}{(2\pi RT)^{D/2}}\int_{\mathbb{R}^D} e^{-\frac{|\mathbf{v}-\mathbf{u}|^2}{2RT}}\,\phi(\mathbf{v})\,d\mathbf{v} \tag{2.11}$$

$$= \frac{\rho}{(2\pi RT)^{D/2}} e^{-\frac{|\mathbf{u}|^2}{2RT}}\int_{\mathbb{R}^D} e^{-\frac{|\mathbf{v}|^2}{2RT}}\,e^{\frac{\mathbf{v}\cdot\mathbf{u}}{RT}}\,\phi(\mathbf{v})\,d\mathbf{v}$$

$$= \frac{\rho}{(2\pi RT)^{D/2}} e^{-\frac{|\mathbf{u}|^2}{2RT}}\int_{\mathbb{R}} e^{-\frac{v_1^2}{2RT}}\ldots\int_{\mathbb{R}} e^{-\frac{v_D^2}{2RT}}\,e^{\frac{\mathbf{v}\cdot\mathbf{u}}{RT}}\,\phi(\mathbf{v})\,dv_D\ldots dv_1$$

$$= \frac{\rho}{(2\pi RT)^{D/2}} e^{-\frac{|\mathbf{u}|^2}{2RT}}\int_{\mathbb{R}} e^{-\frac{v_1^2}{2RT}}\ldots\int_{\mathbb{R}} e^{-\frac{v_D^2}{2RT}}\,\widetilde{\phi}(\mathbf{v})\,dv_D\ldots dv_1 \tag{2.12}$$

where $\widetilde{\phi}(\mathbf{v}) = \exp(\mathbf{v}\cdot(\mathbf{u}/(RT)))\,\phi(\mathbf{v})$. Each of the D integrals in (2.12) is suitable for Gauss-Hermite quadrature. Consider the innermost integral

$$\frac{\rho}{(2\pi RT)^{1/2}}\int_{\mathbb{R}} e^{-\frac{v_D^2}{2RT}}\,\widetilde{\phi}(\mathbf{v})\,dv_D. \tag{2.13}$$

We discretize the Dth dimension of the velocity space as $(v_D)_i = \sqrt{2RT}\xi_i$ where the ξ_i are the zeros of the degree 3 Hermite polynomials; $\xi_i \in \{-\frac{\sqrt{6}}{2}, 0, \frac{\sqrt{6}}{2}\}$. The associated weights are given by the 1-D $w_i \in \{\frac{1}{6}, \frac{2}{3}, \frac{1}{6}\}$ respectively.

Thus,

$$\frac{\rho}{(2\pi RT)^{1/2}}\int_{\mathbb{R}} e^{-\frac{v_D^2}{2RT}}\,\widetilde{\phi}(\mathbf{v})\,dv_D \approx \sum_{i=1}^{3} w_i\,\widetilde{\phi}(v_1,\ldots,v_{D-1},(v_D)_i)$$

where $(v_D)_i \in \{-\sqrt{3RT}, 0, \sqrt{3RT}\}$. The two innermost integrals are then approximated as

$$\frac{\rho}{(2\pi RT)}\int_{\mathbb{R}} e^{-\frac{v_{D-1}^2}{2RT}}\int_{\mathbb{R}} e^{-\frac{v_D^2}{2RT}}\,\widetilde{\phi}(\mathbf{v})\,dv_D\,dv_{D-1}$$

$$\approx \sum_{j=1}^{3} w_j \sum_{i=1}^{3} w_i\,\widetilde{\phi}(v_1,\ldots,v_{D-2},(v_{D-1})_j,(v_D)_i),$$

where,

$$(v_{D-1})_j = \sqrt{2RT}\xi_j$$

and

$$\xi_j \in \left\{-\frac{\sqrt{6}}{2}, 0\frac{\sqrt{6}}{2}\right\}.$$

Proceeding in this way, the integral (2.12) over $\mathbb{R}^D$ would be approximated as the sum of 3^D terms. Each term would involve a weight W_i which is the product of D one dimensional weights. The velocity space $\mathbb{R}^D$ would be discretized using 3^D vectors $\mathbf{v}_i$; the components of $\mathbf{v}_i$ take values in $\{-\sqrt{3RT}, 0, \sqrt{3RT}\}$.

For integrals over $\mathbb{R}^2$, this leads to the popular "D2Q9" (two dimensions, 9 velocities) scheme. shown in Figure 2.3. Λ is the square lattice in $\mathbb{R}^2$ and there are nine admissible velocities shown in Figure 2.3; the admissible velocities are shown at the central node. The velocities $\mathbf{v}_1, \mathbf{v}_2, \mathbf{v}_3$ and $\mathbf{v}_4$ all have the same magnitude and point towards the nearest neighbours of the central node. The velocities $\mathbf{v}_5, \mathbf{v}_6, \mathbf{v}_7$ and $\mathbf{v}_8$ also all have the same magnitude and point towards the next-nearest

neighbours. The ninth velocity $\mathbf{v}_9$ is $\mathbf{0}$.

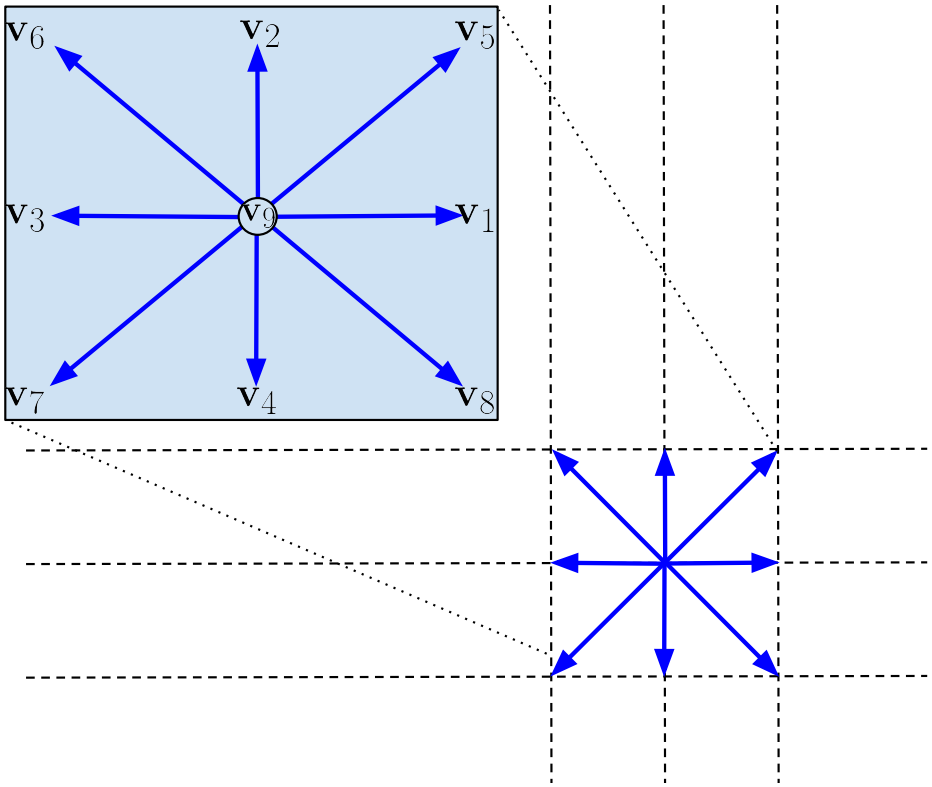

Figure 2.3: The D2Q9 Lattice and Velocity Scheme for $\delta t = 1$.

The components of the velocities and weights are given in Table 2.1.

Table 2.1: D2Q9 Velocity Scheme: $c = \sqrt{3RT}$

i	1	2	3	4	5	6	7	8	9
$\mathbf{v}_i$	(c,0)	(0,c)	(-c,0)	(0,-c)	(c,c)	(-c,c)	(-c,-c)	(c,-c)	(0,0)
W_i	$\frac{1}{9}$	$\frac{1}{9}$	$\frac{1}{9}$	$\frac{1}{9}$	$\frac{1}{36}$	$\frac{1}{36}$	$\frac{1}{36}$	$\frac{1}{36}$	$\frac{4}{9}$

Recalling that the goal was to approximate integrals (2.11) of the continuous equilibrium distribution (2.6), we have

$$\int_{\mathbb{R}^2} f^{\text{eq}}(\mathbf{x}, \mathbf{v}, t)\, \phi(\mathbf{v})\, d\mathbf{v} \approx \rho \sum_{i=1}^{9} W_i e^{\frac{2\mathbf{v}_i \cdot \mathbf{u} - |\mathbf{u}|^2}{2RT}} \phi(\mathbf{v}_i) = \sum_{i=1}^{9} f_i^{\text{eq}} \phi(\mathbf{v}_i) \tag{2.14}$$

where we've defined the discrete equilibrium distribution, $\mathbf{f}^{\text{eq}}$, via

$$f_i^{\text{eq}} := \rho\, W_i\, e^{\frac{2\mathbf{v}_i \cdot \mathbf{u} - |\mathbf{u}|^2}{2RT}}. \tag{2.15}$$

Note that, just like the continuous equilibrium distribution (2.6), the discrete equilibrium distribution $\mathbf{f}^{\text{eq}}$ is a function of $\mathbf{v}$ and depends on the macroscopic quantities $\rho(\mathbf{x}, t)$, $\mathbf{u}(\mathbf{x}, t)$, and $T(\mathbf{x}, t)$. However, in an athermal scheme, we are free to choose a fixed T and thus will choose it to simplify our velocity scheme.

Now, since our quadrature is a direct product of 2 Gauss-Hermite quadratures based on three

points, the bound on the error of each integration will involve the sixth derivative of,

$$\widetilde{\phi}(\mathbf{v}) = e^{(\mathbf{v}\cdot\mathbf{u}/(RT))}\,\phi(\mathbf{v})$$

with respect to $\mathbf{v}$. If we are only interested in expectation values of macroscopic quantities such as density and velocity (or temperature if using a thermal LBM) then the function $\phi(\mathbf{v})$ will be a polynomial of degree two or less. However, even though $\phi(\mathbf{v})$ is a low degree polynomial the $\exp((\mathbf{v}\cdot\mathbf{u})/(RT)$ term in $\widetilde{\phi}(\mathbf{v})$ causes $\widetilde{\phi}$ not to be a polynomial. This leads to errors in the integration. To address this problem one could add more points for the Gauss-Hermite quadrature. However, if one used more than three points to discretize each component of the velocity this would not yield a velocity discretization that led to a lattice in $\mathbf{x}$ [71] requiring additional effort such as those outlined in [72].

However, if one assumes a "low Mach number" approximation, $\frac{|\mathbf{u}|}{\sqrt{RT}} \ll 1$, for the the continuous equilibrium distribution (2.6) then,

$$f^{\text{eq}} \approx \frac{\rho}{(2\pi RT)^{D/2}} e^{-\frac{\mathbf{v}^2}{2RT}} \left\{ 1 - \frac{|\mathbf{u}|^2}{2RT} + \frac{\mathbf{v}\cdot\mathbf{u}}{RT} + \frac{(\mathbf{v}\cdot\mathbf{u})^2}{2(RT)^2} \right\} \tag{2.16}$$

This is the typical approach taken in most LBM simulations and in this case,

$$\widetilde{\phi}(\mathbf{v}) = \left\{ 1 - \frac{|\mathbf{u}|^2}{2RT} + \frac{\mathbf{v}\cdot\mathbf{u}}{RT} + \frac{(\mathbf{v}\cdot\mathbf{u})^2}{2(RT)^2} \right\} \phi(\mathbf{v})$$

which guarantees the integration is exact for $\phi(\mathbf{v})$ of degree 2 or less.

In the low mach number approximation the expression for the moments (2.14) would still hold but with a different discrete form of the equilibrium. Rather than using (2.15), one would use

$$f_i^{\text{eq}} := \rho\, W_i \left\{ 1 - \frac{|\mathbf{u}|^2}{2RT} + \frac{\mathbf{v}_i\cdot\mathbf{u}}{RT} + \frac{(\mathbf{v}_i\cdot\mathbf{u})^2}{2(RT)^2} \right\}. \tag{2.17}$$

The scheme in Table 2.1 was made to ensure the accuracy of integration involving the equilibrium distribution. For integrations involving a general distribution, $f(\mathbf{x},\mathbf{v},t)$, we manipulate the hydrodynamic integral into a form suitable for Gauss-Hermite quadrature and apply the discritization motivated above:

$$\begin{aligned}\int f(\mathbf{x},\mathbf{v},t)\phi(\mathbf{v})\,d\mathbf{v} &= \int \omega(\mathbf{v})\frac{f(\mathbf{x},\mathbf{v},t)}{\omega(\mathbf{v})}\phi(\mathbf{v})\,d\mathbf{v} \\ &\approx \sum_{i=1}^{9} W_i \frac{f(\mathbf{x},\mathbf{v}_i,t)}{\omega(\mathbf{v}_i)}\,\phi(\mathbf{v}_i)\end{aligned}$$

where

$$\omega(\mathbf{v}) = \frac{1}{(2\pi RT)^{D/2}}\, e^{-\frac{|\mathbf{v}|^2}{2RT}}. \tag{2.18}$$

Note that ω is the continuous Maxwell-Boltzmann distribution with unit mass and zero mean velocity.

As is typically done, we can define a discrete distribution $\mathbf{f}(\mathbf{x},t)$ from the continuous distribution $f(\mathbf{x},\mathbf{v},t)$ via

$$\mathbf{f}_i(\mathbf{x},t) = W_i \frac{f(\mathbf{x},\mathbf{v}_i,t)}{\omega(\mathbf{v}_i)} \qquad i \in \{1,2,\ldots,9\}. \tag{2.19}$$

With this notation, in two dimensions the moment based on the continuous distribution f is approx-

imated as:

$$\int f(\mathbf{x},\mathbf{v},t)\phi(\mathbf{v})\,d\mathbf{v} \approx \sum_{i=1}^{9} \mathbf{f}_i(\mathbf{x},t)\ \phi(\mathbf{v}_i) \tag{2.20}$$

If the continuous distribution $f(\mathbf{x},\mathbf{v},t)$ equals $\omega(\mathbf{v})$ — that is if f is the Maxwell-Boltzman distribution with unit mass and zero mean velocity — then the corresponding discrete distribution (2.19) is $\mathbf{W}$. That is, the weights we use in the Gauss-Hermite quadrature *are* the discrete distribution for $\omega(\mathbf{v})$ as given by (2.18).

It is again worth repeating that since the discretization was chosen to minimize integration error involving f^{eq}. This means that if a given distribution f is sufficiently far from f^{eq} the integration accuracy may be quite poor.

In D2Q9 the density, momentum and temperature, (2.1)-(2.3), are calculated form the discrete distribution $\mathbf{f}$ via,

$$\rho(\mathbf{x}_j,t_n) = \sum_{i=1}^{9} \mathbf{f}(\mathbf{x}_j,t_n) \tag{2.21}$$

$$\rho(\mathbf{x}_j,t_n)\,\mathbf{u}(\mathbf{x}_j,t_n) = \sum_{i=1}^{9} \mathbf{f}(\mathbf{x}_j,t_n)\mathbf{v}_i \tag{2.22}$$

2.1.7 Boundary Conditions

We call a node $\mathbf{x}_j \in \Lambda\cap\Omega$ an "internal node" if the neighbouring nodes involved in the streaming step are all in $\Lambda\cap\Omega$. At such nodes, the evolution of the distribution function follows the aforementioned procedure: a local collision step followed by streaming step that constructs $\mathbf{f}^{\text{pre}}$ from the components of $\mathbf{f}^{\text{post}}$ at neighbouring nodes. After the streaming step the internal node has a complete distribution with all components determined: see Figure 2.2b. We call a node $\mathbf{x}_j$ a "boundary node" if any neighbouring nodes required for the streaming step are not in $\mathbf{x}_j \in \Lambda\cap\Omega$. For such a node the streaming step results in some of the components of the distribution not being determined: see Figures 2.4b.

To rectify this situation, a number of methods have been devised to implement various types of boundary conditions. Boundary conditions are a very active area of research for the LBM see [73, 74, 75, 76, 77, 78] amongst others.

No-Slip Boundary Conditions: stationary boundary

No-slip boundary conditions are imposed to ensure that the macroscopic fluid velocity at the boundary equals the velocity of the boundary itself. If the boundary is stationary then the mean velocity of the fluid at the boundary should be $\mathbf{0}$. Due to their simplicity, the most popular methods to impose no-slip boundary conditions for a stationary boundary are the "bounce-back" schemes.

Let $\mathbf{x}_b$ be a boundary node. Because it is a boundary node, after the streaming step $\mathbf{f}^{\text{pre}}(\mathbf{x}_b,t+\delta_t)$ is "missing" some components. That is, $\mathbf{f}_i^{\text{pre}}(\mathbf{x}_b,t+\delta_t)$ is undefined because $\mathbf{x}_b-\mathbf{v}_i\delta_t \notin \Lambda\cap\Omega$ and so there is no $\mathbf{f}_i^{\text{post}}(\mathbf{x}_b-\mathbf{v}_i\delta_t)$. If the "opposite" node $\mathbf{x}_b+\mathbf{v}_i\delta_t$ is in $\Lambda\cap\Omega$ then the bounce-back scheme is to define $\mathbf{f}_i^{\text{pre}}(\mathbf{x}_b,t+\delta_t)$ to be $f_{\bar{i}}^{\text{pre}}(\mathbf{x}_b,t+\delta_t)$ where $\bar{i}$ is the index of the velocity vector that is opposite to the velocity indexed by i. That is, $\mathbf{v}_{\bar{i}} = -\mathbf{v}_i$.

The bounce-back schemes typically come in two classes, full-way bounce-back and half-way bounce-back. The implementation of these bounce-back rules varies, but a common implementation would be to provide auxiliary nodes (sometimes called "ghost nodes" or "solid nodes") that are not part of the fluid domain but allow for distributions to be streamed to and from them. In such auxiliary node implementations, full-way bounce-back can be implemented by treating the auxiliary

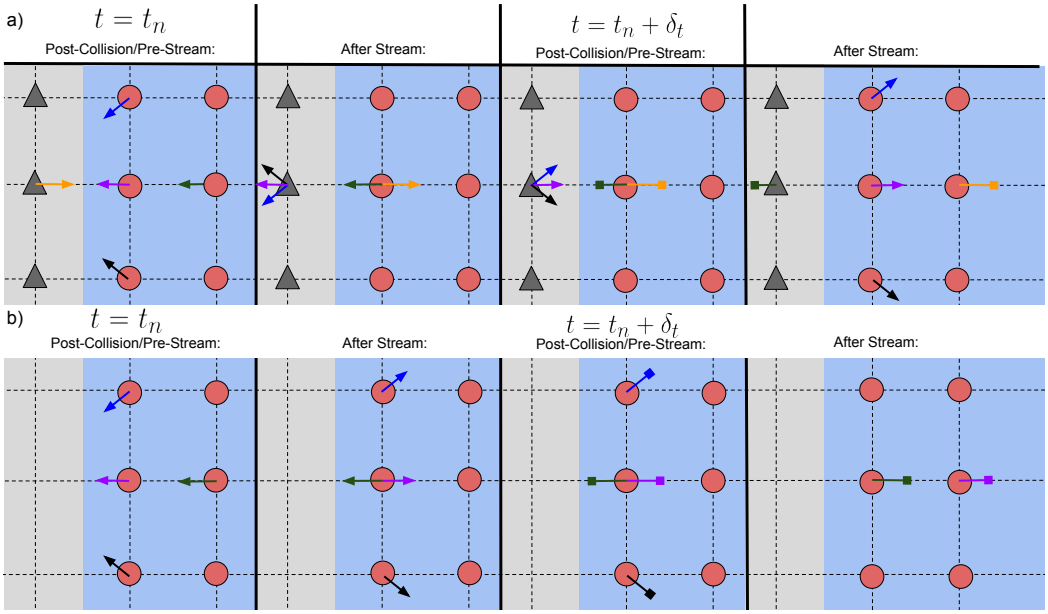

Figure 2.4: a) Full-way bounce-back and b) half-way bounce-back. From left to right: post-collision, after streaming, post-collision, after streaming. Circles represent fluid nodes while triangles denote "ghost nodes." Arrows with square heads indicate populations altered by the collision step.

nodes as fluid nodes, except that the usual collision step at the auxiliary nodes is replaced by an operation that switches the direction of all the components. That is, the only difference between an auxiliary node and a fluid node is the collision step. Alternatively, for the half-way bounce-back, the collision step at the auxiliary nodes is replaced by an operation that switches the direction of all components *and then immediately* streams the missing components back to the fluid node. No collision step is necessary at the auxiliary nodes. For both full-way bounce-back and half-way bounce-back, the actual physical location of the boundary is somewhere between the fluid node and its neighbouring auxiliary node. See Figure 2.4. It can be shown [79, 53] that the actual location of the physical boundary (and thus the accuracy of the method) is crucially linked to the values of the relaxation times.

No-Slip Boundary Conditions: moving boundary

In the case of a moving boundary, the no-slip boundary condition ensures that the mean velocity of the fluid at the boundary equals the velocity of the boundary. A simple way to implement a fixed velocity boundary is to place nodes on the boundary and to use a collision step that simply defines $\mathbf{f}^{\text{post}}$ to be the equilibrium that has the desired macroscopic quantities. We will use this method in this thesis. One should note however that even though simple and effective, setting the distribution to the equilibrium at the boundary may not be appropriate. One reason for this is because having the fluid at equilibrium may not reflect the actual physical conditions at the boundary (although the boundary will have the correct *macroscopic* density and momentum). Other implementations of boundary conditions are possible, see for example [78]. Since our study focuses on comparing the performance of different collision step implementations, the absolute accuracy of the boundary condition implementations is not our immediate concern. Of course, we do use the same boundary conditions for all of our simulations for the sake of consistency.

Now that a typical Lattice Boltzmann simulation procedure has been outlined, we turn our attention to our MinxEnt-LBM procedure, beginning by its foundations in information theory.

Chapter 3

Principle of Minimum Discrimination Information (MinxEnt)

Having given a rough description of the general LBM in §2, we now turn to our specific contribution: the MinxEnt collision step. It comes from an information theoretic approach which we now discuss.

One of the major appeals of the Lattice Boltzmann Method is that it is based on statistical mechanics rather than on tracking individual particles (as is done in other methods like Molecular Dynamics simulations) or solving partial differential equations. The LBM accomplishes this by tracking the evolution of mass expectation distributions with specific velocities and reconstructing macroscopic properties from them.

In Appendix A we show how the mass expectation distribution is directly related to probability distributions which describe probabilities of finding particles with certain properties. With this relationship in mind we take the approach that the fundamental quantity of interest should be these *probability* distributions conditioned at a specific point in space and time. That is, we wish to understand $p(\mathbf{x}, \mathbf{v}, t)$: the probability of finding a particle with velocity $\mathbf{v}$ given that we are at location $\mathbf{x}$ at time t. In Appendix A we show the relationship between f and p and (hence between their corresponding discrete distributions) are related by,

$$\mathbf{f}(\mathbf{x}_j, t) = \rho(\mathbf{x}_j, t)\, \mathbf{p}(\mathbf{x}_j, t). \tag{3.1}$$

In this way, determining the $\mathbf{f}$ required by the LBM is equivalent to determining $\mathbf{p}$.

The question then becomes: how should one collide a discrete probability distribution $\mathbf{p}^{\text{pre}}$ to arrive at $\mathbf{p}^{\text{post}}$? We propose a new way of defining a collision operator to use in the LBM: by appealing to the Principle of Maximum Entropy (MaxEnt) as described by Jaynes in his seminal paper from 1957 [80].

In [80], Jaynes makes a connection between research done by Information Theory pioneer Shannon in his 1948 book [81] and the field of statistical mechanics championed almost 75 years earlier by Boltzmann and others. To make the connection between Information Theory and statistical mechanics, Jaynes argues that,

> previously one constructed a theory based on equations of motion and supplemented by additional hypothesis of ergodicity, metric transitivity or equal a priori probability, and the identification of entropy was made only at the end, by comparison of the resulting

> equations with the laws of phenomenological thermodynamics. Now however, we can take entropy as our starting concept and the fact that a probability distribution maximizes the entropy subject to certain constraints becomes the central fact which justifies the use of that distribution for inference.

Jaynes goes on to point out that, at the time, the objectivists' view of probability was that it was an objective property of the system and that, in principle, it was verifiable in every detail. From this perspective the goal of the observer was to simply figure out the probability distribution which Nature follows. On the other hand, the subjectivist point of view of probability was that it was not an emergent property of a system, rather it was a measure of the ignorance of the observer. That, in some way, probabilities gave us the tool to measure how uncertain we are of the outcome of a process. It is from this viewpoint that Jaynes makes the connection to Shannon's work in information theory.

Shannon wished to quantify the minimum amount of data one would need to transmit in order to send a message. He asked "how uncertain of the message would you be if you only received a certain amount of data?" To answer this, Shannon needed to quantify the amount of uncertainty in a received alphabet character. For example, if one receieves an english 'q', the was a high probability that the next letter will be an english 'u'. In this way, receieving an english 'q' contained more "information" than did receIving an english 't'. In other words Shannon was looking for a way to quantify what our intuition told us; we are more "certain" of the outcome of a process if the corresponding probability distribution is sharply peaked and less certain of the outcome if the corresponding probability distribution was broadly spread.

Suppose we have a probability distribution of n discrete possible outcomes of an event, $p_1, p_2, ..., p_n$. Shannon sought a function H such that,

1. The function should be non-negative: $H(p_1, p_2, ..., p_n) \geq 0$
2. The function $H(p_1, p_2, ..., p_n)$ should be lower for probability distributions associated with greater certainty in the outcome, and higher for probability distributions corresponding to more uncertain outcomes. In particular H should be maximized when all outcomes are equally likely: $p_i = p_j, \forall i \neq j$ (that is, the state of maximum uncertainty).
3. The function should be additive for independent sources of uncertainty. That is, suppose p_B is the probability of an independent event B also occurring. Then this requirement insists that,

$$H(p_1, p_2, ..., p_n, P_B) = H(p_1, p_2, ..., p_n) + H(p_B)$$

4. The function should be continuous and symmetric in all p_i

Shannon found the function,

$$H(p_1, p_2, ..., p_n) = -K \sum_{i=1}^{n} p_i \ln p_i \tag{3.2}$$

satisfied all four criteria. Here K is an arbitrary constant. He called it the Information Entropy due to its similarities to thermodynamic entropy. It is now usually called the "Shannon Entropy;" the quantum version is usually called the "von Neumann Entropy". It was proven by Khinchin in 1957 [82] that (3.2) was in fact the only function that satisfied the four desired properties.

Jaynes showed the connection between Shannon Entropy and thermodynamic entropy and, more importantly, proved that statistical mechanics is a result of maximizing the Shannon Entropy subject to physical constraints. This was in direct contrast to the current view at the time which was that

entropy was an outcome of statistical mechanics, not the foundation on which it stood. Jaynes' approach put statistical mechanics on firmer axiomatic ground. In his concluding paragraph Jaynes wrote,

> The essential point in the arguments presented above is that we accept the von-Neumann-Shannon expression for entropy, very literally, as a measure of the amount of uncertainty represented by a probability distribution; thus entropy becomes the primitive concept with which we work, more fundamental even than energy. If in addition we reinterpret the prediction problem of statistical mechanics in the subjective sense, we can derive the usual relations in a very elementary way without any consideration of ensembles or appeal to the usual arguments concerning ergodicity or equal a priori probabilities. The principles and mathematical methods of statistical mechanics are seen to be of much more general applicability than conventional arguments would lead one to suppose. In the problem of prediction, the maximization of entropy is not an application of a law of physics, but merely a method of reasoning which ensures that no unconscious arbitrary assumptions have been introduced. [80]

It is this argument that we take to be the foundation of our work on the Lattice Boltzmann Method.

The LBM tracks discrete distributions $\mathbf{f}$, and thus equivalently $\mathbf{p}$. However, we must remember that the quantity we are most interested in is the continuous probability distribution function, p. This is the first problem with using the Shannon Entropy in applying the Principle of Maximum Entropy; Shannon Entropy is for discrete probability distributions, and we are trying to track the evolution of a discrete samples of a continuous probability distribution.

Another issue with using the Principle of Maximum Entropy is that the Shannon Entropy was designed to be maximized by a uniform distribution. That is, the Shannon Entropy has built in the assumption that we are at our most ignorant when all outcomes are equally likely. However, it is not always the case that the uniform probability distribution represents maximum uncertainty. For example, if a mispainted die had no face with 3 dots and two faces with 6 dots then the probability distribution that maximizes our ignorance is $p_1 = 1/6$, $p_2 = 1/6$, $p_3 = 0$, $p_4 = 1/6$, $p_5 = 1/6$, $p_6 = 1/3$.

Thus we need a functional that generalizes the Shannon Entropy for situations where 1) the functional acts on continuous probability distributions and 2) the functional can be minimized by a specified nonuniform probability distribution. The functional that does this is the Kullback-Leibler Divergence (KLD) [83, 84],

$$H_{\mathrm{KL}}[p|q] = \iint_{\mathbb{R}^D} p(\mathbf{v}) \ln\left(\frac{p(\mathbf{v})}{q(\mathbf{v})}\right) d\mathbf{v},$$

where q is some predetermined probability distribution for which our uncertainty is maximum. Note that the Kullback-Leibler Divergence, H_{KL}, does not have a negative sign while the Shannon Entropy, H, does. And so the maximization problem for H becomes a minimization problem for H_{KL}. It is important to note that although q may be the distribution that maximizes our uncertainty, it might not (and typically does not) satisfy all of the physical constraints. If q did indeed satisfy all of the physical constraints, then we would simply take $p = q$ to be our chosen probability distribution. Instead, our task is to choose a continuous probability distribution, p, that minimizes the KLD out of the candidates for p that satisfy the physical constraints. This procedure is called the Principle of Minimum Discrimination Information (or Minimum Cross Entropy), MinxEnt. MaxEnt aims to

maximize the function that quantifies our uncertainty while MinxEnt aims to minimize our "distance" from the distribution that maximizes the function that quantifies our uncertainty.

Note that if q is the probability distribution

$$q(\mathbf{v}) = \sum_{i=1}^{n} \frac{1}{n} \delta_{\mathbf{v}_i}(\mathbf{v}) \qquad \mathbf{v}_i \in \{\mathbf{v}_1, \mathbf{v}_2, \dots \mathbf{v}_n\}$$

then H_{KL} is, up to a constant, the negative of the Shannon Entropy H. And so a discrete probability distribution $\mathbf{p}$ that maximizes $H(\mathbf{p})$ will translate directly a continuous probability distribution p that minimizes $H_{\mathrm{KL}}[p|q]$.

Collisions in a physical multi-particle system alter the probability distribution in a tremendously complex way. If the collision step is to assign a probability distribution that represents the changes due to these collisons we *must* choose it in a way that obeys all of the physical knowledge of our system (constraints) but without unconsciously including any other hidden assumptions or bias. Thus we must select the unique probability distribution that agrees with our constraints but maximizes our uncertainty otherwise. If we were to choose *any other* distribution we would be (unwittingly) incorporating assumptions that we have no right to assume. This is the key philisophical basis to our work; it is precisely Jaynes' Principle of Maximum Entropy. Of course, given that our probability distribution is continuous, not discrete, we use MinxEnt. This has the added advantage that it allows for a non-uniform uncertainty maximizer which is crucial for our application

Chapter 4

MinxEnt Lattice Boltzmann Method (MinxEnt-LBM)

As discussed in the introduction, the two common interpretations of the Lattice Boltzmann Method is that of a generalization of the Lattice Gas Automata or as a particular discretization of the Boltzmann Equation. In this section we will describe our new interpretation of the Lattice Boltzmann Method which is a split time scheme where the collision step is a constrained application of the Principle of Minimum Discrimination Information (MinxEnt). We will conclude the chapter with a demonstration that the other LBM variations discussed in this thesis emerge as specific approximations of MinxEnt-LBM.

4.1 The MinxEnt-LBM Collision Step

The main premise of the MinxEnt-LBM is to apply the Principle of Minimum Discrimination Information as the local collision step within the usual LBM framework (see §2.1). That is, in MinxEnt-LBM the only modification to standard LBM methods will be to choose the post-collision probability distribution, $\mathbf{p}^{\text{post}}$, as the probability distribution that minimizes the Kullback-Leibler Divergence subject to constraints. The mass expectation disribution $\mathbf{f}^{\text{post}}$ will then be constructed via $\mathbf{p}^{\text{post}}$ via (3.1). In this section, we will show the general MinxEnt-LBM procedure, followed by the procedure for the specific case of an isotropic Newtonian fluid.

Recall the continuous Kullback-Leibler Divergence:

$$H_{KL}[p|q] = \int_{\mathbb{R}^D} p(\mathbf{v}) \ln\left(\frac{p(\mathbf{v})}{q(\mathbf{v})}\right) d\mathbf{v}. \tag{4.1}$$

In practice, both of the continuous probability distributions p and q are functions of $\mathbf{x}$ and t as well as $\mathbf{v}$. However, we have suppressed the space and time dependence here and in what follows with the understanding that this procedure is carried out at every position, and at each time step independently.

Let $\{C_1, C_2, ..., C_K\}$ be a set of K constraint functionals,

$$C_k : \mathcal{P} \to \mathbb{R} \qquad k = 1, ..., K$$

where $\mathcal{P}$ is the space of all probability distributions on $\mathbb{R}^D$. Let $\{c_1, c_2, ...c_K\}$ be the set of K constraint values. Generally speaking the constraint values $c_1, ...c_K$ will usually depend on the pre-collision probability distribution p^{pre} and also the equilibrium distribution function, p^{eq}. For

example, if momentum is conserved then the D functionals would be, $C_i(p) = \int \mathbf{v}_i\, p(\mathbf{v})\, d\mathbf{v}$ and the D constraints would be $c_i = \mathbf{u}_i$. That is,

$$C_i(p) = c_i \Leftrightarrow \int \mathbf{v}_i\, p(\mathbf{v})\, d\mathbf{v} = \mathbf{u}_i \Leftrightarrow \int \mathbf{v}_i\, f(\mathbf{v})\, d\mathbf{v} = \rho \mathbf{u}_i,$$

where $i \in 1, .., D$.

Armed with H_{KL} and a set of constraints, the MinxEnt-LBM collision step is,

$$\begin{aligned} \text{MinxEnt Collision Step:} \qquad & p^{\text{post}} = \underset{p \in \gamma}{\operatorname{argmin}} \quad H_{KL}[p|q] \\ & \gamma = \left\{ p \mid p \in \mathcal{P} \text{ for all } \mathbf{v} \in \mathbb{R}^D, C_1(p) = c_1, ..., C_K(p) = c_K \right\} \end{aligned} \tag{4.2}$$

4.1.1 Changing to Mass Expectation Distributions

The LBM involves streaming and colliding mass expectation distributions, while MinxEnt involves probability distributions. Before fully specifying the MinxEnt-LBM collision step we will convert the MinxEnt procedure into mass expectation distribution.

From Appendix A, we have that (A.3),

$$p(\mathbf{x}, \mathbf{v}, t) = \frac{f(\mathbf{x}, \mathbf{v}, t)}{\rho(\mathbf{x}, t)}.$$

Thus, the MinxEnt collision step, (4.2) becomes:

$$\begin{aligned} \text{MinxEnt Collision Step:} \qquad & f^{\text{post}} = \underset{f \in \gamma}{\operatorname{argmin}} \quad H_{KL}[f|\rho q] \\ & \gamma = \left\{ f \mid f(\mathbf{v}) > 0 \text{ for all } \mathbf{v} \in \mathbb{R}^D, C_1(f/\rho) = c_1, ..., C_K(f/\rho) = c_K. \right\} \end{aligned} \tag{4.3}$$

For convenience, hereafter we will refer to H_{KL} and related quantities as the "entropy" when discussing the MinxEnt-LBM. The related quantities we will encounter are:

1. the discretized version of $H_{KL}[f|\rho q]$ called $\mathcal{H}_{\mathbf{q}}(\mathbf{f})$
2. A version of $\mathcal{H}_{\mathbf{q}}(\mathbf{f})$ where $\mathbf{q}$ has been explicitly chosen to be the discretized Maxwell-Boltzmann, called $\mathcal{H}(\mathbf{f})$
3. A transformed "moment space" version of $\mathcal{H}_{\mathbf{q}}(\mathbf{f})$ called $\mathcal{S}_{\mathbf{q}}(\mathbf{M})$
4. The analogously transformed version of $\mathcal{H}(\mathbf{f})$ called $\mathcal{S}(\mathbf{M})$

It should be made explicitly clear that we are using "entropy" in the information theory sense, not the thermodynamic sense. For this reason we can define our entropy whether or not we have a well defined temperature in our system.

4.1.2 Discretization Scheme

Using D dimensional, 3 point, Gauss-Hermite quadrature (see §2.1.6) once more we can discretize the entropy,

$$\begin{aligned} H_{KL}[f|\rho q] &= \frac{1}{\rho}\int_{\mathbb{R}^D} f(\mathbf{v}) \ln\left(\frac{f(\mathbf{v})}{\rho q(\mathbf{v})}\right) d\mathbf{v} \\ &\approx \frac{1}{\rho}\sum_{i=1}^{3^D} f_i \ln\left(\frac{f_i}{\rho q_i}\right), \\ &:= \mathcal{H}_{\mathbf{q}}[\mathbf{f}] \end{aligned} \tag{4.4}$$

where $f(\mathbf{v})$ and $\mathbf{f}$ are related via (2.19), as are $q(\mathbf{v})$ and $\mathbf{q}$.

This leads us to the general MinxEnt-LBM collision step,

$$\begin{aligned} \text{MinxEnt-LBM Collision Step:} \qquad \mathbf{f}^{\text{post}} &= \underset{\mathbf{f}\in\gamma}{\operatorname{argmin}} \quad \mathcal{H}_{\mathbf{q}}[\mathbf{f}] \\ \gamma &= \left\{\mathbf{f} \mid \mathbf{f} > \mathbf{0},\ \widetilde{C_1}(\mathbf{f}/\rho) = c_1, ..., \widetilde{C_K}(\mathbf{f}/\rho) = c_K\right\} \end{aligned} \tag{4.5}$$

where the $\widetilde{C}_k$ are the discretized versions of the constraint functionals, C_K. For example if $C_1(p) = \int p(\mathbf{v})\, d\mathbf{v}$, then $\widetilde{C}_1(\mathbf{p}) = \sum_i \mathbf{p}_i$.

Two further problem specific steps are needed. They are, the choice of $q(\mathbf{v})$ and the minimization method.

Regarding the choice of $q(\mathbf{v})$, it will typically differ depending on the system under study, however it must at least meet the requirement,

$$\int_{\mathbb{R}^D} q(\mathbf{v})\, d\mathbf{v} = 1.$$

Addressing the issue of minimization method, we will describe two possible methods here but in principle one could apply any method for constrained optimization. Of course some methods may be more suitable than others for a given problem.

4.1.3 Minimization Method: Newton-Raphson

The first method we consider is Newton-Raphson Minimization. We first convert the constrained minimization problem into an unconstrained one.

Though in principle the MinxEnt-LBM does not explicitly require any specific form on the constraints (except that they are self-consistent), we will limit our discussion here to constraints that are linear in p_i. This may require making linear approximations of nonlinear constraints. In such a case, we can write the discretized constraint functionals as,

$$\widetilde{C}_k(\mathbf{p}) = \sum_{j=1}^{3^D} \mathcal{T}_{kj}\mathbf{p}_j = c_k \qquad k = 1, ..., K$$

and equivalently,

$$\widetilde{C}_k(\mathbf{f}) = \sum_{j=1}^{3^D} \mathcal{T}_{kj}\mathbf{f}_j = \rho c_k \qquad k = 1, ..., K$$

for some $\mathcal{T}_{kj}$ and where $K < 3^D$ (since otherwise we have more constraints than free variables).

Since our constraints are linear in $\mathbf{f}$ we will find it useful to move from distribution space into

"moment space." This will enable us to implement the constraints in a much more straightforward manner during the minimization.

To move into moment space, consider an invertible 3^D by 3^D matrix, $\mathbf{T}$, and define the vector of moments, $\mathbf{M}$,

$$\mathbf{M} := \mathbf{T}\mathbf{f} \tag{4.6}$$

We select $\mathbf{T}$ such that $T_{kj} = \mathcal{T}_{kj}$ for $k \leq K, 1 \leq j \leq 3^D$. In principle the choices for the remaining $K - k$ rows of $\mathbf{T}$ are arbitrary, provided that $\mathbf{T}$ remains invertible and well conditioned. By construction the first K moments are constrained:

$$\begin{aligned} M_1 =& (\mathbf{T}\mathbf{f})_1 = \rho c_1, \\ M_2 =& (\mathbf{T}\mathbf{f})_2 = \rho c_2, \\ &\vdots \\ M_K =& (\mathbf{T}\mathbf{f})_K = \rho c_K, \end{aligned}$$

We define the vector of unconstrained moments by

$$\mathbf{m} = \langle M_{K+1}, M_{K+2}, ..., M_{3^D} \rangle \in \mathbb{R}^{3^D - K}.$$

With this notation, the *full* vector of moments (including constraints) is written,

$$\mathbf{M} = \langle \rho c_1, \ldots, \rho c_K, \mathbf{m} \rangle.$$

Using the definition of $\mathbf{T}$ in (4.6), we now seek the vector $\mathbf{m}$ that minimizes the discretized entropy (4.4) in moment space:

$$\begin{aligned} \mathcal{H}_{\mathbf{q}}[\mathbf{T}^{-1}\mathbf{M}] =& \sum_{i=1}^{3^D} (\mathbf{T}^{-1}\mathbf{M})_i \ln\left((\mathbf{T}^{-1}\mathbf{M})_i \frac{\omega(\mathbf{v}_i)}{\rho\, q_i} \right) \\ :=& \mathcal{S}_{\mathbf{q}}(\mathbf{M}). \end{aligned} \tag{4.7}$$

With the first K components of $\mathbf{M}$ fixed by the K constraints, the constrained minimization problem has become an unconstrained minimization over $3^D - K$ dimensions. The Newton-Raphson minimization procedure involves the gradient of $\mathcal{S}_{\mathbf{q}}$ with respect to $\mathbf{m}$:

$$\begin{aligned} \nabla_k \mathcal{S}(\mathbf{m}) =& \frac{\partial \mathcal{S}_q}{\partial m_k}(\mathbf{M}) \\ =& \sum_{i=1}^{3^D} (\mathbf{T}^{-1})_{ik} \left[\ln\left((\mathbf{T}^{-1}\mathbf{M})_i \frac{\omega(\mathbf{v}_i)}{\rho\, \mathbf{q}_i} \right) + 1 \right] \quad k \in \{K+1, \ldots, 3^D\}. \end{aligned} \tag{4.8}$$

The minmization problem involves finding $\mathbf{m}$ so that $\nabla \mathcal{S}(\mathbf{m}) = \mathbf{0}$.

The Hessian is

$$\begin{aligned} \mathbf{H}_{jk}(\mathbf{m}) =& \frac{\partial^2 \mathcal{S}_q}{\partial m_j \partial m_k}(\mathbf{M}) \\ =& \sum_{i=1}^{3^D} \frac{(T^{-1})_{ik}(T^{-1})_{ij}}{(\mathbf{T}^{-1}\mathbf{M})_i} \quad j, k \in \{K+1, \ldots, 3^D\}. \end{aligned} \tag{4.9}$$

The $n+1$st step of the Newton-Raphson method is

$$\mathbf{m}^{n+1} = \mathbf{m}^n - \mathbf{H}(\mathbf{m}^n)^{-1}\,\nabla\mathcal{S}(\mathbf{m}^n). \tag{4.10}$$

For the initial moments, $\mathbf{m}^0$ we compute the moments of the discretized equilibrium distribution,

$$\mathbf{M}^0 = \mathbf{T}\mathbf{f}^{\mathrm{eq}}.$$

and then take,

$$\mathbf{m}^0 = \langle \mathbf{M}^0_{K+1}, \mathbf{M}^0_{K+1}, ..., \mathbf{M}^0_{3^D} \rangle.$$

Continuing the Newton-Raphson until some convergence criteria is met, and labeling the final distribution $\mathbf{m}^{n_{\mathrm{end}}}$ we construct,

$$\mathbf{M}^{\mathrm{post}} := \langle \rho c_1, \rho c_2, ..., \rho c_K, \mathbf{m}^{n_{\mathrm{end}}} \rangle.$$

and subsequently define the post-collision probability distribution,

$$\mathbf{f}^{\mathrm{post}} = \mathbf{T}^{-1}\mathbf{M}^{\mathrm{post}}$$

This procedure can be summarized by the following algorithm,

1. Calculate pre-collision moments $\mathbf{M}^0 = \mathbf{T}\mathbf{f}^{\mathrm{eq}}$ and constraints $\rho c_1, \rho c_2, ..., \rho c_K$ and calculate $\mathbf{m}^0$.
   (a) Calculate the gradient vector $\nabla\mathcal{S}(\mathbf{m}^n)$ (4.8) and Hessian $\mathbf{H}(\mathbf{m}^n)$ (4.9)
   (b) Perform a Newton-Raphson step, (4.10), for the unconstrained moments, creating $\mathbf{m}^{n+1}$. Construct $\mathbf{M}^{n+1}$.
   (c) Repeat steps (a)-(b) until convergence criteria is met
2. Define the full post-collision moment vector, $\mathbf{M}^{\mathrm{post}} = \mathbf{M}^{\mathrm{end}}$
3. Return to distribution space $\mathbf{f}^{\mathrm{post}} = \mathbf{T}^{-1}\mathbf{M}^{\mathrm{post}}$

Most of the computational overhead of this method involves calculating the Hessian.

4.1.4 Minimization Method: "Iterative Interpolation"

An alternative to the Newton-Raphson is a method we call "Iterative Interpolation" though to our knowledge it has no explicit name. See Figure 4.1. We make no claims about the theoretical properties of the procedure (such as convergence rate, optimal choices of parameters, etc). This is merely a formal description of a possible minimization procedure.

Assume that $q(\mathbf{v})$ is suitably chosen to ensure that the discretized entropy (4.4) is strictly convex in $\mathbf{f}$. Since $\mathcal{H}_{\mathbf{q}}$ is a strictly convex function we know that given $\mathbf{f}$ and $\mathbf{f}'$, and for any $\beta \in (0,1)$,

$$\mathcal{H}_{\mathbf{q}}((1-\beta)\mathbf{f} + \beta\mathbf{f}') < (1-\beta)\mathcal{H}_{\mathbf{q}}(\mathbf{f}) + \beta\mathcal{H}_{\mathbf{q}}(\mathbf{f}'). \tag{4.11}$$

In particular, given a $\mathbf{f}_0$, if we can find a $\mathbf{f}_*$ such that,

$$\mathcal{H}_{\mathbf{q}}(\mathbf{f}_0) = \mathcal{H}_{\mathbf{q}}(\mathbf{f}_*) \quad \forall\beta \in (0,1), \tag{4.12}$$

then (4.11) becomes,

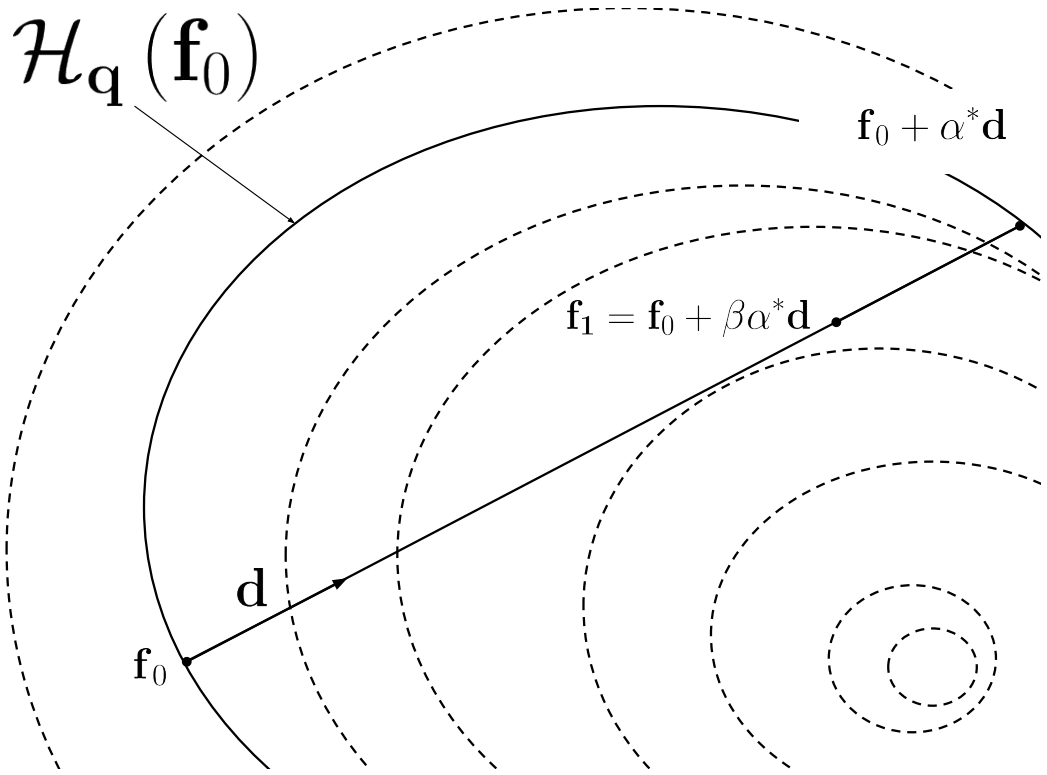

Figure 4.1: The first step in the "Iterative Interpolation" minimization procedure. Contours of the strictly convex function $\mathcal{H}_{\mathbf{q}}$ are shown as curved lines. The solid line is the contour of $\mathcal{H}_{\mathbf{q}}(\mathbf{f}_0)$. $\mathbf{d}$ is a direction vector and α^* is determined by solving $\mathcal{H}_{\mathbf{q}}(\mathbf{f}_0) = \mathcal{H}_{\mathbf{q}}(\mathbf{f}_0 + \alpha^* \mathbf{d})$. $\beta \in (0, 1)$ is a parameter related to the physical constraints. Diagram based on the similar one shown in [28].

$$\mathcal{H}_{\mathbf{q}}((1-\beta)\mathbf{f}_0 + \beta\mathbf{f}_*) < \mathcal{H}_{\mathbf{q}}(\mathbf{f}_0).$$

Setting

$$\mathbf{f}_1 = (1-\beta)\mathbf{f}_0 + \beta\mathbf{f}_*, \tag{4.13}$$

for any $\beta \in (0, 1)$, we are assured that,

$$\mathcal{H}_{\mathbf{q}}(\mathbf{f}_1) < \mathcal{H}_{\mathbf{q}}(\mathbf{f}_0).$$

The choice for $\mathbf{f}_*$ must,

1. Satisfy the entropy constraint, (4.12)
2. When used in (4.13), produces an $\mathbf{f}_1$ that satisfies the physical constraints for some well chosen $\beta \in (0, 1)$.

To address the first of these two conditions we assume the ansatz that $\mathbf{f}_*$ is a linear extension from $\mathbf{f}_0$, in some direction $\mathbf{d} \in \mathbb{R}^{3^D}$,

$$\mathbf{f}_* = \mathbf{f}_0 + \alpha\mathbf{d}, \qquad \alpha \in \mathbb{R}. \tag{4.14}$$

We then calculate α by imposing the entropy constraint (4.12),

$$\mathcal{H}_{\mathbf{q}}(\mathbf{f}_0) = \mathcal{H}_{\mathbf{q}}(\mathbf{f}_0 + \alpha\mathbf{d}), \tag{4.15}$$

and solve for a non-zero value for α (if it exists). Assuming such an α exists we denote this solution α_*.

With condition 1 satisfied, we now attempt to satisfy condition 2 by using our $\mathbf{f}_*$ in (4.13) to obtain,

$$\mathbf{f}_1 = \mathbf{f}_0 + \beta\alpha_*\mathbf{d}.$$

To satisfy our physical constraints we now choose β so that,

$$C_k(\mathbf{f}_1) = C_k(\mathbf{f}_0 + \beta\alpha_*\mathbf{d}) = \rho c_k, \quad k = 1, ..., K. \tag{4.16}$$

In principle, this is likely impossible for all but a few special sets f constraints. However, in athermal fluid simulations which only require a single parameter (the viscosity) this is possible. Since our goal is merely to illustrate that this is the procedure carried out by the Entropic LBM, we will not comment about the feasibility or practicality of this minimization procedure further.

Regarding the choice for $\mathbf{d}$, in principle any direction vector $\mathbf{d}$ is acceptable. However, considering that $\mathbf{d}$ is involved in solving both (4.15) and (4.16), a clever choice for $\mathbf{d}$ is necessary. One simple choice will be given in §4.2.3.

Using $\mathbf{f}^0$ we have constructed $\mathbf{f}_1$ so that $\mathbf{f}_1$ satisfies the constraints and has lower entropy than $\mathbf{f}_0$. One could proceed iteratively, constructing $\mathbf{f}_2$ and so on:

1. Choose $q(\mathbf{v})$ to ensure $\mathcal{H}_{\mathbf{q}}$ is strictly convex in $\mathbf{f}$.
2. Choose starting distribution $\mathbf{f}_0$
3. For $n \geq 0$
   (a) Choose the direction vector $\mathbf{d}$
   (b) Obtain α_*^n by solving for α from the entropy equation (4.15)
   $$\mathcal{H}_{\mathbf{q}}(\mathbf{f}_n) = \mathcal{H}_{\mathbf{q}}(\mathbf{f}_n + \alpha^n\mathbf{d})$$
   (c) Obtain β^n by solving the physical constraint equations
   $$C_k(\mathbf{f}_n + \beta^n\alpha_*^n\mathbf{d}) = \rho c_k, \quad k = 1, ..., K.$$
   (d) Set $\mathbf{f}_{n+1} = \mathbf{f}_n + \beta^n\alpha_*^n\mathbf{d}$
   (e) Set $n = n + 1$ and repeat steps a)-d) until some convergence criteria is met
   (f) Choose $\mathbf{f}^{\text{post}}$ as the result of steps a)-e)

In the context of Minxent-LBM, this procedure would be carried out at each lattice node, at each time step. Even with a clever choice of $\mathbf{d}$, each time this algorithm is used, there is a non-linear equation solve to obtain α_*. This can be computationally very expensive.

4.2 Unification of LBM Methods

In this section we will describe how MRT-LBM and ELBM can be thought of as specific (albeit different) approximations of MinxEnt-LBM. We will see that using the Newton-Raphson minimization procedure (§4.1.3), with some additional approximations, one arrives at MRT-LBM. If one alternatively uses the interative interpolation minimization procedure (§4.1.4) to carry our MinxEnt-LBM, one arrives at ELBM. Finally we will discuss how EF-LBM is also an approximation to MinxEnt-LBM and comment on the recent entropic method (called KBC for Karlin, Bosch and Chikatamarla) suggested in [85, 86].

In §4.1.3 we assumed that the constraint functionals, C_k were linear. We now make an assumption about the constraint values c_k. Specifically, we assume that c_k is determined from the pre-collision and equilibrium distributions by, $\rho c_k = C_k(\mathbf{f}^{\text{pre}}) + B_k\left[C_k(\mathbf{f}^{\text{eq}}) - C_k(\mathbf{f}^{\text{pre}})\right]$ for all $k = 1, ..., K$. The constraints then become,

$$C_k(\mathbf{f}^{\text{post}}) = C_k(\mathbf{f}^{\text{pre}}) + B_k\left[C_k(\mathbf{f}^{\text{eq}}) - C_k(\mathbf{f}^{\text{pre}})\right]. \quad k = 1, ..., K \tag{4.17}$$

It should be noted that if the constraint functional corresponds to a conserved quantity, such as mass or momentum, then one takes $B_k = 0$. We will show later, the case when $B_k \neq 0$ will play a role in determining the physics of the system.

Crucially we point out that the assumption in equation (4.17) is only used to derive MRT-LBM and ELBM. Specifically, MinxEnt-LBM itself does *not* require such a simple relation between the constraint value c_k, $\mathbf{f}^{\text{eq}}$ and $\mathbf{f}^{\text{pre}}$. It is simply an approximation used to derive MRT-LBM and ELBM.

4.2.1 MRT-LBM as an Approximation of MinxEnt-LBM

Recall the MinxEnt-LBM collision step and consider carrying out the minimization with the Newton-Raphson Method in "moment space" (§4.1.3). Recall that the post collision distribution was given by,

$$\mathbf{f}^{\text{post}} = \mathbf{T}^{-1}\mathbf{M}^{\text{post}},$$

where,

$$\mathbf{M}^{\text{post}} = \langle \rho c_1, \rho c_2, ..., \rho c_K, \mathbf{m}^{n_{\text{end}}} \rangle$$

and, $\mathbf{m}^{\text{end}}$ is the vector after n_{end} Newton-Raphson iterations.

Suppose we terminate after a single iteration: $n_{\text{end}} = 1$. Then,

$$\mathbf{m}^{n_{\text{end}}} = \mathbf{m}^0 - \mathbf{H}^{-1}(\mathbf{m}^0)\,\nabla\mathcal{S}(\mathbf{m}^0). \tag{4.18}$$

Further assume that the off-diagonal entries of the Hessian are small and thus we assume that the Hessian can be approximated,

$$\mathbf{H_{jk}}(\mathbf{m^0}) \approx \frac{\partial^{\mathbf{2}}\mathcal{S}_{\mathbf{q}}}{\partial \mathbf{m_k^2}}(\mathbf{m^0})\,\delta_{\mathbf{jk}}.$$

Recall that from §4.1.3 that $\mathbf{m}^0$ is taken to be the 3^{D-K} unconstrained moments of the equilibrium distribution:

$$\mathbf{m}^0 = \langle M^0_{K+1}, ..., M^0_{3D} \rangle = \mathbf{m}^{\text{eq}} := \mathbf{T}\mathbf{f}^{\text{eq}}.$$

and define,

$$\delta^k = \mathbf{m}_k^{\text{pre}} - \mathbf{m}_k^{\text{eq}},$$

where

$$\mathbf{m}_k^{\text{pre}} := \mathbf{T}\mathbf{f}^{\text{pre}}.$$

A fundamental assumption of MRT-LBM is that δ_k is small for all k and so we can use central differences to approximate the Hessian. Making use of the standard basis vectors, $\mathbf{e}_k$,

$$\mathbf{H}_{jk}(\mathbf{m}^0) = \mathbf{H}_{jk}(\mathbf{m}^{\text{eq}}) \approx \frac{\mathcal{S}_{\mathbf{q}}(\mathbf{m}^{\text{eq}} + \delta^k\mathbf{e}_k) - 2\mathcal{S}_{\mathbf{q}}(\mathbf{m}^{\text{eq}}) + \mathcal{S}_{\mathbf{q}}(\mathbf{m}^{\text{eq}} - \delta^k\mathbf{e}_k)}{(\delta^k)^2}\delta_{jk}.$$

Because the Hessian is diagonal, the inverse is approximately,

$$\mathbf{H}_{jk}^{-1}(\mathbf{m}^0) \approx \frac{(\delta^k)^2}{\mathcal{S}_{\mathbf{q}}(\mathbf{m}^{\text{eq}} + \delta^k\mathbf{e}_k) - 2\mathcal{S}_{\mathbf{q}}(\mathbf{m}^{\text{eq}}) + \mathcal{S}_{\mathbf{q}}(\mathbf{m}^{\text{eq}} - \delta^k\mathbf{e}_k)}\delta_{jk}.$$

Likewise, the gradient can be approximated by finite differences, with the kth component approximated by,

$$\nabla_k(\mathbf{m}^0) \approx \frac{\mathcal{S}_{\mathbf{q}}(\mathbf{m}^{\text{pre}}) - \mathcal{S}_{\mathbf{q}}(\mathbf{m}^{\text{eq}})}{\delta^k}.$$

These approximations allow us to approximate our Netwon-Raphson minimization (4.18) with the kth component of $\mathbf{m}^{\text{end}}$ given by,

$$\begin{aligned} m_k^{n_{\text{end}}} &\approx \mathbf{m}^0 - \frac{\mathcal{S}_{\mathbf{q}}(\mathbf{m}^{\text{pre}}) - \mathcal{S}_{\mathbf{q}}(\mathbf{m}^{\text{eq}})}{\mathcal{S}_{\mathbf{q}}(\mathbf{m}^{\text{eq}} + \delta^k\mathbf{e}_k) - 2\mathcal{S}_{\mathbf{q}}(\mathbf{m}^{\text{eq}}) + \mathcal{S}_{\mathbf{q}}(\mathbf{m}^{\text{eq}} - \delta^k\mathbf{e}_k)}\delta^k\delta_{jk}. \\ &= \mathbf{m}^{\text{pre}} + \hat{\mathbf{B}}\left(\mathbf{m}_k^{\text{eq}} - \mathbf{m}_k^{\text{pre}}\right) \end{aligned}$$

where the diagonal matrix $\hat{\mathbf{B}}$ is defined via,

$$\hat{B}_{jk} = \left(\frac{\mathcal{S}_{\mathbf{q}}(\mathbf{m}^{\text{pre}}) - \mathcal{S}_{\mathbf{q}}(\mathbf{m}^{\text{eq}})}{\mathcal{S}_{\mathbf{q}}(\mathbf{m}^{\text{eq}} + \delta^k\mathbf{e}_k) - 2\mathcal{S}_{\mathbf{q}}(\mathbf{m}^{\text{eq}}) + \mathcal{S}_{\mathbf{q}}(\mathbf{m}^{\text{eq}} - \delta^k\mathbf{e}_k)} - 1\right)\delta_{jk}. \tag{4.19}$$

Note that in general the entries for $\hat{\mathbf{B}}$ will depend on space and time, $\hat{B}_{jk} = \hat{B}_{jk}(\mathbf{x}, t)$. However, we will assume $\hat{B}_{jk}$ are constants,

$$\hat{B}_{jk}(\mathbf{x}_j, t_n) \approx \hat{b}_k := \hat{b}_{jk}\delta_{jk} \qquad \forall\, \mathbf{x}_j, t_n.$$

Recalling the assumed form of the constraints, (4.17),

$$\rho c_k = \mathbf{m}_k^{\text{pre}} + B_k(\mathbf{m}^{\text{eq}} - \mathbf{m}^{\text{pre}})_k, \quad k = 1, ..., K,$$

we can combine the constrained and unconstrained moments into one equation,

$$\mathbf{M}^{\text{post}} \approx \mathbf{M}^{\text{pre}} + \mathbf{B}(\mathbf{M}^{\text{eq}} - \mathbf{M}^{\text{pre}}),$$

with,

$$\mathbf{B} = diag(\langle B_1, B_2, ..., B_K, \hat{b}_1, \hat{b}_2, ..., \hat{b}_{3^D-K}\rangle),$$

where $B_1, B_2, ..., B_K$ are user chosen and $\hat{b}_1, ..., \hat{b}_{3^D-K}$ are determined from (4.19). Hence the post collision distribution function can be approximated as,

$$\mathbf{f}^{\text{post}} \approx \mathbf{f}^{\text{pre}} + \mathbf{T}^{-1}\mathbf{B}\mathbf{T}(\mathbf{f}^{\text{eq}} - \mathbf{f}^{\text{pre}}). \tag{4.20}$$

This is precisely the same form of the collision rule for the MRT-LBM with the important difference in how the entries in $\mathbf{B}$ are chosen. This will be discussed later.

Arriving at this expression from MinxEnt-LBM required a number of assumptions and approximations,

1. The Newton-Raphson procedure was terminated after only 1 step
2. Off diagonal entries of the Hessian are small relative to the diagonal
3. The pre-collision distribution is close to the equilibrium distribution
4. The space and time varying values $\hat{B}_{jk}$ can be approximated by constants $\hat{b}_k$
5. The constraints of the system could be written,

$$\rho c_k = \mathbf{m}_k^{\text{pre}} + B_k(\mathbf{m}^{\text{eq}} - \mathbf{m}^{\text{pre}})_k, \quad k = 1, ..., K$$

   for some choice of constants B_k.

It is worth stressing once more that these approximations an assumptions are *not* required for MinxEnt-LBM. They are approximations made that allow one to derive MRT-LBM from MinxEnt-LBM.

An important question becomes how accurate these assumptions are and what impact their associated errors have on simulation using MRT-LBM. In regards to approximation 5, errors in this approximation will decrease the accuracy of results, since the actual physical constraints of the system may not be implemented faithfully.

To address the first 4 approximations one should recall that this procedure was only used to obtain the post-collision values for the unconstrained moments. The actual physical constraints of the system were hard wired into the constrained moments. Thus, up to the errors involved in approximation 5, the accuracy of the system should not be adversely effected. However, approximations 1-4 will lead to an approximation of the correct result of the Newton-Raphson procedure and thus lead to errors in the minimization. In fact, if the approximations are poor, there are no guarantees that collision step will reduce the entropy and may in fact *increase* it leading to what we call an "entropy violation". Since we are operating under the assumption that increases in entropy lead to instabilities, errors in approximations 1-4 may lead to instabilities in simulation where these approximations have significant errors. One should note that a one-step Newton-Raphson minimization outlined above does not prohibit entropy violations, but does recipe to further reduce them (additional iterations, for example.

It is useful to pause here and comment on the differences between the collision steps for MinxEnt-LBM, MRT-LBM, TRT-LBM and SRT-LBM. The fully realized MinxEnt-LBM collision step assigns the post-collision distribution to be the distribution that minimizes the entropy subject to constraints. Should such a distribution exist, this eliminates entropy violations. As outlined above, one method to compute such a distribution would be to use a single step Newton-Raphson procedure with some approximations (such as the ones noted above). This will likely degrade the accuracy of the minimization and increase the likelihood for entropy violations. Working under the hypothesis that entropy violations can lead to an increase in instabilities, these approximations will lead to increased

numerical instability. However, the benefit of making these approximations is that the collision step can be written in a convenient form, (4.20). This form is identical to the MRT-LBM collision step with the important difference being how the entries of $\mathbf{B}$ are chosen. Specifically, rather than being an approximation to a minimization scheme, in MRT-LBM the matrix $\mathbf{B}$ is entirely user chosen *a priori*. This is typically well defined for the entries in $\mathbf{B}$ that correspond to the constrained moments. However, in MRT-LBM, the choice for the entries of $\mathbf{B}$ corresponding to the unconstrained moments are typically chosen somewhat ad hoc, or found by tuning. Because of their ad hoc nature, these choices for the entries of $\mathbf{B}$ increase the likelihood of entropy violation and instabilities. Moreover, since the collision rules for TRT-LBM and SRT-LBM are specific cases of MRT-LBM, the entries of $\mathbf{B}$ are even more restrictive, further increasing the chance of entropy violations and instabilities.

In this way, one can interpret MRT-LBM (and in turn, TRT-LBM and SRT-LBM) as an approximation of a single step Newton-Raphson implementation of MinxEnt-LBM, *without* determining the entries of $\mathbf{B}$ via entropic principles.

4.2.2 SRT-LBM With Ehrenfest Steps as an Approximation of MinxEnt-LBM

The idea of the SRT-LBM With Ehrenfest Steps collision step is to place a limit on the change to the change in the distribution during the collision step if an entropy violation is suspected during the typical collision step. Provided the entropy difference between the equilibrium to the pre-collision distribution is below a certain threshold, the usual SRT-LBM collision step, (1.6), can be taken. If, however, the entropy difference is too large, this is an indication that the pre-collision distribution may be too far from the equilibrium distribution and the usual SRT-LBM step may generate a large entropy violation. In this case, the SRT-LBM step is modified be less drastic, in the hopes this will limit the violation.

The SRT-LBM with Ehrenfest Steps can be summarized as,

$$\mathbf{f}^{\text{post}} = \begin{cases} \mathbf{f}^{\text{pre}} + \frac{1}{\tau}(\mathbf{f}^{\text{eq}} - \mathbf{f}^{\text{pre}}) & \text{if } \Delta S < \text{tolerance} \\ \mathbf{f}^{\text{pre}} + \frac{1}{2\tau}(\mathbf{f}^{\text{eq}} - \mathbf{f}^{\text{pre}}) & \text{if otherwise.} \end{cases},$$

with ΔS given by (2.9).

In the context of MinxEnt-LBM this entropy limiting is to limit the potential entropy violations that the standard SRT-LBM collision step may create. The logic is that if the pre-collision distribution is too far from the equilibrium then the inaccuracies in entropy minimization due to the standard SRT-LBM collision step are reduced by making smaller changes to the distribution during the collision step.

4.2.3 ELBM as an Implementation of MinxEnt-LBM

Rather than use the Newton-Raphson to perform the minimization we could instead elect to use the "Iterative Interpolation" method instead, §4.1.4.

Let the starting distribution of this minimization be $\mathbf{f}_0 = \mathbf{f}^{\text{pre}}$. We then choose a direction vector $\mathbf{d}$ (called the "bare" collision integral, and denoted $\mathbf{\Delta}$ in the literature). Accounting for the form of the constraints (4.17), we choose a $\mathbf{d}$ such that,

$$C_k(\mathbf{d}) = C_k(\mathbf{f}^{\text{eq}}) - C_k(\mathbf{f}^{\text{pre}}). \tag{4.21}$$

For example, considering the linearity of the C_k one can see that an explicit choice of $\mathbf{d}$ could be,

$$\mathbf{d} = \mathbf{f}^{\text{eq}} - \mathbf{f}^{\text{pre}}$$

Having selected $\mathbf{d}$ we then solve the entropy equation,

$$\mathcal{H}_q(\mathbf{f}^{\text{pre}}) = \mathcal{H}_q(\mathbf{f}^{\text{pre}} + \alpha\mathbf{d}).$$

for α and denote the solution α_*.

Setting $\beta = \frac{B_k}{\alpha_*}$ and terminating the procedure after a single step our post-collision distribution is given by,

$$\mathbf{f}^{\text{post}} = \mathbf{f}^{\text{pre}} + \beta\alpha_*\mathbf{d}.$$

This is the typical ELBM procedure. Note that there is only one value for β despite theoretically a number of different B_k values. This apparent inconsistency is not encountered in the literature because ELBM is usually only used in situations with 3 physical constraints $\mathbf{d}$ must satisfy; conservation of mass, conservation of momentum, and the viscosity constraint (discussed in Appendix B). For the conservation constraints, we have that

$$C_k(\mathbf{f}^{\text{eq}}) = C_k(\mathbf{f}^{\text{pre}}),$$

and so these constraints are satisfied trivially from (4.21). This leaves only one other constraint to be satisfied, so that only a single value for β is required.

Arriving at the ELBM from MinxEnt-LBM requires a number of assumptions and approximations,

1. The Iterative Interpolation procedure was terminated after only 1 step
2. The constraints of the system could be written,

$$C_k(\mathbf{f}^{\text{post}}) = C_k(\mathbf{f}^{\text{pre}}) + B_k\left[C_k(\mathbf{f}^{\text{eqm}}) - C_k(\mathbf{f}^{\text{pre}})\right], \quad k = 1, ..., K$$

3. The constraints are such that $\mathbf{d}$ can be found with only a single value of β is required

4.2.4 Conclusion

We conclude this section by noting that starting with the MinxEnt-LBM, other LBM collision steps can be derived. Since these other collision steps involve a number of approximations in their derivation, we would expect the ability to accurately minimize the entropy of these LBMs is greatly reduced. We therefore expect these other methods will experience more severe instabilities than MinxEnt-LBM during simulations. Since the MinxEnt-LBM does not require many of the assumptions and approximations of MRT-LBM (and its special cases) and ELBM.

While beyond the scope of this work, we would also like to comment on the recent work done by Karlin, Bosch and Chikatamarla [85, 86], called KBC-LBM. In these works the authors show that stability improvements can be made by using a entropic multiple relaxation collision step. After careful thought one can interpret the KBC-LBM as another approximation to MinxEnt-LBM. Using a D2Q9 grid, KBC-LBM also seeks to minimize entropy, (4.29) in moment space but they limit the number of free moments that are optimized over to one. This allows them to obtain a closed form approximation for the effective relaxation time of the unconstrained moment. Like MinxEnt-LBM, this effective relaxation time is allowed to vary in space and time. However, unlike MinxEnt-LBM,

all available unconstrained moments are not available for the minimization problem in KBC-LBM. In this way, KBC-LBM is another approximation to MinxEnt-LBM.

MinxEnt-LBM opens doors to explore applications that MRT-LBM and ELBM may not be suitable for. We will, however, find it useful to formulate the MinxEnt-LBM for a specific physical system that MRT-LBM and ELBM have been used extensively for; a 2-D athermal, isotropic, Newtonian fluid. This will allow us to compare and contrast the methods and verify our expectations of the superior performance of MinxEnt-LBM.

4.3 MinxEnt-LBM For An Athermal 2-D Isotropic Newtonian Fluids

With the general MinxEnt-LBM collision step specified, we now discuss its application to the case of an athermal 2 dimensional, isotropic, Newtonian fluid.

4.3.1 Choice of $q(\mathbf{v})$

Consider an infintesimal volume around the point $\mathbf{x}$ and suppose we isolate it (no mass, momentum or energy flow in or out). We now let time go to infinity. The initial probability distribution in the volume would evolve into a state that has decoupled every correlation with the original distribution except for probability (or mass), momentum and energy will have remained the same. This "completely uncorrelated" state should be our choice for $q(\mathbf{v})$ distribution because it contains no other information about the original distribution except the original mass, momentum and energy. This state is usually called the "equilibrium state" (the state as $t \to \infty$). In classical mechanics (such as for fluids and gasses) this distribution is given by the Maxwell-Boltzmann Distribution. Since the system we are considering is a fluid composed of classical particles our choice for $q(\mathbf{v})$ is

$$q(\mathbf{v}) = \frac{1}{(2\pi RT)^{D/2}}\, e^{-\frac{|\mathbf{v}-\mathbf{u}|^2}{2RT}} \tag{4.22}$$

where $\mathbf{u}$ is determined from the pre-collision distribution and T is free to specify due to the athermal nature of our system.

4.3.2 Choice of Constraints

Because we are considering an athermal, isotropic, Netwonian fluid our system satisfies the following constraints:

1. Conservation of mass

$$\int f^{\text{post}}(\mathbf{x},\mathbf{v},t)\,d\mathbf{v} = \int f^{\text{pre}}(\mathbf{x},\mathbf{v},t)\,d\mathbf{v} = \rho(\mathbf{x},t) \tag{4.23}$$

2. Conservation of momentum

$$\int f^{\text{post}}(\mathbf{x},\mathbf{v},t)v_x\,d\mathbf{v} = \int f^{\text{pre}}(\mathbf{x},\mathbf{v},t)v_x\,d\mathbf{v} = \rho(\mathbf{x},t)u_x, \tag{4.24}$$

$$\int f^{\text{post}}(\mathbf{x},\mathbf{v},t)v_y\,d\mathbf{v} = \int f^{\text{pre}}(\mathbf{x},\mathbf{v},t)v_y\,d\mathbf{v} = \rho(\mathbf{x},t)u_y. \tag{4.25}$$

3. Isotropic/Newtonian fluid

In addition to our conservation laws, we assume that our system is an isotropic Newtonian fluid. As such we want to ensure the local stress tensor takes the form,

$$\sigma_{jk}(\mathbf{x},t) = \pi(\mathbf{x},t)\delta_{jk} - 2\mu\varepsilon_{jk}(\mathbf{x},t), \tag{4.26}$$

where π is the hydrostatic pressure, μ is the shear viscosity and ε_{ij} is the strain rate tensor,

$$\varepsilon_{jk} = \frac{1}{2}\left[\frac{\partial u_j}{\partial x_k} + \frac{\partial u_k}{\partial x_j}\right]. \tag{4.27}$$

In terms of the probability distribution function the stress tensor is given by,

$$\sigma_{jk}(\mathbf{x},t) = \int f^{\text{post}}(\mathbf{x},\mathbf{v},t)(\mathbf{v}-\mathbf{u})_j(\mathbf{v}-\mathbf{u})_k \, d\mathbf{v},$$

and thus an additional constraint for this particular system is,

$$\int f^{\text{post}}(\mathbf{x},\mathbf{v},t)(\mathbf{v}-\mathbf{u})_j(\mathbf{v}-\mathbf{u})_k \, d\mathbf{v} = \pi(\mathbf{x},t)\delta_{jk} - 2\mu\varepsilon_{jk}(\mathbf{x},t). \tag{4.28}$$

In Appendix B we show that the standard MRT-LBM relationship between relaxation times and μ arises naturally from the viscosity constraint (4.28) *without* needing to match to the Navier-Stokes equation. This illustrates another benefit of the MinxEnt-LBM scheme; only constraint expressions need to be known, not the governing equations. In principle, this allows MinxEnt-LBM to be extended to systems where the governing equations are unknown.

4.3.3 Discretization in D2Q9

Following the LBM recipe, we need to discretize our space. Since we are considering a 2-D fluid, we choose the popular D2Q9 discretization scheme (§2.1.6).

With this discretization we can show that the frequently used ([34, 32, 87, 50, 49, 37, 51] for example) D2Q9 discretized form of the entropy used in LBM simulations,

$$H(\mathbf{f}) = \sum_i \mathbf{f}_i \ln\left(\frac{\mathbf{f}_i}{W_i}\right) \tag{4.29}$$

To our knowledge the particular derivation here is a new result although an alternative derivation based on Boltzmann's H function and tensor Hermite polynomials is given in [87].

The pre-collision continuous mass expectation distribution f^{pre} determines pre-collision macroscopic properties and thus a Maxwell-Boltzmann distribution (4.22). The entropy conditioned on this distribution is

$$\begin{aligned}
H_{KL}\left[\frac{f}{\rho}|q\right] &= \frac{1}{\rho}\int_{\mathbb{R}^2} f(\mathbf{v}) \ln\left(\frac{f(\mathbf{v})}{\frac{\rho}{(2\pi RT)^{D/2}} e^{-\frac{|\mathbf{v}-\mathbf{u}|^2}{2RT}}}\right) d\mathbf{v} \\
&= \frac{1}{\rho}\int_{\mathbb{R}^D} f(\mathbf{v}) \ln\left(\frac{f(\mathbf{v})}{\frac{\rho}{(2\pi RT)^{D/2}} e^{-\frac{|\mathbf{v}|^2}{2RT}}}\right) d\mathbf{v} - \frac{|\mathbf{u}|^2}{2RT} \\
&= \frac{1}{\rho}\int_{\mathbb{R}^D} f(\mathbf{v}) \ln\left(\frac{f(\mathbf{v})}{\omega(\mathbf{v})}\right) d\mathbf{v} - \frac{|\mathbf{u}|^2}{2RT}
\end{aligned}$$

where ω is given in (2.18).

Since our goal is to find a mass expectation distribution f that minimizes H_{KL}, and this minimization is unaffected by the constant $|\mathbf{u}|^2/(2RT)$ then hereafter this constant is dropped.

We now discretize the minimization problem by discretizing the functional H_{KL} and seeking a discrete mass expectation distribution $\mathbf{f}$. The entropy is discretized using Gauss-Hermite quadrature (2.20),

$$\begin{aligned}\int_{\mathbb{R}^2} f(\mathbf{v}) \ln\left(\frac{f(\mathbf{v})}{\omega(\mathbf{v})}\right) d\mathbf{v} &\approx \sum_{i=1}^{9} \mathbf{f}_i \ln\left(\frac{\mathbf{f}_i}{W_i}\right) \\ &:= \mathcal{H}(\mathbf{f}) \end{aligned} \tag{4.30}$$

where $\mathbf{f}$ and f are related via (2.19) and (3.1): $\mathbf{f}_i = W_i\, f(\mathbf{v}_i)/\omega(\mathbf{v}_i)$, and W_i are related to the weights of the quadrature are given in Table 2.1.

Discretizing the constraints (4.23), (4.24), (4.25) and (4.28) we obtain the discrete constraints,

$$\sum_{i=1}^{9} \mathbf{f}_i^{\text{post}} = \sum_{i=1}^{9} \mathbf{f}_i^{\text{pre}} = \rho \tag{4.31}$$

$$\sum_{i=1}^{9} \mathbf{f}_i^{\text{post}} \mathbf{v}_{x,i} = \sum_{i=1}^{9} \mathbf{f}_i^{\text{pre}} \mathbf{v}_{x,i} = \rho \mathbf{u}_x \tag{4.32}$$

$$\sum_{i=1}^{9} \mathbf{f}_i^{\text{post}} \mathbf{v}_{y,i} = \sum_{i=1}^{9} \mathbf{f}_i^{\text{pre}} \mathbf{v}_{y,i} = \rho \mathbf{u}_y \tag{4.33}$$

$$\sum_{i=1}^{9} \mathbf{f}_i^{\text{post}} \left(\mathbf{v}_{x,i}^2 - \mathbf{v}_{y,i}^2\right) = \sum_{i=1}^{9} \left[\mathbf{f}_i^{\text{pre}} + \frac{1}{\tau}(\mathbf{f}_i^{\text{eq}} - \mathbf{f}_i^{\text{pre}})\right] \left(\mathbf{v}_{x,i}^2 - \mathbf{v}_{y,i}^2\right) = \rho c_8, \tag{4.34}$$

$$\sum_{i=1}^{9} \mathbf{f}_i^{\text{post}} \mathbf{v}_{x,i} \mathbf{v}_{y,i} = \sum_{i=1}^{9} \left[\mathbf{f}_i^{\text{pre}} + \frac{1}{\tau}(\mathbf{f}_i^{\text{eq}} - \mathbf{f}_i^{\text{pre}})\right] (\mathbf{v}_{x,i} \mathbf{v}_{y,i}) = \rho c_9, \tag{4.35}$$

respectively. Constraints (4.34) and (4.35) are derived in Appendix B which is also where we find the relationship between τ and the viscosity ν,

$$\nu = \frac{2\tau - 1}{6} \frac{\delta_x^2}{\delta_t}, \tag{4.36}$$

and pressure and density,

$$\pi = \frac{\rho}{3}. \tag{4.37}$$

Additional constraints can be added to deal with the inaccuracies at the boundary [79, 53],

$$\sum_{i=1}^{9} \mathbf{f}_i^{\text{post}} \left[-5 + 3\left(\mathbf{v}_{x,i}^2 + \mathbf{v}_{y,i}^2\right)\right] \mathbf{v}_{x,i}$$

$$= \sum_{i=1}^{9} \left[\mathbf{f}_i^{\text{pre}} + \frac{1}{\tau_2}(\mathbf{f}_i^{\text{eq}} - \mathbf{f}_i^{\text{pre}})\right] \left[-5 + 3\left(\mathbf{v}_{x,i}^2 + \mathbf{v}_{y,i}^2\right)\right] \mathbf{v}_{x,i} = \rho c_5, \tag{4.38}$$

$$\sum_{i=1}^{9} \mathbf{f}_i^{\text{post}} \left[-5 + 3\left(\mathbf{v}_{x,i}^2 + \mathbf{v}_{y,i}^2\right)\right] \mathbf{v}_{y,i}$$

$$= \sum_{i=1}^{9} \left[\mathbf{f}_i^{\text{pre}} + \frac{1}{\tau_2}(\mathbf{f}_i^{\text{eq}} - \mathbf{f}_i^{\text{pre}})\right] \left[-5 + 3\left(\mathbf{v}_{x,i}^2 + \mathbf{v}_{y,i}^2\right)\right] \mathbf{v}_{y,i} = \rho c_7, \tag{4.39}$$

$$\tag{4.40}$$

where,

$$\tau_2 = \frac{8\tau - 1}{2\tau - 1}.$$

This is in the same spirit as TRT-LBM [56, 69, 88]. These constraints are purely numerical to increase numerical accuracy of the simulation.

To summarize, in the D2Q9 scheme, the MinxEnt-LBM collision for an athermal 2D isotropic Newtonian fluid becomes the constrained optimization problem:

$$\mathbf{f}^{\text{post}} = \underset{\mathbf{f}}{\text{argmin}} \quad \sum_{i=1}^{9} \mathbf{f}_i \ln\left(\frac{\mathbf{f}_i}{W_i}\right)$$

subject either to the constraints (4.31)-(4.35), or to the constraints (4.31)-(4.39).

We call the versions of MinxEnt-LBM with the 5 constraints (4.31)-(4.35) "MinxEnt4." Likewise the name given to the version of MinxEnt-LBM with the 7 constraints (4.31)-(4.39) is "MinxEnt2." The numbers in the names of these sister versions reflect the dimension of parameters that are free to be minimized over.

4.3.4 Choice of Minimization Procedure; MinxEnt-LBM Using Newton-Raphson in Moment Space

Having chosen $q(\mathbf{v})$ and performed the discretization, we now must choose a minimization scheme. In this thesis we will choose the Newton-Raphson minimization. As outlined in §4.1.3, before proceeding with the Newton-Raphson procedure we first move into moment space using invertible matrix, $\mathbf{M} = \mathbf{Tf}$, (4.6) and write the constraints in terms of moments. Given the form of (4.31)-(4.39) it is convenient to define the rows of $\mathbf{T}$ via,

$$\mathbf{M}_1 = (\mathbf{Tf})_1 := \sum_{i=1}^{9} \mathbf{f}_i, \tag{4.41}$$

$$\mathbf{M}_4 = (\mathbf{Tf})_4 := \sum_{i=1}^{9} \mathbf{f}_i \mathbf{v}_{x,i}, \tag{4.42}$$

$$\mathbf{M}_5 = (\mathbf{Tf})_5 := \sum_{i=1}^{9} \mathbf{f}_i \left[-5 + 3\left(\mathbf{v}_{x,i}^2 + \mathbf{v}_{y,i}^2\right)\right] \mathbf{v}_{x,i}, \tag{4.43}$$

$$\mathbf{M}_6 = (\mathbf{Tf})_6 := \sum_{i=1}^{9} \mathbf{f}_i \mathbf{v}_{y,i}, \tag{4.44}$$

$$\mathbf{M}_7 = (\mathbf{Tf})_7 := \sum_{i=1}^{9} \mathbf{f}_i \left[-5 + 3\left(\mathbf{v}_{x,i}^2 + \mathbf{v}_{y,i}^2\right)\right] \mathbf{v}_{y,i}, \tag{4.45}$$

$$\mathbf{M}_8 = (\mathbf{Tf})_8 := \sum_{i=1}^{9} \mathbf{f}_i \left(\mathbf{v}_{x,i}^2 - \mathbf{v}_{y,i}^2\right), \tag{4.46}$$

$$\mathbf{M}_9 = (\mathbf{Tf})_9 := \sum_{i=1}^{9} \mathbf{f}_i \mathbf{v}_{x,i} \mathbf{v}_{y,i} \tag{4.47}$$

(The ordering of these moments is taken to be consistent with the literature). Choosing $\mathbf{T}$ with these properties renders constraints (4.31)-(4.39) into a simpler form,

$$\mathbf{M}_1^{\text{post}} = \mathbf{M}_1^{\text{pre}} = \rho, \tag{4.48}$$

$$\mathbf{M}_4^{\text{post}} = \mathbf{M}_4^{\text{pre}} = \rho \mathbf{u}_x, \tag{4.49}$$

$$\mathbf{M}_5^{\text{post}} = \mathbf{M}_5^{\text{pre}} + \frac{1}{\tau_2}(\mathbf{M}_5^{\text{eq}} - \mathbf{M}_5^{\text{pre}}), \tag{4.50}$$

$$\mathbf{M}_6^{\text{post}} = \mathbf{M}_6^{\text{pre}} = \rho \mathbf{u}_y, \tag{4.51}$$

$$\mathbf{M}_7^{\text{post}} = \mathbf{M}_7^{\text{pre}} + \frac{1}{\tau_2}(\mathbf{M}_7^{\text{eq}} - \mathbf{M}_7^{\text{pre}}), \tag{4.52}$$

$$\mathbf{M}_8^{\text{post}} = \mathbf{M}_8^{\text{pre}} + \frac{1}{\tau}(\mathbf{M}_8^{\text{eq}} - \mathbf{M}_8^{\text{pre}}), \tag{4.53}$$

$$\mathbf{M}_9^{\text{post}} = \mathbf{M}_9^{\text{pre}} + \frac{1}{\tau}(\mathbf{M}_9^{\text{eq}} - \mathbf{M}_9^{\text{pre}}). \tag{4.54}$$

The remaining rows of $\mathbf{T}$ remain to be chosen. In principle they are arbitrary provided $\mathbf{T}$ is invertible however we will use [43],

$$\mathbf{T} = \begin{bmatrix} 1 & 1 & 1 & 1 & 1 & 1 & 1 & 1 & 1 \\ -4 & -1 & -1 & -1 & -1 & 2 & 2 & 2 & 2 \\ 4 & -2 & -2 & -2 & -2 & 1 & 1 & 1 & 1 \\ 0 & 1 & 0 & -1 & 0 & 1 & -1 & -1 & 1 \\ 0 & -2 & 0 & 2 & 0 & 1 & -1 & -1 & 1 \\ 0 & 0 & 1 & 0 & -1 & 1 & 1 & -1 & -1 \\ 0 & 0 & -2 & 0 & 2 & 1 & 1 & -1 & -1 \\ 0 & 1 & -1 & 1 & -1 & 0 & 0 & 0 & 0 \\ 0 & 0 & 0 & 0 & 0 & 1 & -1 & 1 & -1 \end{bmatrix}, \tag{4.55}$$

which satisfies our requirements (4.41)-(4.47) and is a popular choice in the literature.

Continuing as in §4.1.3 we define the vector of unconstrained moments by

$$\mathbf{m} = \begin{cases} \langle m_1, m_2, m_3, m_4 \rangle & \text{MinxEnt4,} \\ \langle m_1, m_2 \rangle & \text{MinxEnt2.} \end{cases}$$

With this notation, the *full* vector of moments (including constraints) is written,

$$\mathbf{M} = \begin{cases} \langle \rho, m_1, m_2, \rho u_x, m_3, \rho u_y, m_4, \rho c_8, \rho c_9 \rangle & \text{MinxEnt4,} \\ \langle \rho, m_1, m_2, \rho u_x, \rho c_5, \rho u_y, \rho c_7, \rho c_8, \rho c_9 \rangle & \text{MinxEnt2.} \end{cases}$$

We now seek the vector $\mathbf{m}$ that minimizes the discretized entropy, (4.30), rewritten in moment space:

$$\mathcal{S}(\mathbf{M}) = \sum_{i=1}^{9} (\mathbf{T}^{-1}\mathbf{M})_i \, \ln\left(\frac{(\mathbf{T}^{-1}\mathbf{M})_i}{W_i}\right). \tag{4.56}$$

Depending on the version of MinxEnt-LBM either five or seven components of $\mathbf{M}$ are fixed by the constraints, and so the constrained minimization problem involves the gradient of $\mathcal{S}$ with respect to the four or two unconstrained moments respectively,

$$\begin{aligned} \nabla_k(\mathbf{m}) &= \frac{\partial \mathcal{S}}{\partial m_k}(\mathbf{M}) \\ &= \sum_{i=1}^{9} (\mathbf{T}^{-1})_{ik} \left[\ln\left(\frac{(\mathbf{T}^{-1}\mathbf{M})_i}{W_i}\right) + 1\right] \quad k \in \{1, ..., 4\} \text{ or } \{1, 2\}. \end{aligned}$$

The Hessian is

$$\begin{aligned} \mathbf{H}_{jk}(\mathbf{m}) &= \frac{\partial^2 \mathcal{S}}{\partial m_j \partial m_k}(\mathbf{M}) \\ &= \sum_{i=1}^{9} \frac{(\mathbf{T}^{-1})_{ik}(\mathbf{T}^{-1})_{ij}}{(\mathbf{T}^{-1}\mathbf{M})_i} \quad j, k \in \{1, ..., 4\} \text{ or } \{1, 2\}. \end{aligned}$$

Following the method in §4.1.3 we then perform the Newton-Raphson procedure,

$$\mathbf{m}^{n+1} = \mathbf{m}^0 - \mathbf{H}^{-1}(\mathbf{m}^n)\, \nabla \mathcal{S}(\mathbf{m}^n)$$

For the initial moments in the Newton-Raphson procedure, $\mathbf{m}^0$ we compute the moments of the discretized equilibrium distribution,

$$\mathbf{M}^0 = \mathbf{T}\mathbf{f}^{\text{eq}}.$$

and then take,

$$\mathbf{m}^0 = \langle M_2^0, M_3^0, M_5^0, M_7^0 \rangle.$$

$$\mathbf{m}^0 = \begin{cases} \langle M_2^0, M_3^0, M_5^0, M_7^0 \rangle & \text{MinxEnt4,} \\ \langle M_2^0, M_3^0 \rangle & \text{MinxEnt2.} \end{cases}$$

According to §4.1.3, the Newton-Raphson procedure should be continued until some convergence

criteria, however to reduce computational overhead we will terminate after a single step,

$$\mathbf{M}^{\text{post}} = \begin{cases} \langle \rho c_1, m_1^1, m_2^1, \rho c_4, m_3^1, \rho c_6, m_4^1, \rho c_8, \rho c_9 \rangle & \text{MinxEnt4,} \\ \langle \rho c_1, m_1^1, m_2^1, \rho c_4, \rho c_5, \rho c_6, \rho c_7, \rho c_8, \rho c_9 \rangle \rangle & \text{MinxEnt2.} \end{cases}$$

and subsequently define the post-collision probability distribution,

$$\mathbf{f}^{\text{post}} = \mathbf{T}^{-1}\mathbf{M}^{\text{post}}$$

This procedure can be summarized by the following algorithm,

1. Calculate pre-collision moments $\mathbf{M}^0 = \mathbf{T}\mathbf{f}^{\text{eq}}$ and constraints
2. Calculate $\mathbf{H}$ and gradient vector $\nabla\mathcal{S}$
3. Perform a single Newton-Raphson step for the unconstrained moments,

$$\mathbf{m}^1 = \mathbf{m}^0 - \mathbf{H}^{-1}(\mathbf{m}^0)\,\nabla\mathcal{S}(\mathbf{m}^0)$$

4. Obtain the full post-collision moment vector, $\mathbf{M}^{\text{post}}$
5. Return to distribution space $\mathbf{f}^{\text{post}} = \mathbf{T}^{-1}\mathbf{M}^{\text{post}}$

Chapter 5

Numerical Applications

To demonstrate the MinxEnt-LBM method a number of numerical simulations of an athermal 2-D, isotropic Newtonian fluid were carried out. For comparison, simulations were also carried out with MRT-LBM, SRT-LBM, TRT-LBM and EF-LBM.

5.1 General Considerations

We assume that flow is athermal and that the macroscopic velocity of the flow, $\mathbf{u}$, is small. This allows us to expand the Maxwell-Boltzmann distribution in a power series in terms of $\mathbf{u}$ and truncate at low order (2.16). Because the flow is athermal we are then free to choose the temperature that appears in the equilibrium distribution. For simplicity we choose the temperature so that so that $RT = 1$. This simplifies the truncated Maxwell-Boltzmann distribution,

$$f^{\mathrm{eq}}(\mathbf{x}, \mathbf{v}, t) = \omega(\mathbf{v})\rho(\mathbf{x}, t)\left\{1 + \mathbf{v}\cdot\mathbf{u} + \frac{1}{2}\left[(\mathbf{v}\cdot\mathbf{u})^2 - |\mathbf{u}|^2\right]\right\}.$$

All LBMs simulated here will use this equilibrium with the exception of EF-LBM.

5.1.1 Velocity Discretization

We use the D2Q9 velocity scheme described in §2.1.6. Using D2Q9 the components of the discrete equilibrium are given by (2.17),

$$\mathbf{f}_i^{\mathrm{eq}}(\mathbf{x}_j, t) = W_i\rho(\mathbf{x}_j, t)\left\{1 + \mathbf{v}_i\cdot\mathbf{u} + \frac{1}{2}[(\mathbf{v}_i\cdot\mathbf{u})^2 - |\mathbf{u}^2]\right\}$$

In the D2Q9 scheme $c := |\mathbf{v}| = \sqrt{3RT}$ and given our choice for T we have that $c = \sqrt{3}$ a for our system.

Most authors work in lattice units (denoted here by a superscript lb). In lattice units,

$$\delta_x^{lb} = 1 = \delta_t^{lb} \quad \Rightarrow \quad |\mathbf{v}^{lb}| = 1.$$

This means that physical and lattice velocities are related by,

$$\mathbf{v} = \sqrt{3}\mathbf{v}^{lb} \Rightarrow \mathbf{u} = \sqrt{3}\mathbf{u}^{lb}.$$

In lattice units our discrete equilibrium becomes,

$$\mathbf{f}_i^{\mathrm{eq}}(\mathbf{x},t) = W_i\rho(\mathbf{x}_j,t)\left\{1+3\mathbf{v}_i^{lb}\cdot\mathbf{u}^{lb}+\frac{9}{2}(\mathbf{v}_i^{lb}\cdot\mathbf{u}^{lb})^2-\frac{3}{2}\left|\mathbf{u}^{lb}\right|^2\right\}.$$

In everything that follows we will operate in lattice units but for notational simplification we will omit the *lb* superscript. This gives the final versions of our equilibria,

$$\mathbf{f}_i^{\mathrm{eq}}(\mathbf{x},t) = \rho(\mathbf{x}_j,t)\,W_i\left\{1+3\mathbf{v}_i\cdot\mathbf{u}+\frac{9}{2}(\mathbf{v}_i\cdot\mathbf{u})^2-\frac{3}{2}\left|\mathbf{u}\right|^2\right\}, \tag{5.1}$$

i	1	2	3	4	5	6	7	8	9
$\mathbf{v}_i^{lb}$	(1,0)	(0,1)	(-1,0)	(0,-1)	(1,1)	(-1,1)	(-1,-1)	(1,-1)	(0,0)
W_i	$\frac{1}{9}$	$\frac{1}{9}$	$\frac{1}{9}$	$\frac{1}{9}$	$\frac{1}{36}$	$\frac{1}{36}$	$\frac{1}{36}$	$\frac{1}{36}$	$\frac{4}{9}$

Table 5.1: The D2Q9 velocity scheme in lattice units and $RT = 1$

In lattice units the D2Q9 velocity scheme is given in Table (5.1),

For the EF-LBM the equilibrium is chosen to be the minimizer of S (1.7) subject to mass and momentum constraints [32]

$$\mathbf{f}_i^{\mathrm{eq}}(\mathbf{x},t_n) = \rho(\mathbf{x}_j,t)\,W_i\prod_{l=1}^{2}\left(2-\sqrt{1+3\mathbf{u}_l^2}\right)\left(\frac{2\mathbf{u}_l+\sqrt{1+3\mathbf{u}_l^2}}{1-\mathbf{u}_l}\right)^{c_{i,l}}. \tag{5.2}$$

For convenience we recall here the discretization formulas in D2Q9 from §2.1.6,

$$\mathbf{f}_i(\mathbf{x}_j,t_n) = W_i\frac{f(\mathbf{x}_j,\mathbf{v}_i,t_n)}{\omega(\mathbf{v}_i)}$$

$$\rho(\mathbf{x}_j,t_n) = \sum_{i=1}^{9}\mathbf{f}_i(\mathbf{x}_j,t_n)$$

$$\rho(\mathbf{x}_j,t_n)\mathbf{u}(\mathbf{x}_j,t_n) = \sum_{i=1}^{9}\mathbf{f}_i(\mathbf{x}_j,t_n)\mathbf{v}_i.$$

Using the fact that in lattice units $\delta_x = 1 = \delta_t$ we have the explicit relationship between viscosity and τ from (4.36),

$$\tau = 3\nu+\frac{1}{2},$$

and recall that

$$\tau_2 = \frac{8\tau-1}{2\tau-1}.$$

5.1.2 Collision Steps

Relaxation Time Methods All MRT-LBM, TRT-LBM, SRT-LBM and EF-LBM collisions are all are based on the same equation,

$$\mathbf{f}^{\mathrm{post}} = \mathbf{f}^{\mathrm{pre}}+\mathbf{T}^{-1}\mathbf{B}\mathbf{T}(\mathbf{f}^{\mathrm{eq}}-\mathbf{f}^{\mathrm{pre}}),$$

where we will utilize the same moment matrix $\mathbf{T}$, (4.55), discussed in §(4.3.4). The various collision rules will differ by the choice of relaxation time matrix, $\mathbf{B}$. The different versions of $\mathbf{B}$ are shown in Table (5.2).

Collision	**B**
MRT-LBM	$diag\left(0, 1.64, 1.54, 0, \frac{1}{\tau_2}, 0, \frac{1}{\tau}2, \frac{1}{\tau}, \frac{1}{\tau}\right)$
TRT-LBM	$diag\left(0, \frac{1}{\tau}, \frac{1}{\tau}, 0, \frac{1}{\tau_2}, 0, \frac{1}{\tau}2, \frac{1}{\tau}, \frac{1}{\tau}\right)$
SRT-LBM	$\frac{1}{\tau}\mathbf{I}$
EF-LBM	$\begin{cases} \frac{1}{\tau}\mathbf{I} & \text{if } \Delta S < \text{tolerance} \\ \frac{1}{2\tau}\mathbf{I} & \text{if otherwise.} \end{cases}$

Table 5.2: Relaxation times for the various LBM collisions. The values 1.64 and 1.54 are chosen to agree with [53, 43]. Tolerance values are given in (5.3). ΔS defined in (2.9)

In some EF-LBM simulations three different tolerances were used,

$$\text{tolerance} = \begin{cases} \infty & \text{if EF1 ,} \\ 10^{-3} & \text{if EF2,} \\ 10^{-5} & \text{if EF3.} \end{cases} \tag{5.3}$$

For the MinxEnt-LBM simulations the probability distribution in the MinxEnt-LBM is first mapped to moment space using the **T** defined above. Constraints in all versions of MinxEnt-LBM are satisfied by fixing,

MinxEnt-LBM Methods We test the two versions of Minxent-LBM outlined in §(4.3), MinxEnt4 and MinxEnt2. MinxEnt4 has the constraints:

1. conservation of probability: $\mathbf{M}_1^{\text{post}} = \mathbf{M}_1^{\text{pre}}$
2. conservation of momentum: $\mathbf{M}_4^{\text{post}} = \mathbf{M}_4^{\text{pre}}$, $\mathbf{M}_6^{\text{post}} = \mathbf{M}_6^{\text{pre}}$
3. viscosity constraint: $\mathbf{M}_k^{\text{post}} = \mathbf{M}_k^{\text{pre}} + \frac{1}{\tau}(\mathbf{M}_k^{\text{eq}} - \mathbf{M}_k^{\text{pre}}), \quad k \in \{8, 9\}$

MinxEnt2 has the additional constraints,

MinxEnt2

4. accuracy constraint: $\mathbf{M}_k^{\text{post}} = \mathbf{M}_k^{\text{pre}} + \frac{1}{\tau_2}(\mathbf{M}_k^{\text{eq}} - \mathbf{M}_k^{\text{pre}}), \quad k \in \{5, 7\}$

After fixing the above constraints, the unconstrained moments are minimized using the Newton-Raphson procedure described in §4.1.3.

5.1.3 Boundary Conditions and Initial Conditions

All no slip boundary, zero velocity conditions are realized by using the full-way bounceback scheme with ghost nodes as explained in §2.1.7.

For distributions on fixed non-zero velocity boundaries, they are assigned the equilibrium distribution according to the macroscopic conditions required at the boundary.

The initial distributions are set to the equilibrium distribution.

5.2 2D Poiseulle Flow Convergence Studies

The first test was a 2D Poiseulle flow (see Figure 5.1) to test for spatial convergence rates. The purpose of this test was to confirm that the MinxEnt-LBM had comparable convergence rates as the other LBM methods. To test for spatial convergence each simulation was carried out until steady-state (determined by the stopping criteria). The number of nodes along the width of the channel, N_x, was varied and the avergaed L_1 norm difference from the analytic solution, $\mathbf{u}_0$, is calculated.

Given a macroscopic force, $\mathbf{F}$ (in lattice units) the implementation of the force was accomplished by shifting the macroscopic velocity that is used by the equilibrium distribution,

$$\hat{\mathbf{u}} = \mathbf{u} + \tau \frac{\mathbf{F}}{\rho}$$

where $\hat{\mathbf{u}}$ replaces $\mathbf{u}$ in the equilibrium distribution.

One should note however, that unlike typical numerical fluid dynamics simulations, increasing the number of nodes in a simulation in lattice units does *not* decrease the grid spacing. The reason for this is because in lattice units the spacing is fixed at $\delta_x = 1$ so the effect of increasing the number of nodes along the width of the channel is to increase the width of the channel (in lattice units). To compensate for this, the force was adjusted to maintain the flow Reynolds Number,

$$Re = \frac{u_y^{\max} N_x}{\nu},$$

where the maximum y-velocity of Poiseulle flow is known to be,

$$u_y^{\max} = \frac{F_y}{8\nu} N_x^2$$

This way, the actual physical flow being simulated remained constant as the number of nodes was changed. The remainder of the simulation setup is summarized in Table 5.3. The Reynolds number was chosen to be 5 to keep the velocities low, and thus make the low mach number approximations as accurate as possible.

5.2.1 Results

The results of the convergence studies are given in Figure 5.2. All LBMs show similar convergence behaviour, including the MinxEnt-LBMs. However, we do notice non-linear behaviour for the EF-LBM methods for flow with a small number of nodes. This phenomena is unique to EF-LBMs and is not present for any other type of LBM collision step, regardless of the number of nodes.

In addition, the convergence is order δ_x^3, which does not agree with previous studies which indicate LBMs should be order δ_x^2 methods. It is unclear at this time what is causing the discrepancy.

5.3 1D Shock tube

A benchmark simulation to test the stability of a simulation is the low viscosity 1D shock tube. Since the zero viscosity limit occurs when $\tau = .5$ (see (4.36)) simulations were performed with values of τ close to .5 in a 1D tube with a density shock. The initial conditions has a density shock located at the centre of the tube. Although it is possible to run a true 1D LBM simulation using a suitable (1 dimensional) velocity scheme, we chose to carry out our simulation in a 2D geometry with periodic conditions in the y direction.

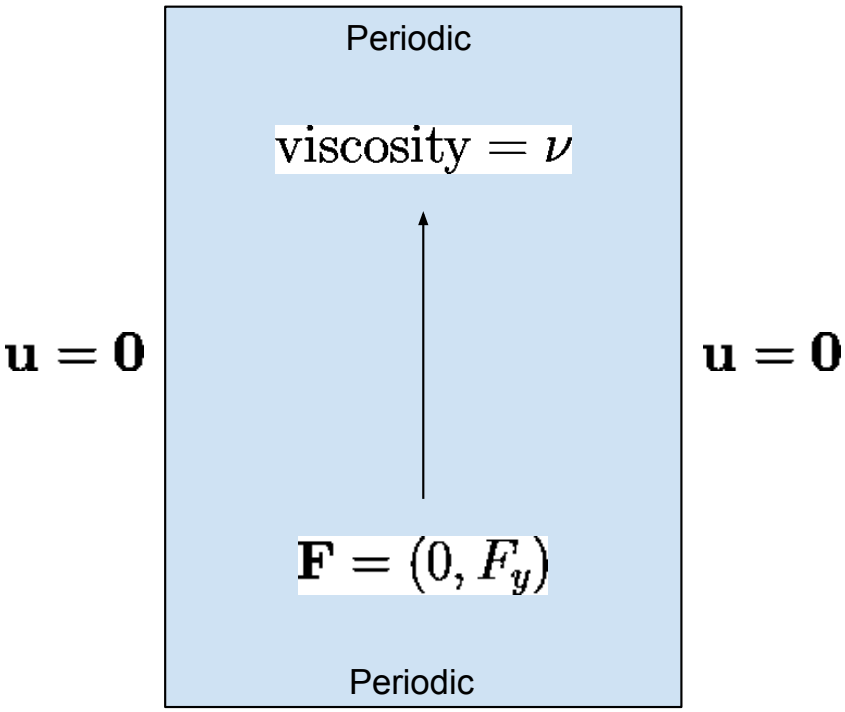

Figure 5.1: Geometry for Poiseulle flow convergence studies

N_x N_y	varied 5
Initial Condition	$\rho = 1$ $\mathbf{u}$=$\mathbf{0}$
Re	5
$\mathbf{F}$	$\left(0, \quad 8\frac{Re\,\nu^2}{N_x^3}\right)$
τ	0.8
$\mathbf{u}_{\text{an}}$	$\left(0, \quad \frac{F_y}{2\nu}x(N_x - x)\right)$
Error	$E = \frac{1}{N_x N_y}\sum_{\mathbf{x}} \|\|\mathbf{u} - \mathbf{u}_{an}\|\|_1$
Stopping Criteria	$\sum_{\mathbf{x}} \|\|\mathbf{u}(t+1) - \mathbf{u}(t)\|\|_2 < 10^{-10}$

Table 5.3: Simulation setup for 2D Poiseulle flow convergence tests

The reason for the 2D simulation was due to the fact if the simulation was carried out in 1D with 3 velocities then the the MinxEnt-LBM would be completely constrained (probability conservation, momentum conservation and viscosity constraint), and no minimization would be required. Thus, in order to perform MinxEnt-LBM on a true 1D grid would require a 1D velocity scheme with more

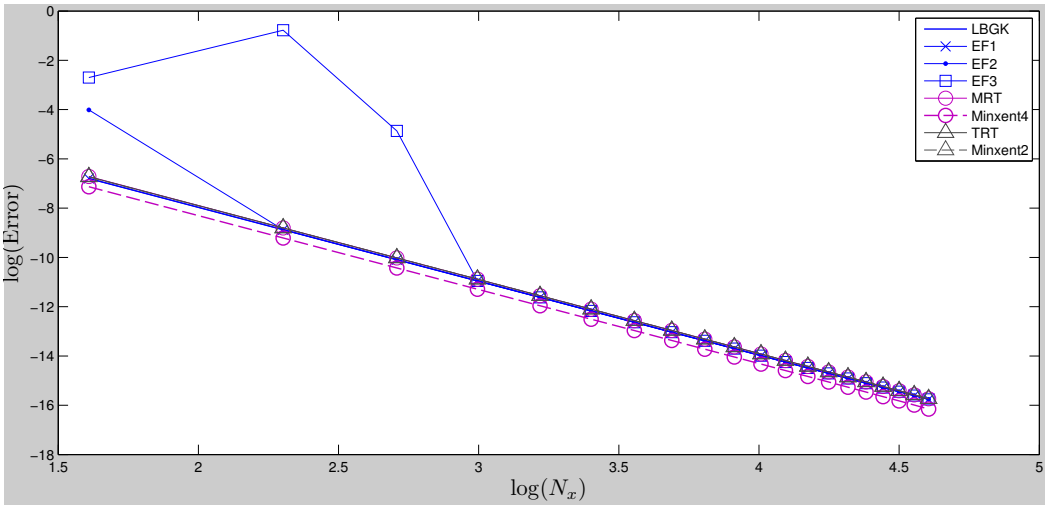

Figure 5.2: Plot of the log error from analytic solution versus log number of nodes in the width of the channel

velocities. However, due to the irrationality of lattice points for higher velocity schemes an additional approximation would be required to properly set up the simulation [71]. To circumvent the lack of unconstrained moments in 1D, the 2D simulation with periodic boundary conditions was employed. The remainder of the simulation setup is summarized in Table 5.4.

N_x	800
N_y	4
Initial Conditions	$\rho = \begin{cases} 1 & \text{if } 0 < x < 400 \\ 0.5 & \text{if } 400 \leq x < 800 \end{cases}$ $\mathbf{u} = \mathbf{0}$
$\mathbf{F}$	$\mathbf{0}$
τ	$0.5 + 10^{-9}$
Stopping Criteria	400 time steps

Table 5.4: Simulation setup for 1D shock tube

5.3.1 Results

Results are shown in Figures 5.3-5.6. Of particular interest is the behaviour near the shock front. It is clear from the plots that SRT-LBM suffers from the worst stability, showing severe oscillation near the shock front in both density and velocity.

In Figures 5.5 and 5.6 we can see that TRT-LBM simulations offer very little in increased stability whereas MRT-LBM has improved stability in both density and velocity. However, we see that the most stable simulations belong to MinxEnt4 and MinxEnt2. These two MinxEnt-LBM based simulations rival the stability of the density and velocity of the highest tolerance EF-LBM simulations (Figures 5.3d and 5.4d respectively).

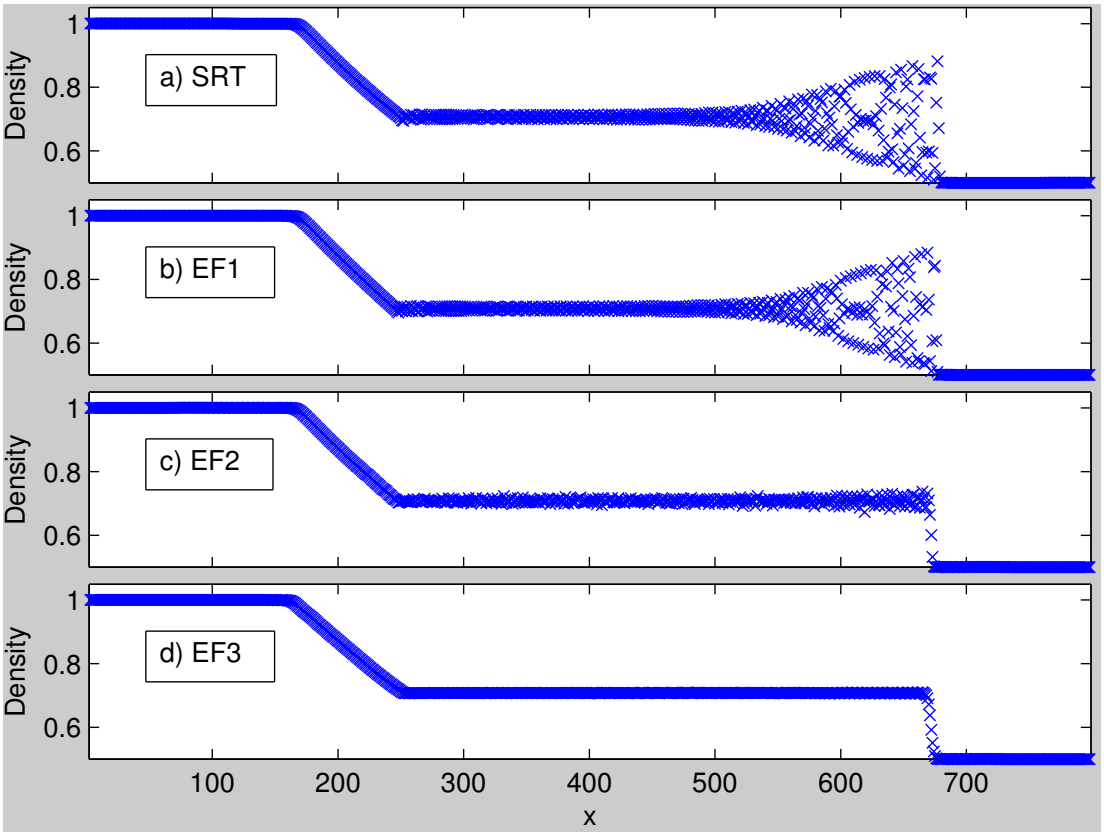

Figure 5.3: 1D shock tube density profiles after 400 times steps. a) SRT-LBM, b) EF1-LBM, c) EF2-LBM, d) EF3-LBM

5.4 Lid-Driven Cavity Flow: Stability Studies

Another benchmark fluid simulation is lid-driven cavity flow (see Figure 5.7). In lid-driven cavity flow the fluid begins at rest and the lid of the cavity is given a constant velocity in the x direction. This creates flow with a number of interesting properties including vortices. This test was conducted to understand the stability of the various LBMs during lid-driven cavity flow. The viscosity relaxation time τ is varied and approaches the zero viscosity limit ($\tau \to 0.5$). For each value of τ, simulations are carried out with a variety of lid velocities. Simulations are considered "stable" if they do not blow up, nor exhibit a negative distribution population, at any time during 1000 time steps. Though not always fatal, a negative distribution population frequently precedes instabilities. This is the reason we choose to label simulations with a negative distribution population as "unstable". The maximum lid velocity at which a simulation is stable is noted for each value of τ. The remainder of the simulation setup is summarized in Table 5.5.

5.4.1 Results

Results of the lid-driven cavity flow stability simulations are shown in Figure 5.8. The first feature of note is the unconditional stability of the EF-LBMs.

The second best performing methods are the MRT-LBM and MinxEnt4 with similar results, with MinxEnt4 consistently fairing better than MRT-LBM.

The worst performing LBMs were TRT-LBM, MinxEnt2 and SRT-LBM was the worst. As seen with MinxEnt4 outperforming its MRT-LBM cousin, we see again that MinxEnt2 consistently achieves better results than its counterpart, TRT-LBM.

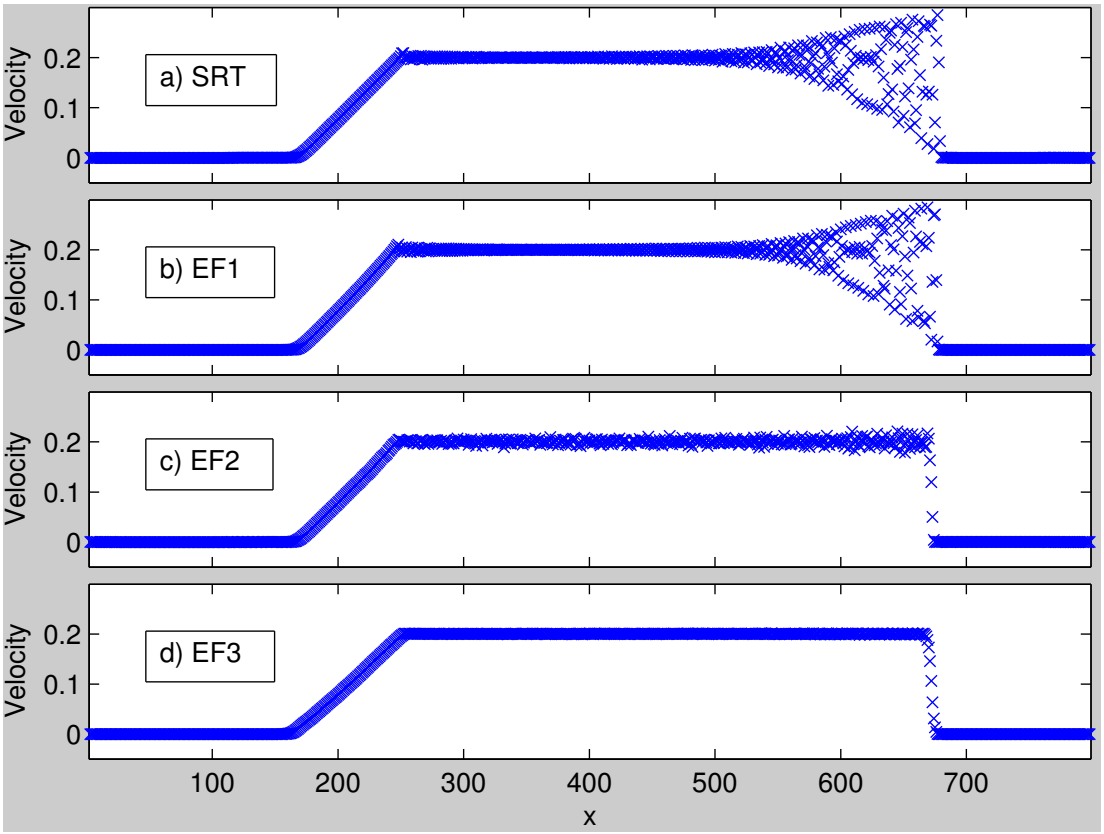

Figure 5.4: 1D shock tube velocity profiles after 400 times steps. a) SRT-LBM, b) EF1-LBM, c) EF2-LBM, d) EF3-LBM

N_x N_y	17 17
Initial Condition	$\rho = 2.7$ $\mathbf{u} = \begin{cases} (u_{\text{lid}}, 0) & \text{if } y = 17 \\ 0 & \text{otherwise} \end{cases}$
$\mathbf{F}$	$\mathbf{0}$
$\mathbf{u}_{\text{lid}}$	varied
τ	varied
Stopping Criteria	1000 time steps, blow up or negative distribution

Table 5.5: Simulation setup for lid-driven flow stability tests

5.5 Lid-Driven Cavity Flow: Accuracy Studies

lid-driven cavity flow on a square grid was performed similar to other studies such as SRT-LBM lid-driven flow (examined by Hou et al. in [89]) and also MRT-LBM lid-driven flow (by Luo et al. [53]). In addition to these, Brownlee and co-workers [51] also studied lid-driven cavity flows at various Reynolds numbers and using various LBM stabilization techniques. To test MinxEnt-LBM we carried out similar lid-driven cavity flow simulations (see Figure 5.7 again for details). Though similar to the work by the aforementioned authors, our simulation does differ in a number of ways and thus cannot be compared directly to them (though the results are very similar). Instead, our focus is on the performance of the various LBMs compared to each other under our experimental set up.

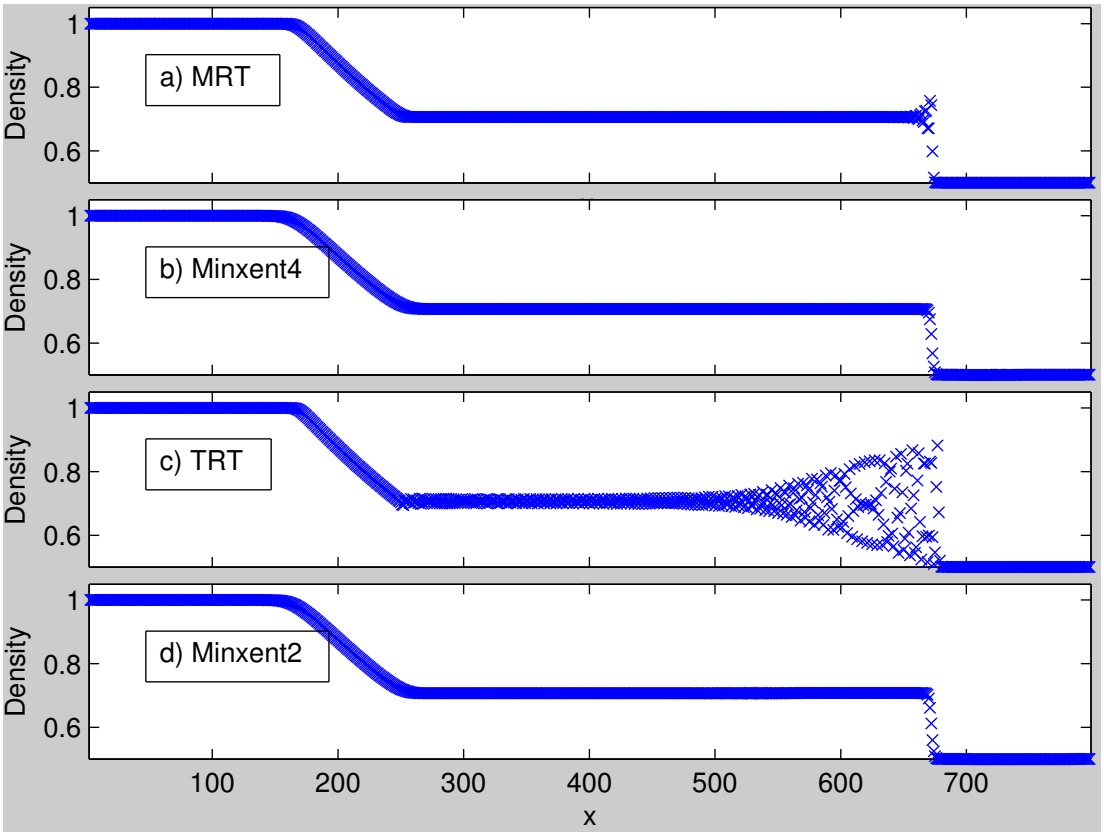

Figure 5.5: 1D shock tube density profiles after 400 times steps. a) MRT-LBM, b) MinxEnt-LBM, c) TRT-LBM, d) MinxEnt2

In each simulation, a square lattice was constructed of either 65×65, 129×129 or 257×257 nodes. A velocity was imparted on the top of the cavity in the x direction.

As a benchmark to compare against simulations using commercial CFD software, COMSOL, were also carried out. One should note however that because of the LBM boundary conditions, the physical system that the LBMs were simulating was *not* a square. Due to the bounce-back boundary at both sides of the cavity, the physical boundary was actually 1/2 a lattice unit beyond the last lattice node. Thus, for a simulation with N_x nodes across the width, the actual physical width of the simulation was N_x is lattice units. However, because bounce-back was not used at the lid boundary, the physical boundary occurred at the last node. This means that the height of the cavity was $N_y - 1/2$ lattice units. Even though the number of nodes were the same in the x and y directions, the actual height of the cavity was always 1/2 of a lattice unit less than its width. One must also be careful when determining the physical location of features for this reason as well.

In light of the above fact, that the lattice nodes do not align with the boundaries, this leads to non-uniform lattice spacing near the boundary. While one could modify Simpson's rule to calculate the stream function,

$$\psi = -\int u_y(\mathbf{x}, t)\, dx$$

integration, we found it simplest to use the trapezoidal rule instead.

The remainder of the simulation setup is summarized in Table 5.6.

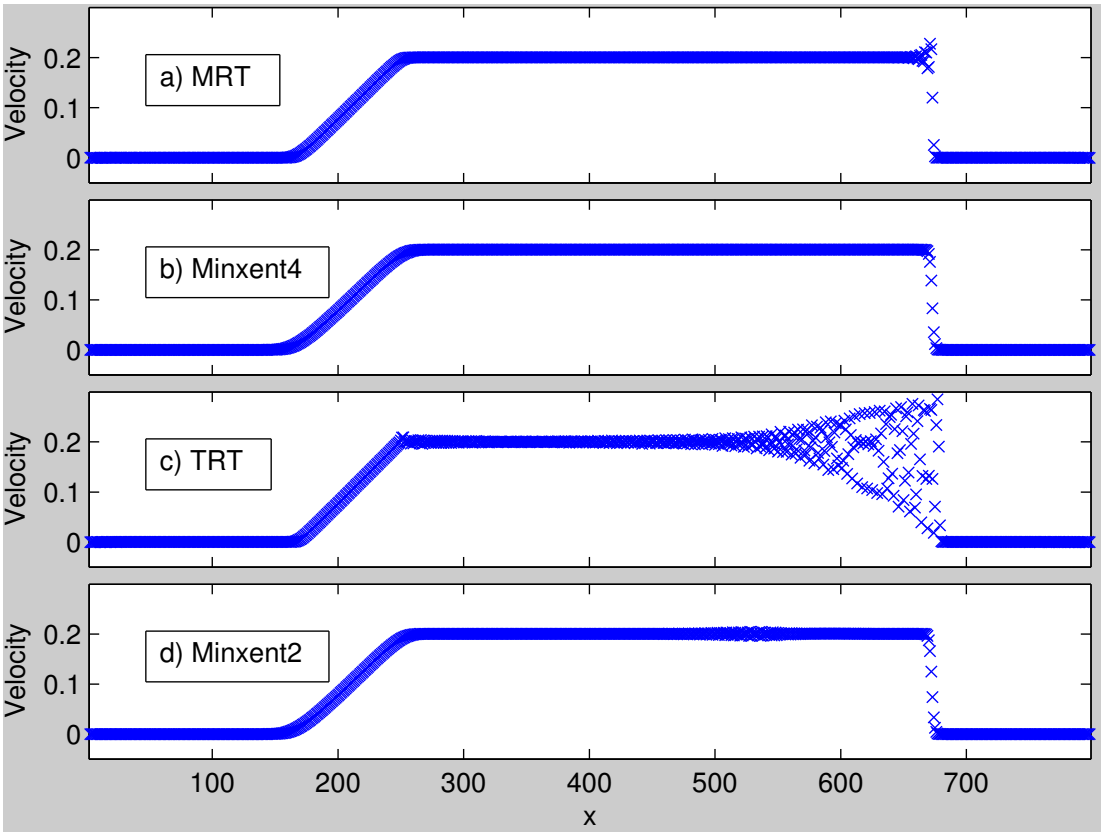

Figure 5.6: 1D shock tube velocity profiles after 400 times steps. a) MRT-LBM, b) MinxEnt-LBM, c) TRT-LBM, d) MinxEnt2

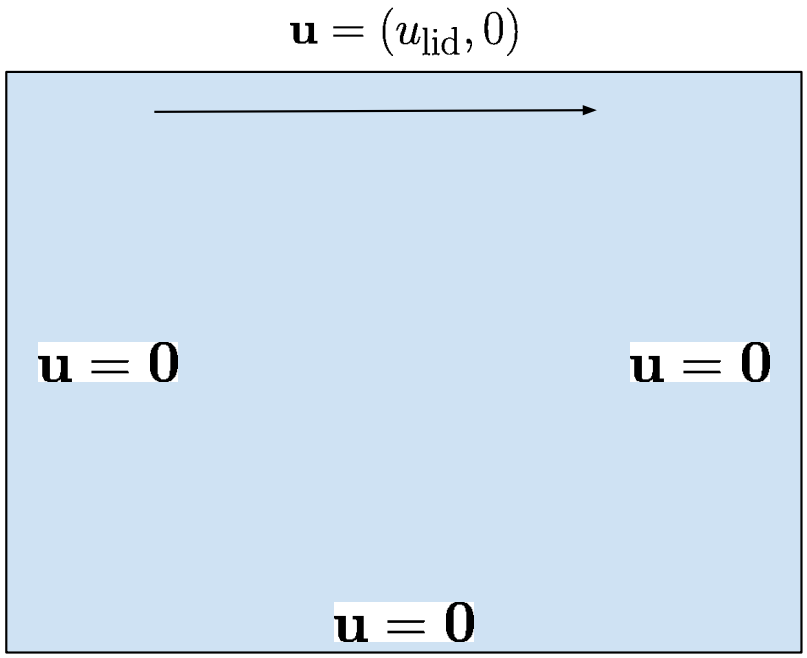

Figure 5.7: Geometry for lid-driven cavity flow

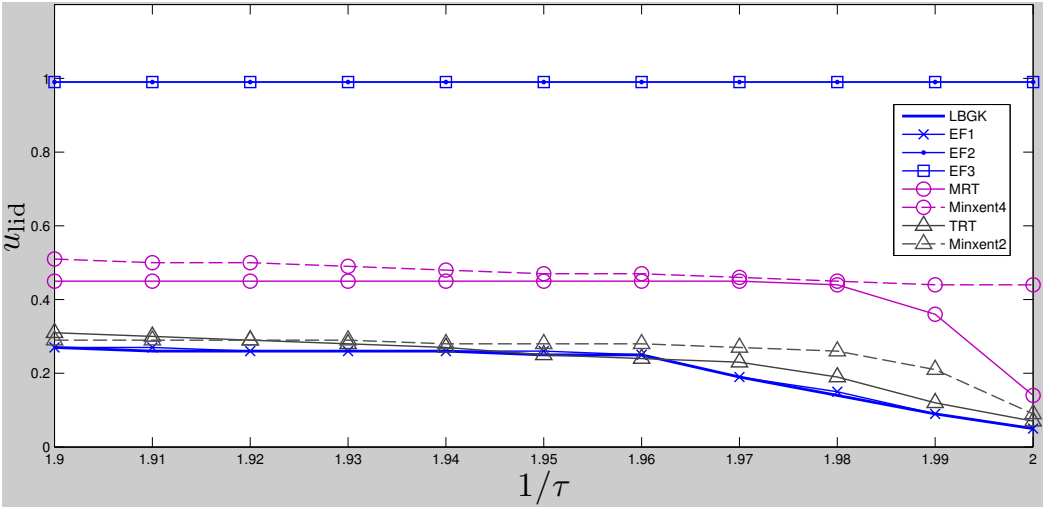

Figure 5.8: Maximum lid velocity in 17^2 nodes Lid-driven cavity flow allowing simulation to survive 1000 time steps for various viscosity relaxation times. SRT-LBM and EF-LBM collisions in blue. MRT-LBM in pink and TRT-LBM in grey. MinxEnt-LBM dashed in pink, MinxEnt2 dashed in grey.

N_x N_y	$65, 129, 257$ $65, 129, 257$
Initial Condition	$\rho_0 = 2.7$ $\mathbf{u} = \begin{cases} (u_{\text{lid}}, 0) & \text{if } y = N_y \\ 0 & \text{otherwise} \end{cases}$
$\mathbf{F}$	$\mathbf{0}$
$\mathbf{u}_{\text{lid}}$	$\begin{cases} (0.01, 0) & \text{if } Re = 100 \\ (0.1, 0) & \text{otherwise} \end{cases}$
Reynolds Number	$\frac{u_{\text{lid}} N_x}{\nu}$
τ	varied
Stopping Criteria	$\psi_{\min}(t + 10000) - \psi_{\min}(t) < 10^{-5}$

Table 5.6: Simulation setup for lid-driven flow

5.5.1 Results

The results of the 257×257 node lid-driven cavity flows are given in Figures 5.9 - 5.17. In all figures, the left column are the pressure deviation contours $\delta\pi$. Recalling the expression for pressure in D2Q9 LBM simulations (4.37), the pressure deviation is given by,

$$\delta\pi = \frac{1}{3}\frac{(\rho - \rho_0)}{\rho_0}.$$

The middle columns of Figures 5.9 - 5.17 are the stream function and the right column is the vorticity. At internal nodes (those that do not send nor receive distribution populations to/from ghost nodes), the vorticity

$$\omega = \frac{\partial u_y}{\partial x} - \frac{\partial u_x}{\partial y}$$

was calculated by centered difference,

$$\omega(x_i, y_j) \approx \frac{u_y(x_{i+1}, y_j) - u_y(x_{i-1}, y_j)}{2h} - \frac{u_x(x_i, y_{j+1}) - u_x(x_i, y_{j-1})}{2h},$$

where $h = \frac{1}{N_x}$.

At non-corner boundary nodes, the vorticity was calculated using finite differences, making use of the macroscopic boundary conditions,

$$\begin{aligned}
\omega(x_1, y_j) &\approx \frac{u_y(x_1, y_j) - 0}{h/2} - \frac{u_x(x_1, y_{j+1}) - u_x(x_1, y_{j-1})}{2h}, \\
\omega(x_{N_x}, y_j) &\approx \frac{0 - u_y(x_{N_x}, y_j)}{h/2} - \frac{u_x(x_{N_x}, y_{j+1}) - u_x(x_{N_x}, y_{j-1})}{2h}, \\
\omega(x_i, y_1) &\approx \frac{u_y(x_{i+1}, y_1) - u_y(x_{i-1}, y_1)}{2h} - \frac{u_x(x_i, y_2) - 0}{h/2}, \\
\omega(x_i, y_{N_y}) &\approx \frac{u_y(x_{i+1}, y_{N_y}) - u_y(x_{i-1}, y_{N_y})}{2h} - \frac{u_{\text{lid}} - u_x(x_i, y_{N_x - 1})}{h/2}.
\end{aligned}$$

Vorticity at the corners was set to,

$$\begin{aligned}
\omega(x_1, y_1) &= 0, \\
\omega(x_{N_x}, y_1) &= 0, \\
\omega(x_1, y_{N_y}) &= 2|\mathbf{u}_{\text{lid}}|, \\
\omega(x_{N_x}, y_{N_y}) &= 2|\mathbf{u}_{\text{lid}}|.
\end{aligned}$$

To standardize the results, the stream function was normalized to the lid velocity

$$\hat{\psi} = \frac{\psi}{|\mathbf{u}_{\text{lid}}|},$$

the pressure deviation was normalized to the square of the lid velocity,

$$\hat{\delta\pi} = \frac{\delta\pi}{\mathbf{u}_{\text{lid}}^2},$$

and the vorticity was normalized to the lid velocity,

$$\hat{\omega} = \frac{\omega}{|\mathbf{u}_{\text{lid}}|}$$

Numerical results are tabulated in Tables 5.7 - 5.15. Presented in the tables are the centres and stengths of the main, lower-left, lower-right vorticies, determined by the extremea of the streamfunction ψ. In addition, the pressure deviation ($\delta\pi$) and vorticity (ω) at these locations is calculated. These values are tabulated for different simulation methods, with different number of lattice nodes, and different Reynolds numbers. Note that no EF3-LBM data is available for $N_x = 65$ since the simulations never reached the convergence threshold.

5.6 Discussion

As we can see from the results above, the choice of collision step had considerable effect on the stability and accuracy of the simulations. The results presented above seem to corroborate the idea that simulations which violate an entropy principle are less stable [20, 21].

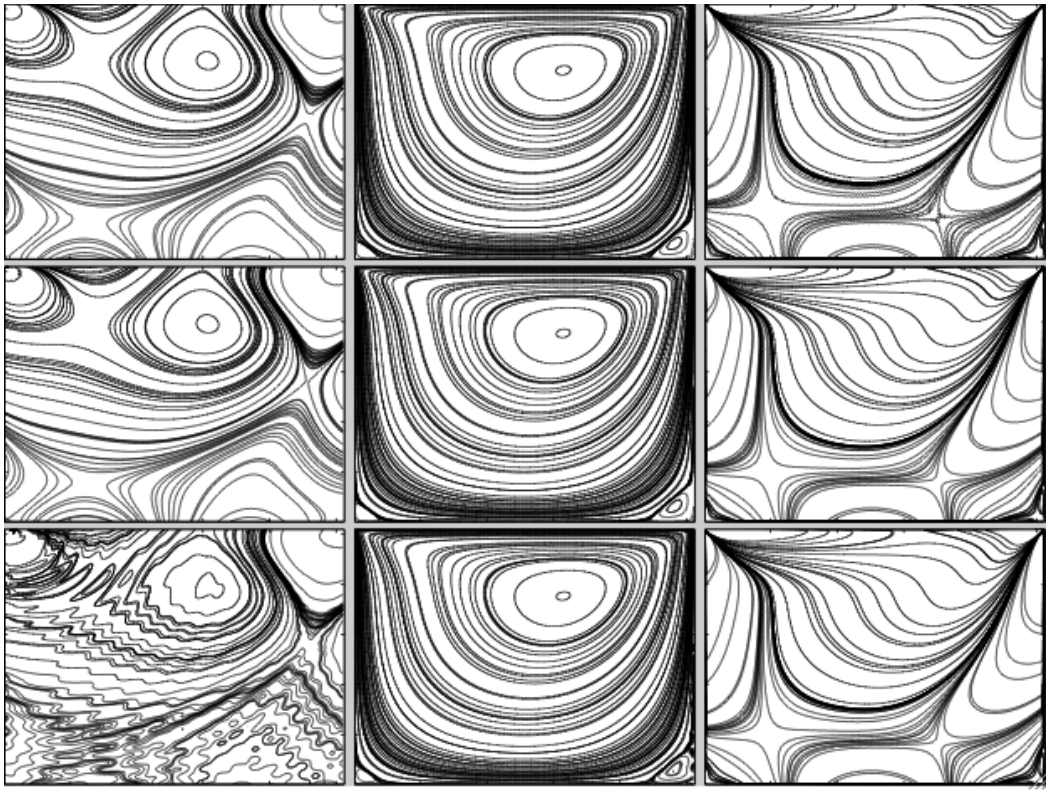

Figure 5.9: Flow contours of lid-driven cavity flow for Re= 100 with $N = 257^2$. Left-Pressure deviation, Middle: Stream Function, Right: Vorticity. Top Row: Comsol, Middle Row: SRT-LBM, Bottom Row: EF3-LBM

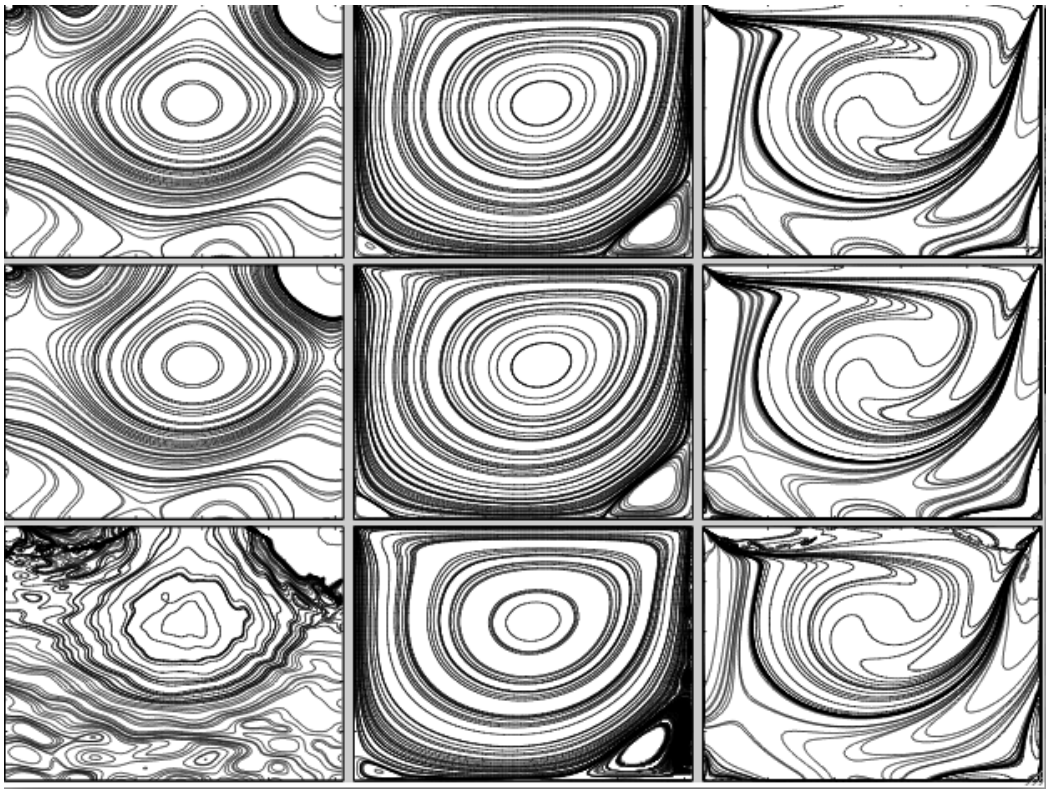

Figure 5.10: Same as Figure 5.9, Re= 400

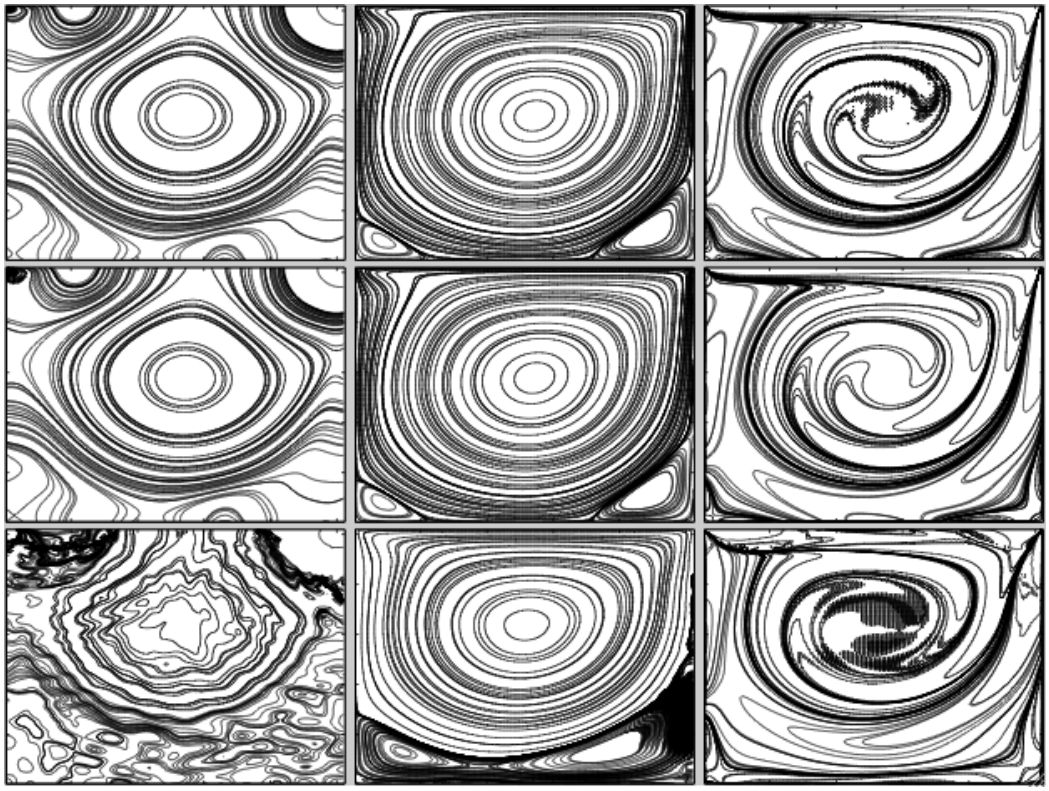

Figure 5.11: Same as Figure 5.9, Re= 1000

Table 5.7: Main Vortex Results, N_x =65

Re=100	N_x	$\hat{\psi}_{\min}$	x	y	$\hat{\delta\pi}$	$\hat{\omega}$
Comsol	65	-0.10332	0.61111	0.72656	-0.077157	-3.1062
LBGK	65	-0.10365	0.61111	0.72656	-0.12638	-3.1323
MRT	65	-0.10346	0.61111	0.72656	-0.079473	-3.1396
Minxent4	65	-0.10374	0.61111	0.72656	-0.080095	-3.1482
TRT	65	-0.10348	0.61111	0.72656	-0.079564	-3.1403
Minxent2	65	-0.10343	0.61111	0.72656	-0.07904	-3.1388
Re=400	N_x	$\hat{\psi}_{\min}$	x	y	$\hat{\delta\pi}$	$\hat{\omega}$
Comsol	65	-0.11374	0.54762	0.60156	-0.077842	-2.2941
LBGK	65	-0.11276	0.54762	0.60156	-0.078925	-2.3031
MRT	65	-0.11169	0.56349	0.60156	-0.077576	-2.2713
Minxent4	65	-0.11263	0.54762	0.60156	-0.078655	-2.2977
TRT	65	-0.11179	0.56349	0.60156	-0.077768	-2.2732
Minxent2	65	-0.11145	0.56349	0.60156	-0.076556	-2.2675
Re=1000	N_x	$\hat{\psi}_{\min}$	x	y	$\hat{\delta\pi}$	$\hat{\omega}$
Comsol	65	-0.11854	0.53175	0.57031	-0.074078	-2.0565
LBGK	65	-0.11845	0.53175	0.55469	-0.076805	-2.0819
MRT	65	-0.11497	0.53175	0.55469	-0.072262	-2.0279
Minxent4	65	-0.11865	0.53175	0.55469	-0.076481	-2.0804
TRT	65	-0.11591	0.53175	0.55469	-0.07366	-2.0459
Minxent2	65	-0.11425	0.53175	0.55469	-0.070133	-2.0186

Indeed, in the 1D shock tube, §5.3, we can see in Figures 5.3 and 5.4 that the stability of the simulations is improved as the tolerance in the EF-LBM is reduced from infinity. By decreasing the

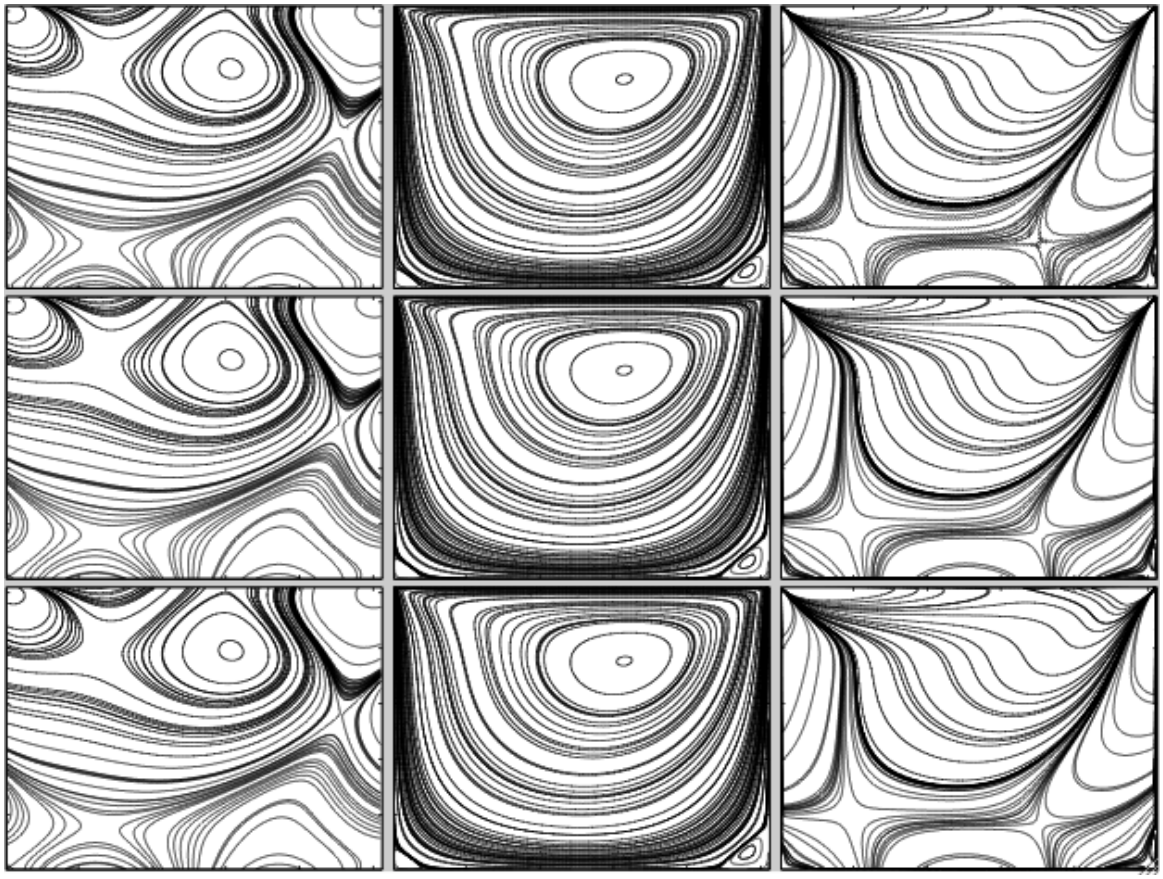

Figure 5.12: Same as Figure 5.9, Top Row: Comsol, Middle Row: MRT-LBM, Bottom Row: MInxEnt4-LBM

entropy violation tolerance we effectively reduce the number of nodes where an increase in entropy is likely.

Similar results were obtained in the lid-driven flow stability tests, §5.4 where EF-LBMs were unconditionally stable, with the exception of EF1-LBM, which had infinite tolerance (and thus was identical to SRT-LBM). This is unsurprising as the method targets nodes where trouble may occur and proportionally adjusts the scheme accordingly, without regard for maintaining accuracy. In fact, one can deduce directly from from the EF-LBM collision rule (2.10) that at troublesome nodes the effective relaxation time doubles, from just above 0.5 to nearly 1. The effect of setting the relaxation time to unity has the effect of setting the post-collision distribution to the equilibrium. We do note, however, that the EF-LBMs were *not* stable at the highest lid velocity tested in our studies ($\mathbf{u}_{\text{lid}} = 1$). This is due to the fact that the equilibrium used by the EF-LBMs was the entropic equilibirum (5.2) which is singular when the velocity is equal to one. Thus, any node on the lid would have immediately diverged. We did not test any lid velocities higher than 1, but we would expect that the EF-LBMs would remain stable above 1 as well.

This relationship between entropy violation and stability seems to hold true for other collision methods as well. Since MinxEnt-LBMs attempt to explicitly minimize the entropy during each collision step, we would expect entropy violations to be less frequent as compared to other LBMs. If the minimization is carried out perfectly we would not expect to see any entropy violations. We see from the 1D shock tube and lid-driven flow stability tests that the MinxEnt4 and MinxEnt2 do indeed exhibit better stability performance than their relaxation time counterparts (MRT-LBM and TRT-LBM respectively). This could be explained by the fact that, in the context of entropy

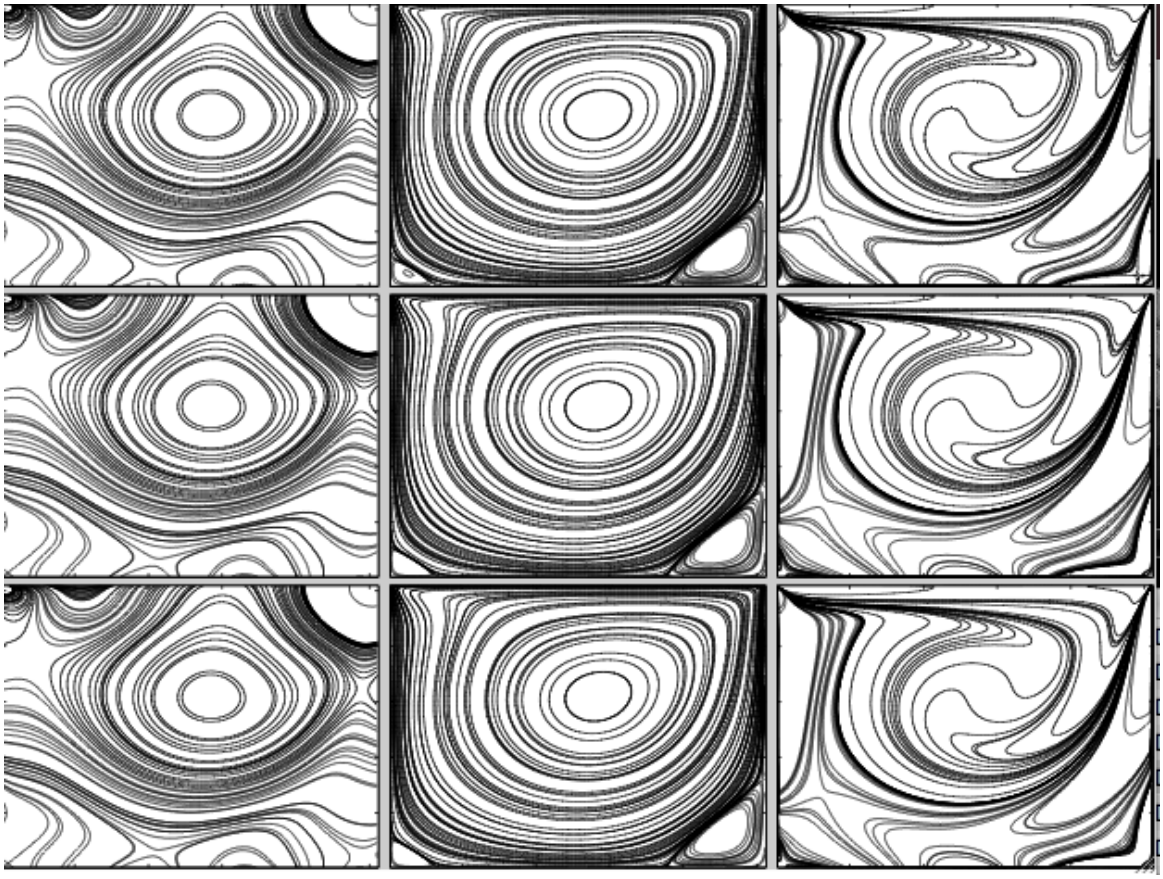

Figure 5.13: Same as Figure 5.12, Re= 400

minimization, MRT-LBM and TRT-LBM are *are* attempting to minimize the entropy, but are not as flexible to do so because their relaxation times are fixed. On the other hand, the MinxEnt-LBMs parameters are variable since their minmization is carried out by a Newton-Raphson method with local Hessian and gradient. We also see further evidence of this when comparing the stability of MinxEnt4 to MinxEnt2 amongst themselves. MinxEnt2 has two additional constraints, which decreases the number of moments available for the Newton-Raphson procedure to minimize over, as compared to MinxEnt4. This restricts the ability of MinxEnt2 to accurately minimize the entropy and raises the likelihood of entropy increase. The result of this restriction is borne out in the decreased stability of the MinxEnt2 compared to the MinxEnt4.

Despite the attractiveness of having increased stability in a simulation, a trade-off usually comes at the cost of accuracy. This can be seen in the Poiseulle flow convergence study §5.2. In Figure 5.2 that the EF2-LBM and EF3-LBM show poor convergence behaviour when the number of nodes is small. We can interpret this by again noting that EF2-LBM alters the collision step (2.10) when entropy violations are likely. With a small number of nodes, these alterations may occur at a large fraction of the lattice nodes. Increasing the number of nodes decreases fraction of nodes that may require alteration, thus increasing the overall accuracy of the method. We also see that the problem is worse for the EF3-LBM, which is consistent with our analysis, since EF3-LBM has less entropy violation tolerance than EF2-LBM, and thus the number of altered nodes is likely to be greater and accuracy degraded.

The degradation of accuracy is even more prevalent in the lid-driven cavity flows §5.5. We see this in demonstrated in Figures 5.9, 5.10, and 5.11. In these figures the bottom row are results using EF3-LBM. We can see considerable inaccuracy compared to the top row (Comsol), particularly in

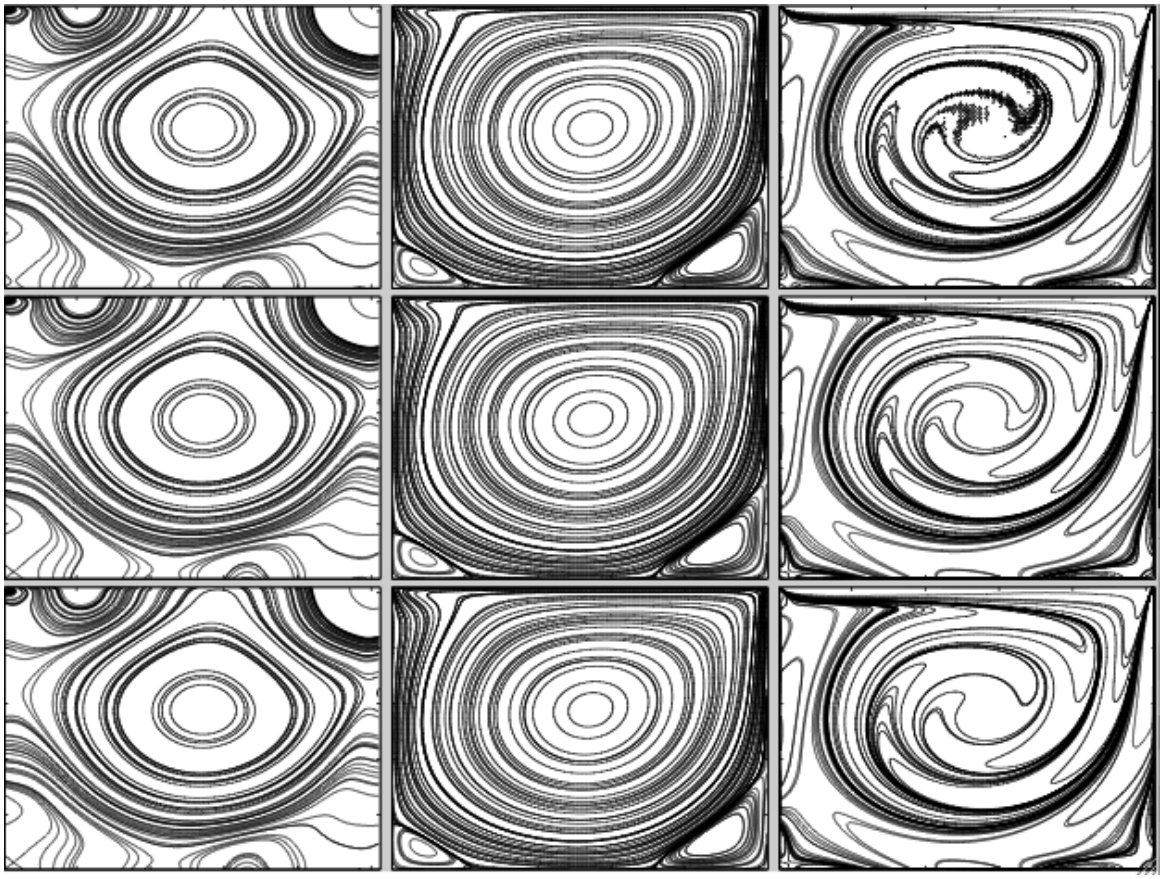

Figure 5.14: Same as Figure 5.12, Re= 1000

the pressure deviation contours. At higher Reynolds numbers we also start to see inaccuracies in the stream function (middle column) and vorticity (right column). This fits with our above analysis since at higher Reynolds numbers, more nodes are likely to require altering in the EF3-LBM scheme.

We can also see the inaccuracies quantitatively in Tables 5.7-5.15. Of note is are the values in the EF3-LBM rows as compared to the Comsol rows. EF3-LBM is consistently more inaccurate than the other LBMs, and generally performs worse as the Reynolds number increases.

Though EF-LBMs and MinxEnt-LBMs performed comparatively when it came to stability, we see from the lid-driven cavity flow data that the MinxEnt-LBMs were able to maintain their accuracy at all Reynolds numbers and lattice spacings. In fact, MinxEnt-LBMs were usually as accurate, if not more accurate than their MRT-LBM cousins.

It should be noted that work done by other authors using EF-LBM such as [51] had similar stability improvements but did not display the same inaccuracy as the studies done here. This is because most of these other studies employed a limit on the number of nodes that were allowed to be altered. This leads to a practical difficulty that of finding the optimal way to choose the parameters of the model. Before commencing a simulation it is not known *a priori* what the entropy violation tolerance should be in order to adequately stabilize the simulation. Moreover, the limit on the number of altered nodes is also not known beforehand. This leads one to either be skeptical of results obtained with EF-LBMs or requires repeated simulation runs in order to tune the parameters properly.

A similar situation exists with MRT-LBMs in that some of their fixed relaxation times are not known *a priori*, and are usually taken to be values that are popular in the literature or have been successful in similar simulations. As evidenced by the stability improvements of MRT-LBM over

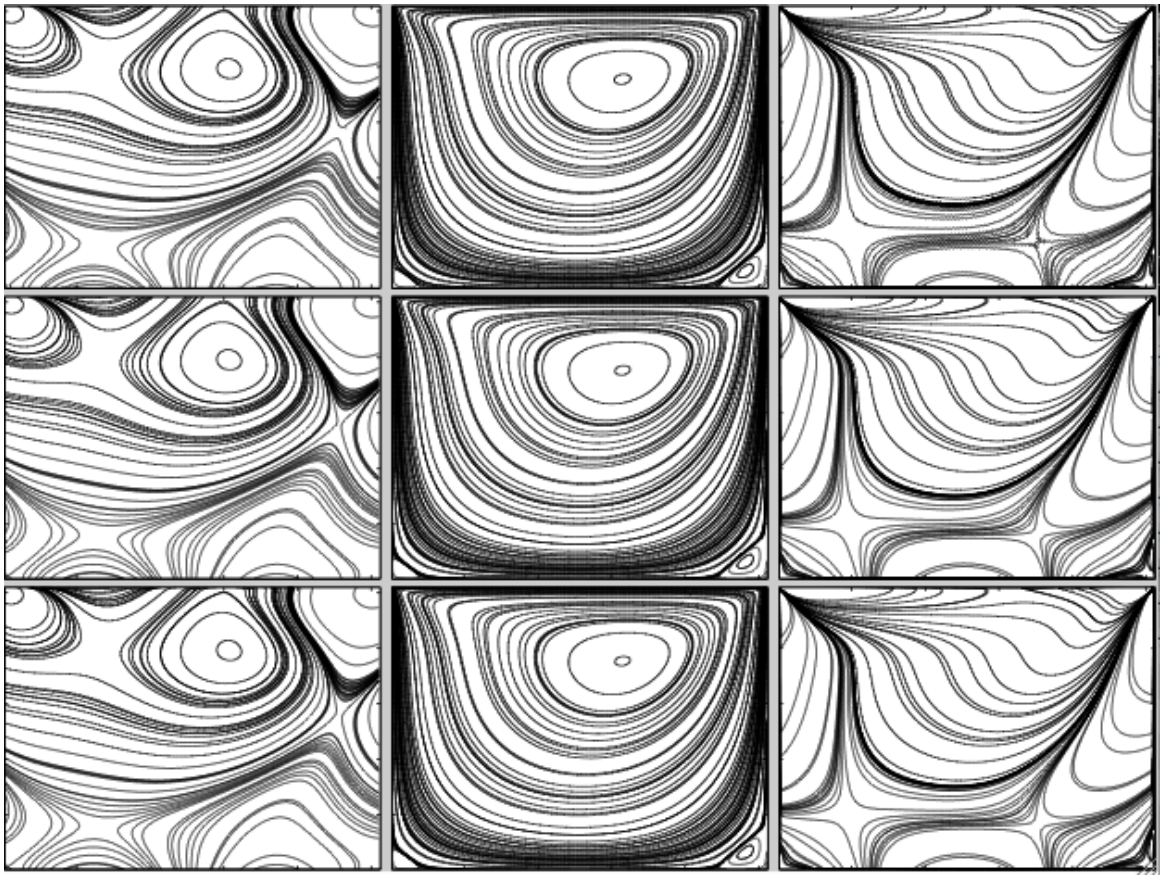

Figure 5.15: Same as Figure 5.9, Top Row: Comsol, Middle Row: TRT-LBM, Bottom Row: MinxEnt2

TRT-LBM it stands to reason that choosing the relaxation times differently can have a dramatic effects on the stability of simulations. This suggests that if one could find the proper relaxation times, perhaps one could achieve the stability performance that was exhibited by the MinxEnt-LBM simulations. However, this returns us to the problem faced by the EF-LBM. That is, the need to conduct numerous simulations and tune the relaxation times for optimal stability and accuracy.

These tuning procedures are *not* required by the MinxEnt-LBMs. In effect, the MinxEnt-LBMs adjust their "relaxation times" on-the-fly and locally, negating the need to find the "optimal" relaxation times or other model parameters. It is also worth mentioning that recent work done in [85, 86] demonstrated an MRT like LBM, based on entropy methonds, wwhere the relaxation times were *not* fixed. This LBM was briefly discussed as also being an approximation to MinxEnt-LBM in §4.2.4.

From all of the results shown here, the LBM which has the greatest stability while maintaining the accuracy of the method are the Minxent-LBMs. Stability wise they are able to perform comparably to the alterations experienced with robust EF-LBMs, while at the same time maintaining accuracy. Crucially the MinxEnt-LBMs are able to achieve these results without tuning or *a priori* knowledge that are required with the other LBMs presented here.

In the context of the performance of the other LBMs, it seems reasonable to conclude that the power of the MinxEnt-LBMs rests with their ability to more accurately minimize the entropy during the collision step which reduces the number of times entropy is increased. This works seems to validate the notion that entropy likely plays a necessary role in maintaining the stability of simulations that has been suggested by numerous other authors and their results.

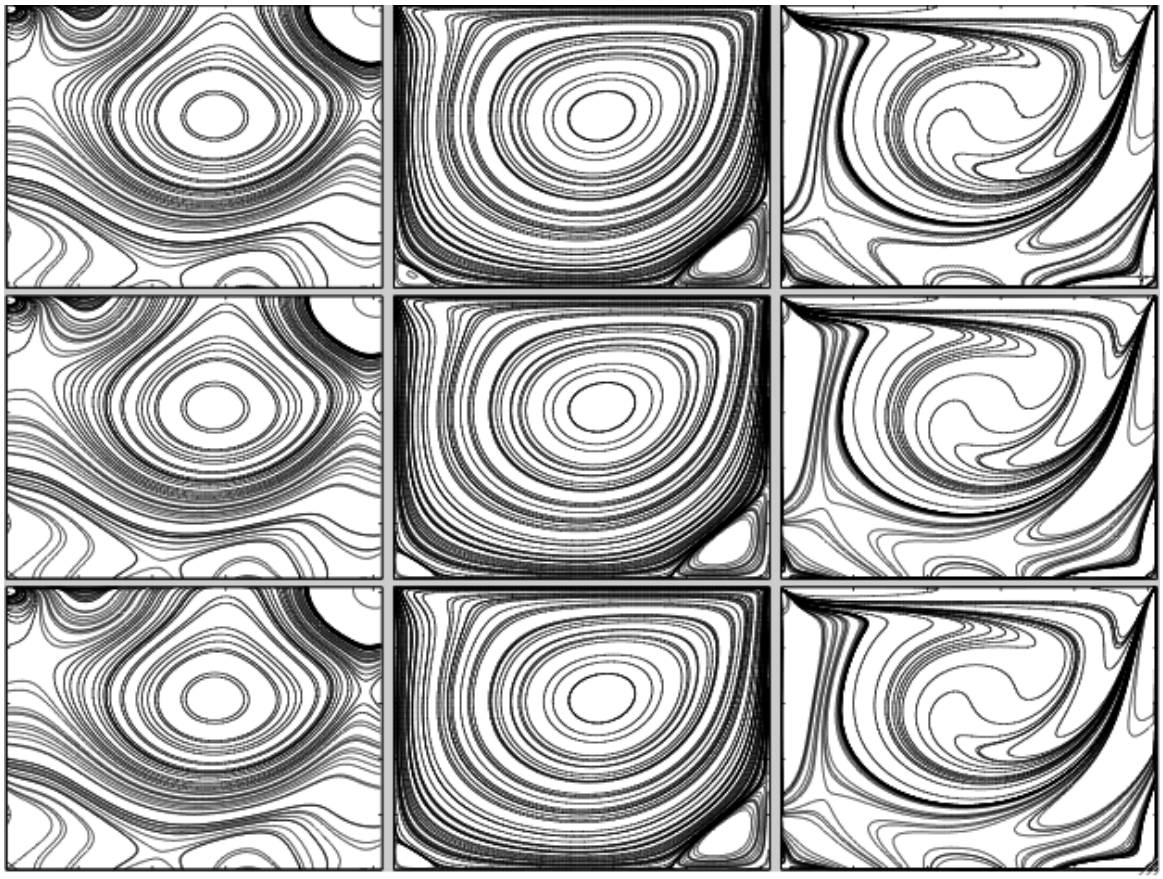

Figure 5.16: Same as Figure 5.15, Re= 400

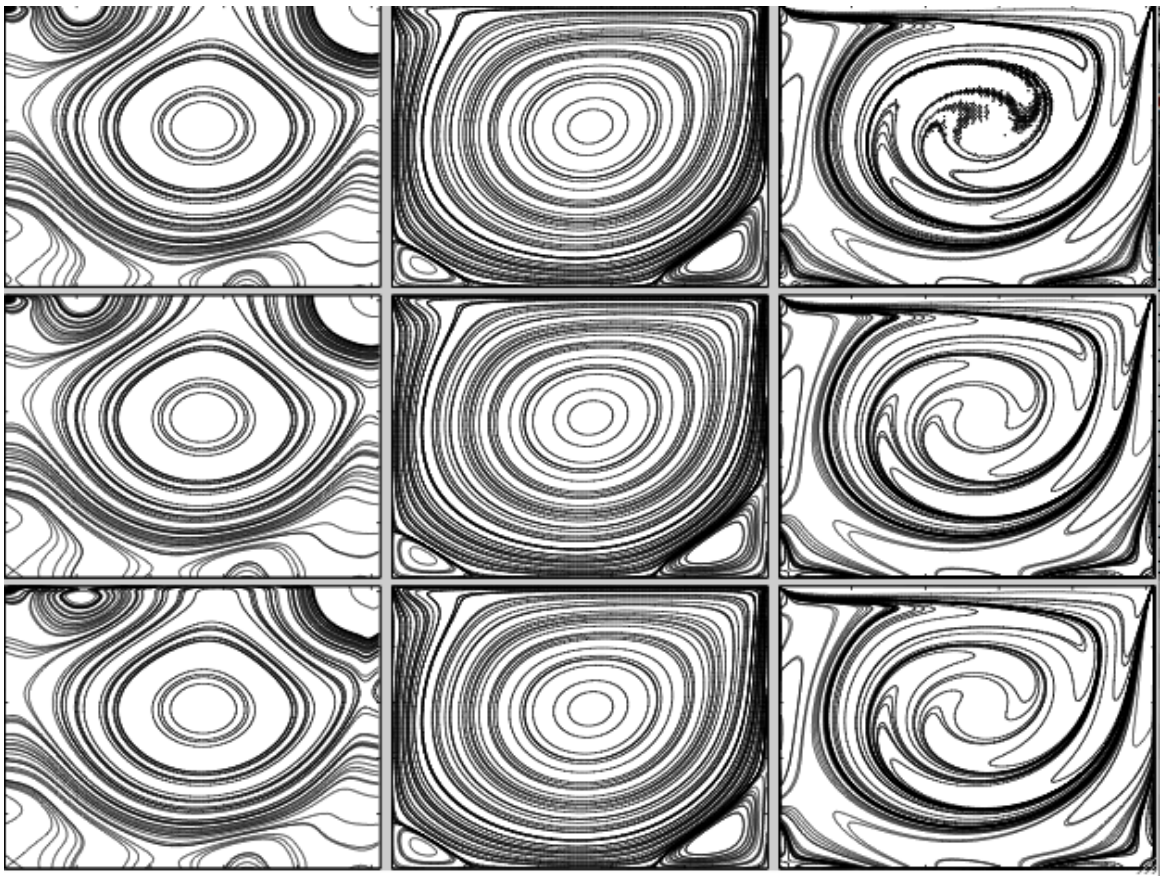

Figure 5.17: Same as Figure 5.15, Re= 1000

Table 5.8: Main Vortex Results, N_x =129

Re=100	N_x	$\hat{\psi}_{\min}$	x	y	$\hat{\delta\pi}$	$\hat{\omega}$
Comsol	129	-0.10345	0.61811	0.73828	-0.077497	-3.1943
LBGK	129	-0.10352	0.61811	0.73047	-0.077679	-3.1841
EF3	129	-0.10366	0.61811	0.73047	-0.10345	-3.1858
MRT	129	-0.10344	0.61811	0.73047	-0.077751	-3.1814
Minxent4	129	-0.10352	0.61811	0.73047	-0.077893	-3.1841
TRT	129	-0.10343	0.61811	0.73047	-0.077764	-3.1814
Minxent2	129	-0.10343	0.61811	0.73047	-0.077554	-3.1814
Re=400	N	$\hat{\psi}_{\min}$	x	y	$\hat{\delta\pi}$	$\hat{\omega}$
Comsol	129	-0.11387	0.55512	0.60547	-0.077692	-2.2904
LBGK	129	-0.11269	0.55512	0.60547	-0.07716	-2.2835
EF3	129	-0.13721	0.5315	0.67578	-0.14495	-3.4764
MRT	129	-0.11244	0.55512	0.60547	-0.076837	-2.2801
Minxent4	129	-0.11256	0.55512	0.60547	-0.076972	-2.278
TRT	129	-0.11244	0.55512	0.60547	-0.076841	-2.2801
Minxent2	129	-0.11242	0.55512	0.60547	-0.076742	-2.2798
Re=1000	N_x	$\hat{\psi}_{\min}$	x	y	$\hat{\delta\pi}$	$\hat{\omega}$
Comsol	129	-0.11874	0.5315	0.56641	-0.074017	-2.0615
LBGK	129	-0.11832	0.5315	0.55859	-0.074487	-2.0658
EF3	129	-0.14152	0.51575	0.66797	-0.15399	-3.6574
MRT	129	-0.11767	0.5315	0.55859	-0.073686	-2.0563
Minxent4	129	-0.11825	0.5315	0.55859	-0.074309	-2.0615
TRT	129	-0.11775	0.5315	0.55859	-0.073815	-2.0577
Minxent2	129	-0.1175	0.5315	0.55859	-0.07321	-2.0535

Table 5.9: Main Vortex Results, N_x =257

Re=100	N_x	$\hat{\psi}_{\min}$	x	y	$\hat{\delta\pi}$	$\hat{\omega}$
Comsol	257	-0.10347	0.61765	0.73633	-0.077177	-3.1783
LBGK	257	-0.10336	0.61765	0.73633	-0.077439	-3.1849
EF3	257	-0.1034	0.61765	0.73633	-0.077155	-3.1854
MRT	257	-0.10333	0.61765	0.73633	-0.077375	-3.1839
Minxent4	257	-0.10336	0.61765	0.73633	-0.077414	-3.1846
TRT	257	-0.10332	0.61765	0.73633	-0.077376	-3.1838
Minxent2	257	-0.10333	0.61765	0.73633	-0.077336	-3.1839
Re=400	N_x	$\hat{\psi}_{\min}$	x	y	$\hat{\delta\pi}$	$\hat{\omega}$
Comsol	257	-0.1139	0.5549	0.60352	-0.07765	-2.292
LBGK	257	-0.11259	0.5549	0.60352	-0.076446	-2.2807
EF3	257	-0.1305	0.53137	0.62305	-0.1078	-2.721
MRT	257	-0.11253	0.5549	0.60352	-0.076367	-2.2797
Minxent4	257	-0.11251	0.5549	0.60352	-0.076361	-2.2758
TRT	257	-0.11253	0.5549	0.60352	-0.076363	-2.2797
Minxent2	257	-0.11254	0.5549	0.60352	-0.076453	-2.28
Re=1000	N_x	$\hat{\psi}_{\min}$	x	y	$\hat{\delta\pi}$	$\hat{\omega}$
Comsol	257	-0.11881	0.53137	0.56445	-0.074009	-2.0634
LBGK	257	-0.11818	0.53137	0.56445	-0.073636	-2.06
EF3	257	-0.14223	0.50784	0.62305	-0.12897	-2.8944
MRT	257	-0.11802	0.53137	0.56445	-0.073445	-2.0576
Minxent4	257	-0.11808	0.53137	0.56445	-0.073515	-2.0552
TRT	257	-0.11802	0.53137	0.56445	-0.07345	-2.0576
Minxent2	257	-0.11801	0.53137	0.56445	-0.073452	-2.0574

Table 5.10: Lower Right Vortex Results, N_x =65

Re=100	N_x	$\hat{\psi}_{\max}\,(10^{-5})$	x	y	$\hat{\delta\pi}\,(10^{-2})$	$\hat{\omega}\,(10^{-2})$
Comsol	65	2.0524	0.99206	0.35156	1.0364	-6.0868
LBGK	65	2.0683	0.99206	0.32031	2.2206	-2.3269
MRT	65	2.4288	0.99206	0.35156	0.8597	-7.5582
Minxent4	65	2.1569	0.99206	0.33594	1.1365	-6.9639
TRT	65	2.4182	0.99206	0.35156	0.8695	-7.5803
Minxent2	65	2.4489	0.99206	0.35156	0.90453	-7.5212
Re=400	N_x	$\hat{\psi}_{\max}\,(10^{-4})$	x	y	$\hat{\delta\pi}\,(10^{-2})$	$\hat{\omega}\,(10^{-1})$
Comsol	65	6.6322	0.88095	0.11719	2.8919	4.3576
LBGK	65	6.0882	0.88095	0.11719	2.6579	4.3657
MRT	65	6.3413	0.88095	0.11719	2.6155	4.316
Minxent4	65	6.1493	0.88095	0.11719	2.6751	4.3558
TRT	65	6.3768	0.88095	0.11719	2.6126	4.3043
Minxent2	65	6.2676	0.88095	0.11719	2.6842	4.3641
Re=1000	N_x	$\hat{\psi}_{\max}\,(10^{-3})$	x	y	$\hat{\delta\pi}\,(10^{-2})$	$\hat{\omega}$
Comsol	65	1.7195	0.86508	0.11719	3.4531	1.1257
LBGK	65	1.5709	0.86508	0.11719	3.2124	1.1265
MRT	65	1.7228	0.86508	0.11719	3.0807	1.1088
Minxent4	65	1.6023	0.86508	0.11719	3.3216	1.1284
TRT	65	1.707	0.86508	0.11719	3.0895	1.0742
Minxent2	65	1.823	0.86508	0.11719	3.2199	1.1583

Table 5.11: Lower Right Vortex Results, N_x =129

Re=100	N_x	$\hat{\psi}_{\max}\,(10^{-5})$	x	y	$\hat{\delta\pi}\,(10^{-2})$	$\hat{\omega}\,(10^{-2})$
Comsol	129	1.2346	0.94094	0.058594	2.03	3.3841
LBGK	129	1.1956	0.94094	0.058594	1.9812	3.3754
EF3	129	16.291	0.99606	0.33984	2.9701	-2.2103
MRT	129	1.2456	0.94094	0.058594	1.9824	3.3987
Minxent4	129	1.2055	0.94094	0.058594	1.9903	3.3773
TRT	129	1.2458	0.94094	0.058594	1.9813	3.3988
Minxent2	129	1.2454	0.94094	0.058594	2.001	3.3989
Re=400	N_x	$\hat{\psi}_{\max}(10^{-4})$	x	y	$\hat{\delta\pi}\,(10^{-2})$	$\hat{\omega}\,(10^{-1})$
Comsol	129	6.5059	0.88583	0.12109	2.9161	4.3441
LBGK	129	6.2807	0.88583	0.12109	2.7841	4.3278
EF3	129	13.807	0.80709	0.11328	0.012344	2.8654
MRT	129	6.3231	0.88583	0.12109	2.7714	4.316
Minxent4	129	6.2799	0.88583	0.12109	2.7767	4.3226
TRT	129	6.3236	0.88583	0.12109	2.7714	4.316
Minxent2	129	6.3171	0.88583	0.12109	2.7768	4.3177
Re=1000	N_x	$\hat{\psi}_{\max}\,(10^{-3})$	x	y	$\hat{\delta\pi}\,(10^{-2})$	$\hat{\omega}$
Comsol	129	1.7229	0.8622	0.11328	3.5042	1.1407
LBGK	129	1.6922	0.8622	0.11328	3.4109	1.1415
EF3	129	2.1583	0.77559	0.18359	2.3824	0.61059
MRT	129	1.7113	0.8622	0.11328	3.3699	1.1317
Minxent4	129	1.693	0.8622	0.11328	3.4136	1.1409
TRT	129	1.7124	0.8622	0.11328	3.371	1.1308
Minxent2	129	1.7167	0.8622	0.11328	3.3927	1.1386

Table 5.12: Lower Right Vortex Results, N_x =257

Re=100	N_x	$\hat{\psi}_{\max}\,(10^{-5})$	x	y	$\hat{\delta\pi}\,(10^{-2})$	$\hat{\omega}\,(10^{-2})$
Comsol	257	1.2457	0.94314	0.060547	2.0433	3.4253
LBGK	257	1.2455	0.94314	0.060547	2.0196	3.3532
EF3	257	1.2365	0.93922	0.052734	2.0395	2.9944
MRT	257	1.2539	0.94314	0.060547	2.0184	3.3586
Minxent4	257	1.2477	0.94314	0.060547	2.0213	3.3539
TRT	257	1.2539	0.94314	0.060547	2.0183	3.3586
Minxent2	257	1.254	0.94314	0.060547	2.0227	3.3585
Re=400	N_x	$\hat{\psi}_{\max}\,(10^{-4})$	x	y	$\hat{\delta\pi}\,(10^{-2})$	$\hat{\omega}\,(10^{-1})$
Comsol	257	6.4492	0.88431	0.12305	2.935	4.7086
LBGK	257	6.303	0.88431	0.12305	2.8272	4.5192
EF3	257	10.19	0.86863	0.14648	3.1812	5.5647
MRT	257	6.2994	0.88431	0.12305	2.8279	4.5172
Minxent4	257	6.2862	0.88431	0.12305	2.8188	4.5149
TRT	257	6.2993	0.88431	0.12305	2.8281	4.5172
Minxent2	257	6.3046	0.88431	0.12305	2.8189	4.5169
Re=1000	N_x	$\hat{\psi}_{\max}\,(10^{-3})$	x	y	$\hat{\delta\pi}\,(10^{-2})$	$\hat{\omega}$
Comsol	257	1.7192	0.86471	0.11133	3.5281	1.0996
LBGK	257	1.7092	0.86471	0.11133	3.4585	1.0812
EF3	257	3.6034	0.7549	0.13477	3.2223	1.1831
MRT	257	1.7125	0.86471	0.11133	3.447	1.0784
Minxent4	257	1.7071	0.86471	0.11133	3.4503	1.0801
TRT	257	1.7126	0.86471	0.11133	3.4468	1.0784
Minxent2	257	1.7128	0.86471	0.11133	3.4446	1.0786

Table 5.13: Lower Left Vortex Results, N_x=65

Re=100	N_x	$\hat{\psi}_{\max}\,(10^{-6})$	x	y	$\hat{\delta\pi}\,(10^{-2})$	$\hat{\omega}\,(10^{-2})$
Comsol	65	1.0982	0.039683	0.023438	1.6134	0.86636
LBGK	65	0.09497	0.039683	0.023438	1.346	0.93154
MRT	65	1.1721	0.039683	0.023438	1.4454	0.91345
Minxent4	65	0.11672	0.02381	0.023438	1.4741	0.28755
TRT	65	1.1531	0.039683	0.023438	1.4411	0.90138
Minxent2	65	1.2201	0.039683	0.023438	1.5134	0.93364
Re=400	N_x	$\hat{\psi}_{\max}\,(10^{-5})$	x	y	$\hat{\delta\pi}\,(10^{-2})$	$\hat{\omega}\,(10^{-2})$
Comsol	65	1.0932	0.055556	0.039063	3.5813	4.7404
LBGK	65	0.74957	0.055556	0.039063	3.3114	4.5015
MRT	65	1.LBGK4	0.055556	0.039063	3.2633	4.5903
Minxent4	65	0.83092	0.055556	0.039063	3.3339	4.5133
TRT	65	1.1083	0.055556	0.039063	3.2676	4.5883
Minxent2	65	1.0901	0.055556	0.039063	3.3058	4.6056
Re=1000	N_x	$\hat{\psi}_{\max}\,(10^{-4})$	x	y	$\hat{\delta\pi}\,(10^{-2})$	$\hat{\omega}\,(10^{-1})$
Comsol	65	2.0277	0.087302	0.070313	4.4541	3.1701
LBGK	65	1.8388	0.087302	0.070313	4.1189	3.0663
MRT	65	1.9182	0.087302	0.070313	4.0079	3.0087
Minxent4	65	1.8264	0.087302	0.070313	4.2898	3.0681
TRT	65	1.9459	0.087302	0.070313	4.0818	3.0275
Minxent2	65	1.939	0.087302	0.070313	4.0693	2.9862

Table 5.14: Lower Left Vortex Results, N_x =129

Re=100	N_x	$\hat{\psi}_{\max}(10^{-6})$	x	y	$\hat{\delta\pi}(10^{-2})$	$\hat{\omega}(10^{-2})$
Comsol	129	1.4813	0.035433	0.035156	1.6337	1.6403
LBGK	129	1.3208	0.035433	0.035156	1.5642	1.5854
EF3	129	0	0	0	0	0
MRT	129	1.6117	0.035433	0.035156	1.5639	1.6115
Minxent4	129	1.3759	0.035433	0.035156	1.5731	1.5919
TRT	129	1.6123	0.035433	0.035156	1.5628	1.6115
Minxent2	129	1.6135	0.035433	0.035156	1.5826	1.6121
Re=400	N_x	$\hat{\psi}_{\max}(10^{-5})$	x	y	$\hat{\delta\pi}(10^{-2})$	$\hat{\omega}(10^{-2})$
Comsol	129	1.2735	0.051181	0.042969	3.5971	5.0593
LBGK	129	1.2243	0.051181	0.042969	3.4392	4.8987
EF3	129	64.155	0.50787	0.042969	3.0591	29.683
MRT	129	1.2871	0.051181	0.042969	3.4249	4.9082
Minxent4	129	1.2423	0.051181	0.042969	3.4334	4.9066
TRT	129	1.2873	0.051181	0.042969	3.4249	4.9083
Minxent2	129	1.2857	0.051181	0.042969	3.4296	4.907
Re=1000	N_x	$\hat{\psi}_{\max}(10^{-4})$	x	y	$\hat{\delta\pi}(10^{-2})$	$\hat{\omega}(10^{-1})$
Comsol	129	2.183	0.082677	0.074219	4.4655	3.2451
LBGK	129	2.1756	0.082677	0.074219	4.3529	3.1771
EF3	129	20.367	0.19291	0.16797	3.3597	5.1709
MRT	129	2.1942	0.082677	0.074219	4.3132	3.1633
Minxent4	129	2.1835	0.082677	0.074219	4.3571	3.1804
TRT	129	2.1981	0.082677	0.074219	4.3182	3.1662
Minxent2	129	2.1887	0.082677	0.074219	4.3234	3.158

Table 5.15: Lower Left Vortex Results, N_x =257

Re=100	N_x	$\hat{\psi}_{\max}(10^{-6})$	x	y	$\hat{\delta\pi}(10^{-2})$	$\hat{\omega}(10^{-2})$
Comsol	257	1.6489	0.033333	0.033203	1.6384	1.3439
LBGK	257	1.6893	0.033333	0.033203	1.6029	1.3356
EF3	257	1.7749	0.033333	0.037109	1.617	1.5947
MRT	257	1.7358	0.033333	0.033203	1.6012	1.3394
Minxent4	257	1.7009	0.033333	0.033203	1.6046	1.3366
TRT	257	1.7358	0.033333	0.033203	1.6011	1.3394
Minxent2	257	1.7356	0.033333	0.033203	1.6056	1.3394
Re=400	N_x	$\hat{\psi}_{\max}(10^{-5})$	x	y	$\hat{\delta\pi}(10^{-2})$	$\hat{\omega}(10^{-2})$
Comsol	257	1.3374	0.052941	0.044922	3.6042	5.6698
LBGK	257	1.3307	0.052941	0.044922	3.4853	5.5808
EF3	257	3.8934	0.076471	0.037109	4.5367	6.7884
MRT	257	1.3405	0.052941	0.044922	3.4778	5.5812
Minxent4	257	1.3331	0.052941	0.044922	3.4734	5.5837
TRT	257	1.3406	0.052941	0.044922	3.478	5.5813
Minxent2	257	1.3412	0.052941	0.044922	3.4722	5.5813
Re=1000	N_x	$\hat{\psi}_{\max}(10^{-4})$	x	y	$\hat{\delta\pi}(10^{-2})$	$\hat{\omega}(10^{-1})$
Comsol	257	2.2514	0.084314	0.076172	4.4704	3.5089
LBGK	257	2.2549	0.084314	0.076172	4.3907	3.4114
EF3	257	13.627	0.13922	0.12695	5.4204	6.4293
MRT	257	2.2569	0.084314	0.076172	4.3797	3.4068
Minxent4	257	2.255	0.084314	0.076172	4.382	3.4119
TRT	257	2.2571	0.084314	0.076172	4.3797	3.4069
Minxent2	257	2.2562	0.084314	0.076172	4.3764	3.406

Chapter 6

Conclusions

6.1 Conclusions

We began this thesis by describing the traditional interpretations of the single relaxation time Lattice Boltzmann Method; as a generalization of the Lattice Gas Automata or as a discretization of the Boltzmann Equation. In the pursuit of increasing the stability of the LBM some researchers attempted to equip the LBM with an H-Theorem. The H-Theorem would provide an equilibrium that is the minimizer of some entropy function and would also act as an attractor. It is hypothesized that an equilibrium with these features would help stabilize the method. The most popular of these methods is called the Entropic Lattice Boltzmann Method (ELBM).

The ELBM has been criticized by other researchers who believed that the most promising and practical route to stabilization was by using multiple relaxation times. This has led to somewhat of a split in the LBM community; those who embrace entropic methods such as ELBM and entropic limiters, and those who prefer multiple relaxation times.

We however believe that these two seemingly dissimilar approaches are specific implementations of our unified interpretation of LBM. We proposed that the LBM is a split-time scheme that implements the principle of Minimum Discrimination INformation (MinxEnt). Indeed we show that the entropic methods and relaxation time methods are specific approximations of MinxEnt-LBM. In this way we unify the entropic and relaxation time schemes.

Because the entropic and relaxation time schemes are approximations of MinxEnt-LBM, we expect that MinxEnt-LBM should have superior stability characteristics. This indeed was shown in numerical simulations carried out here. The only scheme that performed superior to MinxEnt-LBM was the entropy limiting scheme of the LBM based on Ehrenfest Steps (EF-LBM). However, lid driven cavity flow simulations showed that without tuning the parameters involved in EF-LBM schemes they suffered from a degradation of accuracy. We can conclude that, of the LBM schemes tested, MinxEnt-LBM had the best combination of stability and accuracy.

An important practical consideration should also be noted here. EF-LBM and MRT-LBM require specification of parameters which need to be tuned and optimal values are not known *a priori*. This is not the case for the MinxEnt-LBM.

Finally, the development of the MinxEnt-LBM scheme was based on constraints and an entropy function only, and did not use the Navier-Stokes equations to obtain values for its parameters. This cannot be said about the other LBM schemes described here. This means that the MinxEnt-LBM is much more suited to be applied to non-fluid systems or systems in which the governing macroscopic equations are unknown.

6.2 Future Work

The MinxEnt-LBM described here used a single step Newton-Raphson method to perform the minimizations. It is hypothesized here that instabilities occur in the LBM due to inaccuracies in these minimizations. This suggests a route for enhancing stability; use more sophisticated, robust and accurate methods than Newton-Raphson to perform the minimization.

Also, due to the aforementioned general nature of the MinxEnt-LBM, work that uses MinxEnt-LBM to simulate non-fluid related physical systems may be explored. In fact, nothing in development of the MinxEnt-LBM scheme suggested that it could only be applied to mass transport type problems. This would make MinxEnt-LBM a promising method to explore systems which have no pre-defined governing equations. One possible application may be to simulate a system at the microscopic level (using other methods such as Molecular Dynamics simulations, or Density Functional Theory) to obtain constraints inherent (and non-obvious) of the system. These constraints could then be used in the MinxEnt-LBM scheme to simulate the mesoscopic or macroscopic evolution of the system. In this way, the macroscopic governing equations would be an *emergent* property of the method, and not a crucial ingredient.

Our novel interpretation of the Lattice Boltzmann Method not only improves the stability and accuracy of the current implementations of the LBM, but also provides a unifying framework on which to base them on. This framework opens a large number of different possibilities for future improvements to the Lattice Boltzmann Method and a much wider range of possible application.

Appendices

Appendix A

Probability and Mass Expectation Distributions

Consider a classical system, of a large number, N, of identical particles of mass m in D dimensions. Rather than track the particles individually we treat the position and velocity of each particle as random variables.

$$X(t) = \{\mathbf{X}_j(t) \,|\, j = 1 \ldots N\},$$
$$V(t) = \{\mathbf{V}_j(t) \,|\, j = 1 \ldots N\},$$

where $\mathbf{X}_j$ and $\mathbf{V}_j$ are random variables describing the jth particle's position and velocity respectively. We define a "microscopic state," Γ, to be a vector of specific realizations of the random positions and velocities of the particles. That is,

$$\Gamma(t) = \langle \mathbf{X}_1(t) = \mathbf{x}_1, \ldots, \mathbf{X}_N(t) = \mathbf{x}_N, \mathbf{V}_1(t) = \mathbf{v}_1, \ldots \mathbf{V}_N(t) = \mathbf{v}_N \rangle.$$

Imagine that we would like to predict the value of a macroscopic observable quantity that is a function of the positions and velocities of all of the particles in the system. Call this function $G(\Gamma(t))$. Rather than measure actual values for G, laboratory devices usually measure time averages of G. That is, devices measure G_{obs} which is given by,

$$G_{obs}(t) = \frac{1}{\Delta t} \int_t^{t+\Delta t} G(\Gamma(s))\, ds.$$

This suggests that following the precise location of all the particles at all times may in fact give us more information than we could actually use. With this in mind we wish to find a way to track these averaged quantities instead.

Given a specific position $\mathbf{x}$ and velocity $\mathbf{v}$ we denote the joint probability of finding a particle with velocity $\mathbf{v}$ *and* at position $\mathbf{x}$ at time t as,

$$p_{\text{joint}}(\mathbf{x}, \mathbf{v}, t) \equiv P\left[\bigcup_{j=1}^{N} \left(\mathbf{X}_j(t) = \mathbf{x} \bigcap \mathbf{V}_j(t) = \mathbf{v}\right)\right], \tag{A.1}$$

where $P(Y)$ denotes the probability of event Y occurring. We also denote the conditional probability

of finding a particle with velocity $\mathbf{v}$ *given* that it is located at position $\mathbf{x}$ as,

$$p(\mathbf{x}, \mathbf{v}, t) \equiv P\left[\bigcup_{j=1}^{N} (\mathbf{V}_j(t) = \mathbf{v} \mid \mathbf{X}_j(t) = \mathbf{x})\right].$$

Finally the marginal probability of finding a particle at position $\mathbf{x}$ at time t (regardless of its velocity) as,

$$p_{\text{marg}}(\mathbf{x}, t) \equiv P\left[\bigcup_{j=1}^{N} (\mathbf{X}_j(t) = \mathbf{x})\right].$$

We now define the the mass expectation density, f, to be,

$$f(\mathbf{x}, \mathbf{v}, t) := Nmp_{\text{joint}}(\mathbf{x}, \mathbf{v}, t), \tag{A.2}$$

and note that f has the following properties,

$$\int f(\mathbf{x}, \mathbf{v}, t) d\mathbf{v} = \rho(\mathbf{x}, t) = Nmp_{\text{marg}}(\mathbf{x}, t),$$
$$\int f(\mathbf{x}, \mathbf{v}, t)\, d\mathbf{v} d\mathbf{x} = Nm,$$

where $\rho(\mathbf{x}, t)$ is the mass density at position $\mathbf{x}$ at time t.

The relationship between f and p can be found by using the definition of conditional probability. For events A and B, the conditional probability is defined by,

$$P(A|B) = \frac{P(A \cap B)}{P(B)},$$

which for us becomes,

$$p(\mathbf{x}, \mathbf{v}, t) = \frac{p_{\text{joint}}(\mathbf{x}, \mathbf{v}, t)}{p_{\text{marg}}(\mathbf{x}, t)}$$

And so for our system,

$$\begin{aligned} f(\mathbf{x}, \mathbf{v}, t) &= Nmp_{\text{joint}}(\mathbf{x}, \mathbf{v}, t) \\ &= Nmp(\mathbf{x}, \mathbf{v}, t)p_{\text{marg}}(\mathbf{x}, t), \\ &= p(\mathbf{x}, \mathbf{v}, t) \int f(\mathbf{x}, \mathbf{v}, t)\, d\mathbf{v}, \\ &= p(\mathbf{x}, \mathbf{v}, t)\rho(\mathbf{x}, t), \end{aligned}$$

and thus, if the mass density is non-zero then,

$$p(\mathbf{x}, \mathbf{v}, t) = \frac{f(\mathbf{x}, \mathbf{v}, t)}{\rho(\mathbf{x}, t)}. \tag{A.3}$$

Note that for all positions and times, p is a probability distribution with respect to $\mathbf{v}$,

$$\int p(\mathbf{x}, \mathbf{v}, t)\, d\mathbf{v} = 1,$$

Consider a vector of k macroscopic quantities

$$\mathbb{M}(t) := \langle \mathbb{M}_1(\mathbf{X}(t), \mathbf{V}(t)), .., \mathbb{M}_k(\mathbf{X}(t), \mathbf{V}(t)) \rangle,$$

such as density, mean velocity, temperature, etc. Further, let $\mathcal{M}(t)$ denote a vector of k realizations of these macroscopic quantities at a given time t,

$$\mathcal{M}(t) := \langle \mathcal{M}_1, ..., \mathcal{M}_k \rangle.$$

In this case we say that at time t a system is in the "macroscopic state," $\mathcal{M}(t)$.

A system in a given macroscopic state could be in any of a large number of different microscopic states. The set of all microscopic states that share the same macroscopic state is called the *ensemble*; denoted $\mathcal{E}$,

$$\mathcal{E}(\mathcal{M}(t)) := \{\Gamma(t) \,|\, \mathbb{M}(t) = \mathcal{M}(t)\}$$

Now, suppose that at a given time t, and that the system is in macroscopic state, $\mathcal{M}(t)$. We can define the following quantities,

$$\begin{aligned}
P(\Gamma(t)) :=& \text{probability that the system is in microscopic state } \Gamma(t) \\
P\left[\Gamma(t)|\mathcal{M}(t)\right] :=& \text{probability of the system being in microscopic state } \Gamma(t) \\
& \text{given it's in macroscopic state } \mathcal{M}(t) \\
P\left[(\mathbf{x}, \mathbf{v}, t) \cap \Gamma(t)\right] :=& \text{probability of a particle being at position } \mathbf{x} \text{ with velocity } \mathbf{v} \\
& \textit{and} \text{ that the system is in microscopic state } \Gamma(t) \\
P\left[\Gamma \,|\, (\mathbf{x}, \mathbf{v}, t)\right] :=& \text{ probability that the system is in microscopic state } \Gamma(t) \\
& \text{given that there is a particle at position } \mathbf{x} \text{ with velocity } \mathbf{v}
\end{aligned}$$

Using these definitions and the axioms of probability we can calculate the ensemble average, $\langle G \rangle$, of observable G. Let $d\Gamma = d\mathbf{x}_1 ... d\mathbf{x}_N d\mathbf{v}_1 ... d\mathbf{v}_N$ be the differential change in the microscopic state then we have,

$$\begin{aligned}
\langle G \rangle(t) &= \int_{\Gamma \in \mathcal{E}} P(\Gamma)\, G(\Gamma)\, d\Gamma \\
&= \int_{\Gamma \in \mathcal{E}} \iint P\left[(\mathbf{x}', \mathbf{v}', t) \cap \Gamma\right]\, G(\Gamma)\, d\mathbf{x}'\, d\mathbf{v}'\, d\Gamma \\
&= \int_{\Gamma \in \mathcal{E}} \iint p_{\text{joint}}(\mathbf{x}', \mathbf{v}', t)\, P\left[\Gamma|(\mathbf{x}', \mathbf{v}', t)\right]\, G(\Gamma)\, d\mathbf{x}'\, d\mathbf{v}'\, d\Gamma \\
&= \iint p_{\text{joint}}(\mathbf{x}', \mathbf{v}', t) \int_{\Gamma \in \mathcal{E}} P\left[\Gamma|(\mathbf{x}', \mathbf{v}', t)\right]\, G(\Gamma)\, d\mathbf{x}'\, d\mathbf{v}'\, d\Gamma \\
&= \iint p_{\text{joint}}(\mathbf{x}', \mathbf{v}', t)\, g(\mathbf{x}', \mathbf{v}', t)\, d\mathbf{x}'\, d\mathbf{v}'
\end{aligned} \tag{A.4}$$

where we have defined

$$g(\mathbf{x}', \mathbf{v}', t) \equiv \int_{\Gamma \in \mathcal{E}} P(\Gamma|(\mathbf{x}', \mathbf{v}', t))\, G(\Gamma)\, d\Gamma. \tag{A.5}$$

One can think of $g(\mathbf{x}, \mathbf{v}, t)$ as representing the expectation value of the observable, G, given that there is a particle located at position $\mathbf{x}$, with velocity $\mathbf{v}$, at time t.

Assuming the ergodic hypothesis holds, we can equate the ensemble average and the time average

and so,

$$G_{\text{obs}}(t) = \langle G \rangle(t) = \iint p_{\text{joint}}(\mathbf{x}', \mathbf{v}', t)\, g(\mathbf{x}', \mathbf{v}', t)\, d\mathbf{x}'\, d\mathbf{v}'.$$

For example, to evaluate the observed macroscopic density, ρ, at position $\mathbf{x}$ at time t we would use $g(\mathbf{x}', \mathbf{v}', t) = Nm\,\delta(\mathbf{x}' - \mathbf{x})$ in (A.4),

$$\rho(\mathbf{x}, t) = \iint Nmp_{\text{joint}}(\mathbf{x}', \mathbf{v}', t)\, \delta(\mathbf{x}' - \mathbf{x})\, d\mathbf{x}'\, d\mathbf{v}' \tag{A.6}$$

For the macroscopic momentum, $\rho\,\mathbf{u}$, at position $\mathbf{x}$ at time t at position $\mathbf{x}$ at time t we would use $g(\mathbf{x}', \mathbf{v}', t) = Nm\mathbf{v}'\,\delta(\mathbf{x}' - \mathbf{x})$,

$$\rho(\mathbf{x}, t)\mathbf{u}(\mathbf{x}, t) = \iint \mathbf{v}' Nmp_{\text{joint}}(\mathbf{x}', \mathbf{v}', t)\, \delta(\mathbf{x}' - \mathbf{x})\, d\mathbf{x}'\, d\mathbf{v}' \tag{A.7}$$

Recalling the mass expectation density, (A.2), we can write,

$$\begin{aligned}
\rho(\mathbf{x}, t) &= \iint f(\mathbf{x}', \mathbf{v}', t)\, \delta(\mathbf{x}' - \mathbf{x})\, d\mathbf{x}'\, d\mathbf{v}' \\
&= \int f(\mathbf{x}, \mathbf{v}', t)\, d\mathbf{v}' \\
\rho(\mathbf{x}, t)\mathbf{u}(\mathbf{x}, t) &= \iint f(\mathbf{x}', \mathbf{v}', t)\mathbf{v}'\, \delta(\mathbf{x}' - \mathbf{x})\, d\mathbf{x}'\, d\mathbf{v}' \\
&= \int f(\mathbf{x}, \mathbf{v}', t)\, \mathbf{v}'\, d\mathbf{v}'
\end{aligned}$$

It is still an area of active research as to the conditions under which the ergodic hypothesis holds. However, we will assume that it holds.

Appendix B

D2Q9 Fluid Constraint

B.1 Isotropic Newtonain Fluids

From continuum mechanics we know that any continuum that obeys conservation of mass follows the Cauchy momentum equation,

$$\rho \frac{d\mathbf{u}}{dt} = \nabla \cdot \sigma + \rho \mathbf{g}$$

where ρ is the mass density, $\mathbf{u}$ is the macroscopic velocity, σ is the Cauchy stress tensor and $\mathbf{g}$ is a body force. In kinetic theory σ is related to the mass expectation distribution by,

$$\begin{aligned}\sigma_{jk}(\mathbf{x}, t) &= \int f(\mathbf{x}, \mathbf{v}, t)(\mathbf{v} - \mathbf{u})_j (\mathbf{v} - \mathbf{u})_k \, d\mathbf{v} \\ &= \int f(\mathbf{x}, \mathbf{v}, t)\mathbf{v}_j \mathbf{v}_k \, d\mathbf{v} - \rho \mathbf{u}_j \mathbf{u}_k\end{aligned}$$

For an isotropic Newtonian fluid the stress tensor is related to the strain-rate tensor by,

$$\sigma_{jk} = -\pi \delta_{jk} + 2\mu \varepsilon_{jk} \tag{B.1}$$

where π is the hydrostatic pressure, μ is the kinematic viscosity and ε is the strain-rate tensor,

$$\varepsilon_{jk} = \frac{1}{2}\left[\frac{\partial u_j}{\partial x_k} + \frac{\partial u_k}{\partial x_j}\right].$$

In what follows we will derive the constraints that need to be applied to the collision step to ensure (B.1) holds and thus allow an LBM simulation to simulate an isotropic Newtonian fluid.

B.2 D2Q9 LBM Configuration

Recall the two dimensional, 9 velocity LBM. The velocity set is given in Table B.1.

Table B.1: D2Q9 Velocity Scheme: $c = \sqrt{3RT}$

i	1	2	3	4	5	6	7	8	9
$\mathbf{v}_i$	(c,0)	(0,c)	(-c,0)	(0,-c)	(c,c)	(-c,c)	(-c,-c)	(c,-c)	(0,0)
W_i	$\frac{1}{9}$	$\frac{1}{9}$	$\frac{1}{9}$	$\frac{1}{9}$	$\frac{1}{36}$	$\frac{1}{36}$	$\frac{1}{36}$	$\frac{1}{36}$	$\frac{4}{9}$

The streaming step and the discrete polynomial equilibrium is given in equations (B.2) and (B.3) respectively,

$$\mathbf{f}_i(\mathbf{x} + \mathbf{v}_i\delta_t, t + \delta_t) = \mathbf{f}_i^{\text{post}}(\mathbf{x}, t), \tag{B.2}$$

$$\mathbf{f}_i^{\text{eq}} = \rho\, W_i \left\{1 - \frac{3|\mathbf{u}|^2}{2c^2} + \frac{3\mathbf{v}_i \cdot \mathbf{u}}{c^2} + \frac{9(\mathbf{v}_i \cdot \mathbf{u})^2}{2c^4}\right\}. \tag{B.3}$$

B.3 D2Q9 Tensor Identities

From the expression for the equilibrium distribution (B.3), one can easily show that in D2Q9 we have the following identities [11],

$$\sum_{i=1}^{9} \mathbf{f}_i^{\text{eq}} = \rho, \tag{B.4}$$

$$\sum_{i=1}^{9} \mathbf{f}_i^{\text{eq}} \mathbf{v}_{i,j} = \rho \mathbf{u}_j, \tag{B.5}$$

$$\sum_{i=1}^{9} \mathbf{f}_i^{\text{eq}} \mathbf{v}_{i,j} \mathbf{v}_{i,k} = \frac{1}{3} c^2 \rho \delta_{jk} + \rho \mathbf{u}_j \mathbf{u}_k, \tag{B.6}$$

$$\sum_{i=1}^{9} \mathbf{f}_i^{\text{eq}} \mathbf{v}_{i,j} \mathbf{v}_{i,k} \mathbf{v}_{i,l} = \frac{1}{3} c^2 \rho \left(\delta_{jk}\mathbf{u}_l + \delta_{kl}\mathbf{u}_j + \delta_{jl}\mathbf{u}_k\right), \tag{B.7}$$

B.4 Chapman-Enskog Expansion

We will perform a procedure based on the one outlined in the appendix of [11] (commonly known as Chapman-Enskog analysis). For brevity, we introduce the expansion parameter $\epsilon = \delta_t$ and assume that $\epsilon << 1$.

Performing a Taylor expansion,

$$\mathbf{f}_i(\mathbf{x} + \mathbf{v}_i\delta_t, t + \delta_t) = \sum_{n=0}^{\infty} \frac{\epsilon^n}{n!} D^n f^{\text{pre}} \tag{B.8}$$

where we define the multi-scale expansions,

$$\begin{aligned} D &:= D_0 + \epsilon D_1 + \mathcal{O}(\epsilon^2), \\ D_0 &:= \frac{\partial}{\partial t_0} + \sum_{k=1}^{2} \mathbf{v}_{i,k} \frac{\partial}{\partial x_k}, \\ D_1 &:= \frac{\partial}{\partial t_1} \\ \frac{\partial}{\partial t} &= \frac{\partial}{\partial t_0} + \epsilon \frac{\partial}{\partial t_1} + \mathcal{O}(\epsilon^2). \end{aligned}$$

We also expand the pre-collision distribution,

$$\mathbf{f}_i^{\text{pre}} = \mathbf{f}_i^{\text{eq}} + \epsilon \mathbf{f}_i^1 + \mathcal{O}(\epsilon^2). \tag{B.9}$$

We will also find it useful to define,

$$\Pi^0_{jk} := \sum_{i=1}^{9} \mathbf{f}_i^{\text{eq}} \mathbf{v}_{i,j} \mathbf{v}_{i,k} \tag{B.10}$$

$$\Pi^1_{jk} := \sum_{i=1}^{9} \mathbf{f}_i^{1} \mathbf{v}_{i,j} \mathbf{v}_{i,k} \tag{B.11}$$

With these expansions in hand, we now show that choosing the equilibrium as (B.3) and ensuring the collision has 3 important properties has the consequence that we recover the LBM version of the Cauchy momentum equation and satisfy (B.1).

B.5 Consequences of Equilibrium and Collision Constraints

Theorem B.5.1. If the equilibrium distribution is given as in (B.3), and the collision step satisfies the following three properties,

1. $\sum_{i=1}^{9} \mathbf{f}_i^{\text{post}} = \sum_{i=1}^{9} \mathbf{f}_i^{\text{pre}}$
2. $\sum_{i=1}^{9} \mathbf{f}_i^{\text{post}} \mathbf{v}_{i,j} = \sum_{i=1}^{9} \mathbf{f}_i^{\text{pre}} \mathbf{v}_{i,j}$
3. $\sum_{i=1}^{9} D_0 f^{\text{eq}} \mathbf{v}_{i,j} \mathbf{v}_{i,k} = -\frac{1}{\tau} \sum_{i=1}^{9} \mathbf{f}_i^{1} \mathbf{v}_{i,j} \mathbf{v}_{i,k}$

then the D2Q9 version of LBM will simulate the continuity equation and modified Cauchy momentum equation,

$$\frac{\partial \rho}{\partial t} + \nabla \cdot (\rho \mathbf{u}) = 0$$
$$\rho \frac{d\mathbf{u}}{dt} = \nabla \cdot \sigma^{\text{LBM}}$$

where,

$$\sigma^{\text{LBM}} = -\frac{c^2}{3}\rho + 2\mu\varepsilon_{jk},$$

and

$$\mu = \epsilon\rho\frac{c^2}{3}\left(\frac{2\tau - 1}{2}\right),$$

up to $\mathcal{O}(\epsilon^2)$ and $\mathcal{O}(\mathbf{u}^3)$

Proof. Before beginning we make note of the following fact,

$$\begin{aligned}\rho &= \sum_{i=1}^{9} \mathbf{f}_i^{\text{pre}} \\ &= \sum_{i=1}^{9} \mathbf{f}_i^{\text{eq}} + \epsilon \mathbf{f}_i^{1} + \mathcal{O}(\epsilon^2) \\ &= \rho + \epsilon \mathbf{f}_i^{1} + \mathcal{O}(\epsilon^2)\end{aligned}$$

and thus,

$$\sum_{i=1}^{9} \mathbf{f}_i^{1} = \mathcal{O}(\epsilon). \tag{B.12}$$

Similarly,

$$\begin{aligned}\rho\mathbf{u} &= \sum_{i=1}^{9} \mathbf{f}_i^{\text{pre}} \mathbf{v}_i \\ &= \sum_{i=1}^{9} \mathbf{f}_i^{\text{eq}} \mathbf{v}_i + \epsilon \mathbf{f}_i^1 \mathbf{v}_i + \mathcal{O}(\epsilon^2) \\ &= \rho\mathbf{u} + + \epsilon \mathbf{f}_i^1 \mathbf{v}_i + \mathcal{O}(\epsilon^2)\end{aligned}$$

And so,

$$\sum_{i=1}^{9} \mathbf{f}_i^1 \mathbf{v}_i = \mathcal{O}(\epsilon). \tag{B.13}$$

Starting with the local conservation of mass property of the collision step and making use of the streaming step (B.2) and expansion (B.9) we have,

$$\begin{aligned}\sum_{i=1}^{9} \mathbf{f}_i^{\text{post}} &= \sum_{i=1}^{9} \mathbf{f}_i^{\text{pre}}, \\ \sum_{i=1}^{9} \mathbf{f}_i(\mathbf{x} + \mathbf{v}_i\delta_t, t + \delta_t) &= \sum_{i=1}^{9} \mathbf{f}_i^{\text{pre}}, \\ &= \sum_{i=1}^{9} \mathbf{f}_i^{\text{eq}} + \epsilon \mathbf{f}_i^1 + \mathcal{O}(\epsilon^2)\end{aligned}$$

and thus from the Taylor expansion (B.8),

$$\sum_{i=1}^{9} \sum_{n=0}^{\infty} \frac{\epsilon^n}{n!} D^n \mathbf{f}_i^{\text{pre}} = \sum_{i=1}^{9} \mathbf{f}_i^{\text{eq}} + \epsilon \mathbf{f}_i^1 + \mathcal{O}(\epsilon^2).$$

Equating orders of ϵ we obtain,

$$\mathcal{O}(\epsilon) : \sum_{i=1}^{9} D_0 \mathbf{f}_i^{\text{eq}} = 0 \tag{B.14}$$

$$\mathcal{O}(\epsilon^2) : \sum_{i=1}^{9} D_0 \mathbf{f}_i^1 + \frac{1}{2} D_0^2 \mathbf{f}_i^{\text{eq}} + D_1 \mathbf{f}_i^{\text{eq}} = \mathcal{O}(\epsilon^2) \tag{B.15}$$

Likewise from the local conservation of momentum property of the collision step we get,

$$\sum_{i=1}^{9} \sum_{n=0}^{\infty} \frac{\epsilon^n}{n!} D^n \mathbf{f}_i^{\text{pre}} \mathbf{v}_i = \sum_{i=1}^{9} \mathbf{f}_i^{\text{eq}} \mathbf{v}_i + \epsilon \mathbf{f}_i^1 \mathbf{v}_i + \mathcal{O}(\epsilon^2)$$

Again equating orders of ϵ,

$$\mathcal{O}(\epsilon) : \sum_{i=1}^{9} D_0 \mathbf{f}_i^{\text{eq}} \mathbf{v}_i = \mathbf{0} \tag{B.16}$$

$$\mathcal{O}(\epsilon^2) : \sum_{i=1}^{9} D_0 \mathbf{f}_i^1 \mathbf{v}_i + \frac{1}{2} D_0^2 \mathbf{f}_i^{\text{eq}} \mathbf{v}_i + D_1 \mathbf{f}_i^{\text{eq}} \mathbf{v}_i = \mathcal{O}(\epsilon^2) \tag{B.17}$$

Note that,

$$\begin{aligned}\sum_{i=1}^{9} D_0^2 \mathbf{f}_i^{\mathrm{eq}} &= \sum_{i=1}^{9} D_0 D_0 \mathbf{f}_i^{\mathrm{eq}} \\ &= \sum_{i=1}^{9} \left(\frac{\partial}{\partial t_0} + \sum_{k=1}^{2} \mathbf{v}_{i,k} \frac{\partial}{\partial x_k} \right) D_0 \mathbf{f}_i^{\mathrm{eq}} \\ &= \frac{\partial}{\partial t_0} \sum_{i=1}^{9} D_0 \mathbf{f}_i^{\mathrm{eq}} + \sum_{k=1}^{2} \frac{\partial}{\partial x_k} \sum_{i=1}^{9} D_0 \mathbf{f}_i^{\mathrm{eq}} \mathbf{v}_{i,k}.\end{aligned}$$

Using (B.14) and (B.16) we have,

$$\sum_{i=1}^{9} D_0^2 \mathbf{f}_i^{\mathrm{eq}} = 0. \tag{B.18}$$

Similarly we can use (B.16) and the assumed third property of the collision step to show,

$$\sum_{i=1}^{9} D_0^2 \mathbf{f}_i^{\mathrm{eq}} \mathbf{v}_{i,j} = -\frac{1}{\tau} \sum_{i=1}^{9} D_0 \mathbf{f}_i^{1} \mathbf{v}_{i,j}. \tag{B.19}$$

Equations (B.18) and (B.19) allow (B.14) and (B.15) to become,

$$\mathcal{O}(\epsilon) : \frac{\partial \rho}{\partial t_0} + \nabla \cdot (\rho \mathbf{u}) = 0, \tag{B.20}$$

$$\mathcal{O}(\epsilon^2) : \frac{\partial \rho}{\partial t_1} = \mathcal{O}(\epsilon^2), \tag{B.21}$$

as well as (B.16) and (B.17) to become,

$$\mathcal{O}(\epsilon) : \frac{\partial \rho \mathbf{u}}{\partial t_0} + \nabla \cdot \Pi^0 = 0 \tag{B.22}$$

$$\mathcal{O}(\epsilon^2) : \frac{\partial \rho \mathbf{u}}{\partial t_1} + \left(\frac{2\tau - 1}{2\tau} \right) \nabla \cdot \Pi^1 = \mathcal{O}(\epsilon^2) \tag{B.23}$$

Taking $(B.20) + \epsilon(B.21)$,

$$\frac{\partial \rho}{\partial t} + \nabla \cdot (\rho \mathbf{u}) = \mathcal{O}(\epsilon^3), \tag{B.24}$$

and $(B.22) + \epsilon(B.23)$,

$$\frac{\partial \rho \mathbf{u}}{\partial t} + \nabla \cdot \left[\Pi^0 + \epsilon \left(\frac{2\tau - 1}{2\tau} \right) \Pi^1 \right] = \mathcal{O}(\epsilon^3). \tag{B.25}$$

Recalling the definitions (B.10) and (B.11) we can use the identities from (B.4)-(B.7) to rewrite (B.25) as,

$$\rho \frac{d\mathbf{u}}{dt} = \nabla \cdot \sigma^{\mathrm{LBM}} + \mathcal{O}(\epsilon^2),$$

where $\frac{d}{dt}$ is the material derivative,

$$\frac{d}{dt} = \frac{\partial}{\partial t} + \mathbf{u} \cdot \nabla,$$

and

$$\sigma^{\mathrm{LBM}} = -\frac{c^2}{3}\rho\delta_{jk} - \epsilon\left(\frac{2\tau-1}{2\tau}\right)\Pi^1. \tag{B.26}$$

From the third assumed collision property we have,

$$\Pi^1_{jk} = \sum_{i=1}^{9} \mathbf{f}_i^1 \mathbf{v}_{i,j}\mathbf{v}_{i,k} = -\tau\sum_{i=1}^{9} D_0\mathbf{f}_i^{\mathrm{eq}}\mathbf{v}_{i,j}\mathbf{v}_{i,k}$$

and quoting an important result from the appendix of [11],

$$-\tau\sum_{i=1}^{9} D_0\mathbf{f}_i^{\mathrm{eq}}\mathbf{v}_{i,j}\mathbf{v}_{i,k} = \\ \tau\left[\frac{c^2}{3}\left(u_j\nabla_k\rho + u_k\nabla_j\rho\right) + \rho\left(u_j(\mathbf{u}\cdot\nabla)u_k + u_k(\mathbf{u}\cdot\nabla)u_j\right) - 2\frac{c^2}{3}\rho\varepsilon_{jk}\right],$$

we arrive at,

$$\Pi^1_{jk} = \tau\left[\frac{c^2}{3}\left(u_j\nabla_k\rho + u_k\nabla_j\rho\right) + \rho\left(u_j(\mathbf{u}\cdot\nabla)u_k + u_k(\mathbf{u}\cdot\nabla)u_j\right) - 2\frac{c^2}{3}\rho\varepsilon_{jk}\right] \tag{B.27}$$

As done in [11] we neglect terms of order $\mathbf{u}^3$ and higher in (B.27) to considerably simplify the expression to,

$$\Pi^1_{jk} = -2\tau\frac{c^2}{3}\rho\varepsilon_{jk}$$

so that,

$$\sigma^{\mathrm{LBM}} = -\frac{c^2}{3}\rho + 2\epsilon\rho\frac{c^2}{3}\left(\frac{2\tau-1}{2}\right)\varepsilon_{jk}$$

Comparing to (B.1) we see that we can recover a Newtonian fluid if we choose τ so that,

$$\mu = \epsilon\rho\frac{c^2}{3}\left(\frac{2\tau-1}{2}\right)$$

which can be written alternatively as,

$$\nu = \frac{(2\tau-1)}{6}\frac{\delta_x^2}{\delta_t}.$$

Note that in order to onbtain the correct stress-strain rate relationship we are forced to interpret the hydrostatic pressure to be,

$$\pi = \frac{c^2}{3}\rho.$$

□

B.6 Discussion

An important note to the above derivation is that for a D2Q9 LBM simulation to obey the proper stress-strain rate relationship (B.1) for an isotropic Newtonian fluid (up to $\mathcal{O}(\epsilon^2)$ and $\mathcal{O}(\mathbf{u}^3)$) the only conditions we needed were the choice of equilibrium and to constrain our collision step so that

it has the aforementioned properties,

$$\sum_{i=1}^{9} \mathbf{f}_i^{\text{post}} = \sum_{i=1}^{9} \mathbf{f}_i^{\text{pre}} \tag{B.28}$$

$$\sum_{i=1}^{9} \mathbf{f}_i^{\text{post}} \mathbf{v}_{i,j} = \sum_{i=1}^{9} \mathbf{f}_i^{\text{pre}} \mathbf{v}_{i,j} \tag{B.29}$$

$$\sum_{i=1}^{9} D_0 f^{\text{eq}} \mathbf{v}_{i,j} \mathbf{v}_{i,k} = -\frac{1}{\tau} \sum_{i=1}^{9} \mathbf{f}_i^1 \mathbf{v}_{i,j} \mathbf{v}_{i,k} \tag{B.30}$$

Of course way to implement the constraint (B.30) is the usual MRT-LBM expression,

$$\sum_{i=1}^{9} \mathbf{f}_i^{\text{post}} \mathbf{v}_{i,j} \mathbf{v}_{i,k} = \sum_{i=1}^{9} \mathbf{f}_i^{\text{pre}} \mathbf{v}_{i,j} \mathbf{v}_{i,k} + \frac{1}{\tau} \left(\mathbf{f}_i^{\text{eq}} - \mathbf{f}_i^{\text{pre}} \right) \mathbf{v}_{i,j} \mathbf{v}_{i,k}, \tag{B.31}$$

which in the moment description of §4.3.4 was written as,

$$\mathbf{M}_k^{\text{post}} = \mathbf{M}_k^{\text{pre}} + \frac{1}{\tau} \left(\mathbf{M}_k^{\text{eq}} - \mathbf{M}_k^{\text{pre}} \right), \quad k \in \{8, 9\}.$$

This realization has an interesting consequence. Namely that one does not need a collision step as restrictive as the SRT-LBM expression,

$$\sum_{i=1}^{9} \mathbf{f}_i^{\text{post}} = \sum_{i=1}^{9} \mathbf{f}_i^{\text{pre}} + \frac{1}{\tau} \left(\mathbf{f}_i^{\text{eq}} - \mathbf{f}_i^{\text{pre}} \right),$$

in order to simulate a Newtonian fluid. All that is required is that (B.28)-(B.30) are satisfied. In fact, we can take this interpretation further and state that it is not even necessary for the collision step to assume the usual MRT-LBM form (B.31). In principle, any constraints on the collision step will suffice provided they have properties (B.28)-(B.30). This opens the door to new ways of constraining the collision step yet still ensuring the proper physics.

Bibliography

[1] Haihu Liu et al. "Multiphase lattice Boltzmann simulations for porous media applications – a review". In: (Apr. 2014), p. 51. arXiv: 1404.7523.

[2] Guy R McNamara and Gianluigi Zanetti. "Use of the Boltzmann equation to simulate lattice-gas automata". In: Physical Review Letters 61.20 (1988), p. 2332.

[3] FJ J Higuera, S Succi, and R Benzi. "Lattice gas dynamics with enhanced collisions". In: EPL (Europhysics Letters) 345.4 (June 1989), pp. 345–349. DOI: 10.1209/0295-5075/9/4/008.

[4] F J Higuera and J Jimenez. "Boltzmann approach to lattice gas simulations". In: EPL (Europhysics Letters) 9.7 (1989), p. 663.

[5] Shiyi Chen et al. "Lattice Boltzmann model for simulation of magnetohydrodynamics". In: Physical Review Letters 67.27 (1991), p. 3776.

[6] Roberto Benzi, Sauro Succi, and Massimo Vergassola. "The lattice Boltzmann equation: theory and applications". In: Physics Reports 222.3 (1992), pp. 145–197.

[7] Hudong Chen, Shiyi Chen, and William H Matthaeus. "Recovery of the Navier-Stokes equations using a lattice-gas Boltzmann method". In: Physical Review A 45.8 (1992), R5339.

[8] YH Qian, D D'Humières, and P Lallemand. "Lattice BGK models for Navier-Stokes equation". In: EPL (Europhysics Letters) 479 (1992).

[9] J.-P. Rivet and J. P. Boon. Lattice Gas Hydrodynamics. Cambridge University Press, 2005, p. 312.

[10] Bastien Chopard and Michel Droz. Cellular Automata Modeling of Physical Systems. Cambridge University Press, 2005, p. 341.

[11] Xiaoyi He and LS Luo. "A priori derivation of the lattice Boltzmann equation". In: Physical Review E 55.6 (1997), pp. 6333–6336.

[12] Xiaoyi He and Li-Shi Luo. "Lattice Boltzmann Model for the Incompressible NavierStokes Equation". In: Journal of Statistical Physics 88.3/4 (Aug. 1997), pp. 927–944. DOI: 10.1023/B:JOSS.0000015179.12689.e4.

[13] Xiaoyi He and Li-Shi Luo. "Theory of the lattice Boltzmann method: From the Boltzmann equation to the lattice Boltzmann equation". In: Physical Review E 56.6 (Dec. 1997), pp. 6811–6817. DOI: 10.1103/PhysRevE.56.6811.

[14] M. K. Banda, W. A. Yong, and A. Klar. "A Stability Notion for Lattice Boltzmann Equations". In: SIAM Journal on Scientific Computing 27.6 (Jan. 2006), pp. 2098–2111. DOI: 10.1137/040606211.

[15] JD Sterling and S Chen. "Stability analysis of lattice Boltzmann methods". In: Journal of Computational Physic 206.123 (1996), pp. 196–206.

[16] Yanbing Li et al. "Numerical study of flow past an impulsively started cylinder by the lattice-Boltzmann method". In: Journal of Fluid Mechanics 519 (2004), pp. 273–300.

[17] F. Tosi et al. "Numerical stability of Entropic versus positivity-enforcing Lattice Boltzmann schemes". In: Mathematics and Computers in Simulation 72.2-6 (Sept. 2006), pp. 227–231. DOI: 10.1016/j.matcom.2006.05.007.

[18] B. M. BM Boghosian et al. "Entropic lattice Boltzmann methods". In: Proceedings of the Royal Society A: Math 457.2007 (Mar. 2001), pp. 717–766. DOI: 10.1098/rspa.2000.0689.

[19] Ludwig Boltzmann. "Further Studies on the Thermal Equilibrium of Gas Molecules". In: The Kinetic Theory of Gases. Vol. Volume 1. History of Modern Physical Sciences. Imperial College Press, July 2003, pp. 262–349. DOI: doi:10.1142/9781848161337_0015.

[20] Hudong Chen and Chris Teixeira. "H-theorem and origins of instability in thermal lattice Boltzmann models". In: Computer Physics Communications 129.1-3 (July 2000), pp. 21–31. DOI: 10.1016/S0010-4655(00)00089-8.

[21] Sauro Succi, Iliya Karlin, and Hudong Chen. "Colloquium: Role of the H theorem in lattice Boltzmann hydrodynamic simulations". In: Reviews of Modern Physics 74.4 (Nov. 2002), pp. 1203–1220. DOI: 10.1103/RevModPhys.74.1203.

[22] Santosh Ansumali and Iliya Karlin. "Stabilization of the lattice Boltzmann method by the H theorem:A numerical test". In: Physical Review E 62.6 (Dec. 2000), pp. 7999–8003. DOI: 10.1103/PhysRevE.62.7999.

[23] Bruce Boghosian et al. "Galilean-invariant lattice-Boltzmann models with H theorem". In: Physical Review E 68.2 (Aug. 2003), p. 025103. DOI: 10.1103/PhysRevE.68.025103. arXiv: 0211093v1 [arXiv:cond-mat].

[24] Sauro Succi. The Lattice Boltzmann Equation: For Fluid Dynamics and Beyond. Oxford University Press, 2001, p. 288.

[25] IV Iliya Karlin and S. Succi. "Equilibria for discrete kinetic equations". In: Physical Review E 58.4 (Oct. 1998), pp. 4053–4056. DOI: 10.1103/PhysRevE.58.R4053.

[26] Iliya Karlin et al. "Maximum Entropy Principle for Lattice Kinetic Equations". In: Physical Review Letters 81.1 (July 1998), pp. 6–9. DOI: 10.1103/PhysRevLett.81.6.

[27] A Renda et al. "Thermohydrodynamic lattice BGK schemes with non-perturbative equilibria". en. In: Europhysics Letters (EPL) 41.3 (Feb. 1998), pp. 279–284. DOI: 10.1209/epl/i1998-00143-x.

[28] IV Karlin, A Ferrante, and HC Öttinger. "Perfect entropy functions of the lattice Boltzmann method". In: EPL (Europhysics Letters) 47.July (1999), pp. 182–188.

[29] Alexander J. Wagner. "An H-Theorem for the Lattice Boltzmann Approach to Hydrodynamics". In: EPL (Europhysics Letters) 29.April 1995 (Aug. 1998), p. 6. DOI: 10.1209/epl/i1998-00448-8. arXiv: 9808052 [cond-mat].

[30] Bruce M Boghosian, Peter Love, and Jeffrey Yepez. "Entropic lattice Boltzmann model for Burgers's equation." In: Philosophical transactions. Series A, Mathematical, physical, and engineering sciences 362.1821 (Aug. 2004), pp. 1691–701. DOI: 10.1098/rsta.2004.1410.

[31] Santosh Ansumali and Iliya Karlin. "Single relaxation time model for entropic lattice Boltzmann methods". In: Physical Review E 65.5 (May 2002), p. 056312. DOI: 10.1103/PhysRevE.65.056312.

[32] S. Ansumali et al. "Minimal entropic kinetic models for hydrodynamics". In: EPL (Europhysics Letters) 798.September (2003), pp. 798–804.

[33] SANTOSH ANSUMALI et al. "Entropic Lattice Boltzmann Simulation of the Flow Past Square Cylinder". In: International Journal of Modern Physics C 15.03 (Mar. 2004), pp. 435–445. DOI: 10.1142/S012918310400584X. arXiv: 0311156v1 [arXiv:cond-mat].

[34] S. Ansumali et al. "Entropic lattice Boltzmann method for microflows". In: Physica A: Statistical Mechanics and 359 (Jan. 2006), pp. 289–305. DOI: 10.1016/j.physa.2005.04.039.

[35] Sunder et al. "Entropic Lattice Boltzmann method on non-uniform grids". In: 3516 (2005), pp. 72–79.

[36] F Tosi and S Succi. "An Introduction to Entropic Lattice Boltzmann Scheme". In: SIMAI e-Lecture Notes 1 (2008), pp. 1–42. DOI: 10.1685/SELN08004.

[37] R.A. A Brownlee, A.N. N. Gorban, and J. Levesley. "Nonequilibrium entropy limiters in lattice Boltzmann methods". In: Physica A: Statistical Mechanics and its Applications 387.2-3 (Mar. 2008), pp. 385–406. DOI: 10.1016/j.physa.2007.09.031. arXiv: 0704.0043.

[38] A. N. Gorban. "Basic Types of Coarse-Graining". In: Model Reduction and Coarse-Graining Approaches for ... (Feb. 2006), pp. 117–176. arXiv: 0602024 [cond-mat].

[39] R. A Brownlee, A. N Gorban, and J. Levesley. "Stabilization of the lattice Boltzmann method using the Ehrenfests coarse-graining idea". In: Physical Review E 74.3 (Sept. 2006), p. 037703. DOI: 10.1103/PhysRevE.74.037703. arXiv: 0605359 [cond-mat].

[40] R A Brownlee, A N Gorban, and J Levesley. "Stabilisation of the lattice-Boltzmann method using the Ehrenfests' coarse-graining". In: 1 (May 2006), p. 4. DOI: 10.1103/PhysRevE.74.037703. arXiv: 0605359 [cond-mat].

[41] D'Humières. "Rarefied Gas Dynamics: Theory and Simulations. Prog". In: Aeronaut. Astronaut 159 (1992), p. 450.

[42] Dominique D'Humieres. "Generalized lattice-Boltzmann equations". In: Rarefied gas dynamics- Theory and sim (1994), pp. 450–458.

[43] P Lallemand and Ls Luo. "Theory of the lattice boltzmann method: dispersion, dissipation, isotropy, galilean invariance, and stability". In: Physical review. E, Statistical physics, plasmas, fluids, and relat 61.6 Pt A (June 2000), pp. 6546–62.

[44] Dominique D'Humières et al. "Multiple-relaxation-time lattice Boltzmann models in three dimensions." In: Philosophical transactions. Series A, Mathematical, physical, and engineering sciences 360.1792 (Mar. 2002), pp. 437–51. DOI: 10.1098/rsta.2001.0955.

[45] Michael McCracken and John Abraham. "Multiple-relaxation-time lattice-Boltzmann model for multiphase flow". In: Physical Review E 71.3 (Mar. 2005), p. 036701. DOI: 10.1103/PhysRevE.71.036701.

[46] Rui Du, Baochang Shi, and Xingwang Chen. "Multi-relaxation-time lattice Boltzmann model for incompressible flow". In: Physics Letters A 359.6 (Dec. 2006), pp. 564–572. DOI: 10.1016/j.physleta.2006.07.074.

[47] Feng Chen et al. "Multiple-relaxation-time lattice Boltzmann approach to compressible flows with flexible specific-heat ratio and Prandtl number". In: EPL (Europhysics Letters) 90.5 (June 2010), p. 54003. DOI: 10.1209/0295-5075/90/54003. arXiv: 1004.5442.

[48] Rui Du and Wenwen Liu. "A New Multiple-relaxation-time Lattice Boltzmann Method for Natural Convection". In: Journal of Scientific Computing 56.1 (Dec. 2012), pp. 122–130. DOI: 10.1007/s10915-012-9665-9.

[49] R. Brownlee, a. Gorban, and J. Levesley. "Stability and stabilization of the lattice Boltzmann method". In: Physical Review E 75.3 (Mar. 2007), p. 036711. DOI: 10.1103/PhysRevE.75.036711.

[50] R Brownlee, A N Gorban, and J Levesley. "Stable simulation of fluid flow with high-Reynolds number using Ehrenfests steps". In: Numerical Algorithms 45.1-4 (May 2007), pp. 389–408. DOI: 10.1007/s11075-007-9087-1. arXiv: arXiv:0705.4371v1.

[51] R. A. Brownlee et al. "Add-ons for Lattice Boltzmann Methods: Regularization, Filtering and Limiters". In: (Oct. 2011). arXiv: 1110.0270.

[52] Alexander N. Gorban and Dave Packwood. "Allowed and forbidden regimes of entropy balance in lattice Boltzmann collisions". In: Physical Review E 86.2 (Aug. 2012), p. 025701. DOI: 10.1103/PhysRevE.86.025701.

[53] Li-Shi Luo et al. "Numerics of the lattice Boltzmann method: Effects of collision models on the lattice Boltzmann simulations". In: Physical Review E 83.5 (May 2011), p. 056710. DOI: 10.1103/PhysRevE.83.056710.

[54] L de la Fuente and David Ingram. "Enhancing stability of Lattice-Boltzmann simulations via new boundary conditions". In: ... Journal of Modern ... 14.1 (Jan. 2003), pp. 29–40. DOI: 10.1142/S0129183103004176.

[55] Joris Verschaeve. "Analysis of the lattice Boltzmann Bhatnagar-Gross-Krook no-slip boundary condition: Ways to improve accuracy and stability". In: Physical Review E 80.3 (Sept. 2009), p. 036703. DOI: 10.1103/PhysRevE.80.036703.

[56] Irina Ginzburg. "Equilibrium-type and link-type lattice Boltzmann models for generic advection and anisotropic-dispersion equation". In: Advances in Water Resources 28.11 (Nov. 2005), pp. 1171–1195. DOI: 10.1016/j.advwatres.2005.03.004.

[57] H. Hammou, I. Ginzburg, and M. Boulerhcha. "Two-relaxation-times Lattice Boltzmann schemes for solute transport in unsaturated water flow, with a focus on stability". In: Advances in Water Resources 34.6 (June 2011), pp. 779–793. DOI: 10.1016/j.advwatres.2011.04.008.

[58] A Kuzmin and J Derksen. Introduction to the Lattice Boltzmann Method. 2011.

[59] Yusong Li, Eugene LeBoeuf, and P. Basu. "Least-squares finite-element scheme for the lattice Boltzmann method on an unstructured mesh". In: Physical Review E 72.4 (Oct. 2005), p. 046711. DOI: 10.1103/PhysRevE.72.046711.

[60] Jonas Latt and Bastien Chopard. "Lattice Boltzmann method with regularized pre-collision distribution functions". In: Mathematics and Computers in Simulation 72.2-6 (Sept. 2006), pp. 165–168. DOI: 10.1016/j.matcom.2006.05.017.

[61] D. N. Siebert, L. A. Hegele, and P. C. Philippi. "Lattice Boltzmann equation linear stability analysis: Thermal and athermal models". In: Physical Review E 77.2 (Feb. 2008), p. 026707. DOI: 10.1103/PhysRevE.77.026707.

[62] Wen-An Yong. "An Onsager-like relation for the lattice Boltzmann method". In: Computers & Mathematics with 58.5 (Sept. 2009), pp. 862–866. DOI: 10.1016/j.camwa.2009.02.010.

[63] Ahmed Mezrhab et al. "Double MRT thermal lattice Boltzmann method for simulating convective flows". In: Physics Letters A 374.34 (July 2010), pp. 3499–3507. DOI: 10.1016/j.physleta.2010.06.059.

[64] Bastien Chopard, Pascal O Luthi, and J-F Wagen. "Lattice boltzmann method for wave propagation in urban microcells". In: IEE Proceedings-Microwaves, Antennas and Propagation 144.4 (1997), pp. 251–255.

[65] R A Brownlee, Alexander N Gorban, and Jeremy Levesley. "Stabilization of the lattice Boltzmann method using the Ehrenfests coarse-graining idea". In: Physical Review E 74.3 (2006), p. 37703.

[66] Richard L Liboff. Kinetic theory: classical, quantum, and relativistic descriptions. Springer Science & Business Media, 2003.

[67] Li-Shi Luo. "Unified Theory of Lattice Boltzmann Models for Nonideal Gases". In: Physical Review Letters 81.8 (Aug. 1998), pp. 1618–1621. DOI: 10.1103/PhysRevLett.81.1618.

[68] P. Bhatnagar, E. Gross, and M. Krook. "A Model for Collision Processes in Gases. I. Small Amplitude Processes in Charged and Neutral One-Component Systems". In: Physical Review 94.3 (May 1954), pp. 511–525. DOI: 10.1103/PhysRev.94.511.

[69] Irina Ginzburg, Frederik Verhaeghe, and Dominique D'Humieres. "Two-relaxation-time lattice Boltzmann scheme: About parametrization, velocity, pressure and mixed boundary conditions". In: Communications in computational physics 3.2 (2008), pp. 427–478.

[70] Paul Ehrenfest and Tatiana Ehrenfest. The conceptual foundations of the statistical approach in mechanics. Courier Corporation, 1990.

[71] Shyam Chikatamarla and Iliya Karlin. "Entropy and Galilean Invariance of Lattice Boltzmann Theories". In: Physical Review Letters 97.19 (Nov. 2006), p. 190601. DOI: 10.1103/PhysRevLett.97.190601.

[72] A Bardow, I V Karlin, and A A Gusev. "General characteristic-based algorithm for off-lattice Boltzmann simulations". In: EPL (Europhysics Letters) 75.3 (2006), p. 434.

[73] Stephen Wolfram. "Cellular automaton fluids 1: Basic theory". In: Journal of Statistical Physics 45.3-4 (1986), pp. 471–526.

[74] Paul Lavallee, Jean Pierre Boon, and Alain Noullez. "Boundaries in lattice gas flows". In: Physica D: Nonlinear Phenomena 47.1 (1991), pp. 233–240.

[75] P A Skordos. "Initial and boundary conditions for the lattice Boltzmann method". In: Physical Review E 48.6 (1993), p. 4823.

[76] David R Noble et al. "A consistent hydrodynamic boundary condition for the lattice Boltzmann method". In: Physics of Fluids (1994-present) 7.1 (1995), pp. 203–209.

[77] Robert S Maier, Robert S Bernard, and Daryl W Grunau. "Boundary conditions for the lattice Boltzmann method". In: Physics of Fluids (1994-present) 8.7 (1996), pp. 1788–1801.

[78] Qisu Zou and Xiaoyi He. "On pressure and velocity boundary conditions for the lattice Boltzmann BGK model". In: Physics of Fluids 9.6 (1997).

[79] I Ginzbourg and P M Adler. "Boundary flow condition analysis for the three-dimensional lattice Boltzmann model". In: Journal de Physique II 4.2 (1994), pp. 191–214.

[80] ET Jaynes. "Information theory and statistical mechanics". In: Physical review (1957).

[81] Claude E Shannon. "The Bell Technical Journal,". In: A mathematical theory of communication 27.4 (1948), pp. 379–423.

[82] A I Khinchin. "Mathematical Foundations of Information Theory Dover Publications Inc". In: New York (1957).

[83] S. Kullback and R. A. Leibler. "On Information and Sufficiency". EN. In: The Annals of Mathematical Statistics 22.1 (Mar. 1951), pp. 79–86.

[84] Shunsuke Ihara. Information theory for continuous systems. Vol. 2. World Scientific, 1993.

[85] I V Karlin, F Bösch, and S S Chikatamarla. "Gibbs' principle for the lattice-kinetic theory of fluid dynamics". In: Physical Review E 90.3 (2014), p. 31302.

[86] Fabian Bösch, Shyam S Chikatamarla, and Ilya Karlin. "Entropic Multi-Relaxation Models for Simulation of Fluid Turbulence". In: arXiv preprint arXiv:1507.02509 (2015).

[87] Santosh Ansumali and Iliya V. Karlin. "Kinetic boundary conditions in the lattice Boltzmann method". In: Physical Review E 66.2 (Aug. 2002), p. 26311.

[88] Irina Ginzburg. "Generic boundary conditions for lattice Boltzmann models and their application to advection and anisotropic dispersion equations". In: Advances in Water Resources 28.11 (Nov. 2005), pp. 1196–1216. DOI: 10.1016/j.advwatres.2005.03.009.

[89] Shuling Hou et al. "Simulation of Cavity Flow by the Lattice Boltzmann Method". In: Journal of Computational 118.2 (May 1995), pp. 329–347. DOI: http://dx.doi.org/10.1006/jcph.1995.1103.